Chapter 3

Laser induced fluorescence of atmospheric polycyclic aromatic hydrocarbons

3.1 INTRODUCTION

Polycyclic aromatic hydrocarbons (PAHs) are emitted from a number of anthropogenic sources, including combustion processes. They are of environmental concern due to their potential toxicity, particularly carcinogenicity. PAH monitoring campaigns have thus been conducted globally, focusing on such sources as vehicles (Marr et al., 1999 and 2004; Tang et al., 2001; Koziel et al., 2001; and Odziemkowski et al., 2001), biomass burning (Yang et al., 2006; Hays et al., 2003; Fang et al., 1999; and dos Santos et al. 2002) and incineration (Chiang et al., 1992).

PAHs consist of aggregates of condensed aromatic rings (as shown in Figure 3.1), which may be formed from low molar mass hydrocarbons via pyrosynthesis at temperatures above 500 ^{o}C, under oxygen deficient conditions. Free radicals are formed upon cleavage of the carbon-carbon and carbon-hydrogen bonds of these hydrocarbon precursors. The radicals then undergo dehydrogenation and combine to form aromatic ring structures. PAHs may also be formed from free radicals produced during pyrolysis of higher alkanes (Manahan, 2000).

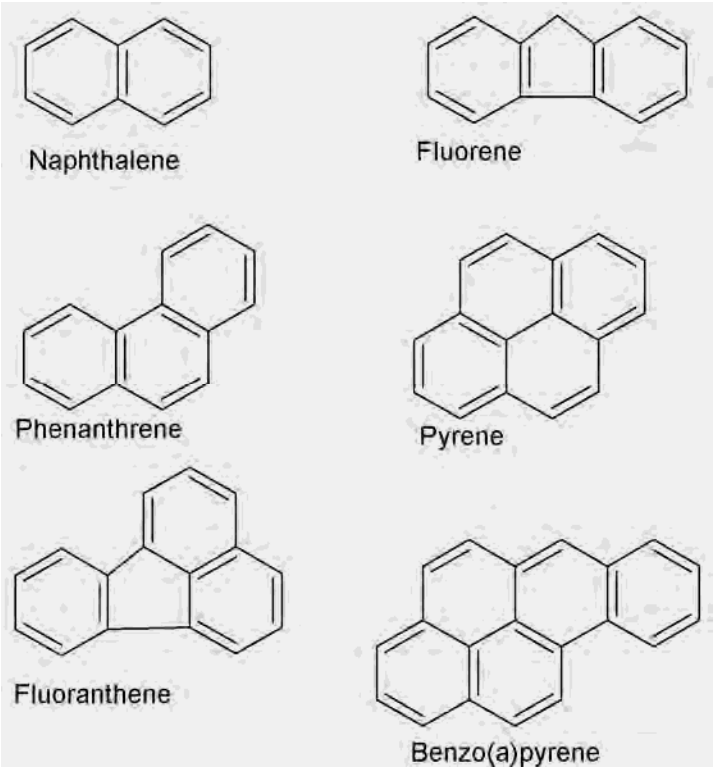

Figure 3.1: Structure of selected PAHs.

The larger ring structures (> 5 rings) are usually predominantly particle bound under ambient conditions, whilst the smaller species (2- and 3-ring PAHs) are usually in the gas phase, with 4- membered rings being found in both phases (Ohura et al., 2004a and Ono-Ogasawara and Smith, 2004). In terms of health effects, it is important that both of phases be monitored (Chang et al., 2006 and Westerholm et al., 1991).

3.1.1 Problem statement and aim

Current analytical methods for atmospheric PAH determinations are time consuming and usually require the use of solvent extraction of samples. This may limit the widespread sampling and analysis of PAH samples for spatial and temporal trend determinations.

A technique was therefore to be developed and investigated, which would allow for the rapid screening of samples for the presence of PAHs, prior to comprehensive, quantitative analysis, if required.

This method would be based on the sampling of air onto a multi-channel silicone rubber trap, in which the polydimethylsiloxane (PDMS) serves as a solvent for the analyte species. The inert nature of the silicone minimizes the possibility of artifact formation and the low pressure drop across the trap allows for a large volume of air to be drawn through the traps by means of a small, battery operated portable pump. Two traps can also be coupled in series, in order to verify the absence of breakthrough of analytes from the first trap.

Laser-induced fluorescence (LIF) was to be employed to selectively excite the PAH(s) of interest on the trap, and the resulting fluorescence would be determined at the wavelength characteristic for the target PAH. The technique would be basically non-destructive, thus enabling the subsequent GC-MS analysis of samples of interest, for example those containing the target analytes at levels exceeding a specified threshold concentration. It would also lend itself to real-time monitoring and the provision of chemical "finger-prints" via the fluorescence spectra (Gridin et al., 2000).

This chapter provides a background to PAHs in the environment and the use of fluorescence based methods for monitoring these compounds. The development and optimization of our laser induced fluorescence screening method is then described, including the results of repeatability, sensitivity, breakthrough volume and photodegradation studies.

3.1.2 PAHs in the environment

PAHs are classified as persistent organic pollutants, and may be subject to long range atmospheric transport. Although man has a long history of burning materials, such as coal, oil, petrol and wood, which inevitably has resulted in substantial releases of PAHs worldwide, they were first subjected to international emission controls under the United Nations Economic Commission for Europe protocol in 1998 (Prevedouros et al., 2004).

PAHs are derived from a number of different sources, and it has been found that the specific PAHs present in an atmospheric sample can be used as source fingerprints, as indicated in Table 3.1.

Table 3.1: Main PAHs emitted from various sources, which can be used for source fingerprinting (Harrison et al., 1996).

Source	**PAH markers**
Coal combustion	Anthracene; phenanthrene; fluoranthene; pyrene; benz(*a*)anthracene; chrysene
Coke production	Anthracene; phenanthrene; benz(*a*)pyrene; benzo(*ghi*)perylene
Incineration	Phenanthrene; fluoranthene; pyrene
Wood combustion	Anthracene; phenanthrene; fluoranthene; pyrene
Oil burning	Fluoranthene; pyrene
Petrol fueled automobiles	Fluoranthene; pyrene; benzo(*ghi*)perylene; coronene
Diesel fueled automobiles	Similar to petrol fueled automobiles

Emission inventories for the United Kingdom (UK) estimated that domestic burning contributes ~80 % of the total PAH emissions annually, and four PAHs, namely phenanthrene, fluoranthene, fluorene and pyrene, contributed ~75 % to this total (Lohmann et al., 2000). Another UK source inventory and budget estimated that over 100 tons of PAHs are emitted into the UK atmosphere per annum from primary combustion sources, with over 95 % derived from domestic coal burning, unregulated fires and vehicle emissions (Wild and Jones, 1995).

In a European study spanning 22 countries, which was based on passive polyurethane foam (PUF) sampling of PAHs, fluorene, phenanthrene, fluoranthene, pyrene, chrysene and 1-methylphenanthrene were detected in all samples (Jaward et al., 2004). Three- and four-ring PAHs, specifically phenanthrene, fluorene, fluoranthene and pyrene, also comprised ~90 % of the total PAHs detected in a similar passive sampler campaign in Kuwait, with phenanthrene contributing ~35 % (Gevao et al., 2006).

These trends are to be expected when considering the information presented in Table 3.1, as it is evident that phenanthrene, fluoranthene and pyrene are emitted from most of the sources, thus they were chosen as the PAHs of interest in this study, as further elaborated under section 3.1.6.

As previously mentioned, PAHs are of environmental concern due to their potential toxicity. Exposure to naphthalene, for example, which can be smelled at a concentration of 84 ppb in air (Agency for Toxic Substances and Disease Registry (ATSDR), 2005), may lead to hemolytic anemia, as a result of damage and destruction of red blood cells. Naphthalene is also a possible human carcinogen (EPA Group C rating) (ATSDR, 2005).

As naphthalene was covered in most detail in our study, due to the analytical challenges it presented, the sources of this compound are of relevance. The main source of naphthalene is from the burning of wood and fossil fuels, followed by the use of moth repellents. Studies have been conducted to determine naphthalene (and *p*-dichlorobenzene and camphor) concentration profiles in a wardrobe containing moth repellents, using passive sampling onto PDMS stir bars for 120 hours, although equilibrium is reached after approximately 2 hours (De Coensel et al., 2008), where the results indicate momentary concentrations to which the stir bars are exposed. Solvent extraction of exposed clothing indicated that the clothing could also serve as a secondary source of airborne naphthalene, as a result of re-volatilisation.

Gasoline and diesel engine exhausts, with concomitant vaporization from fuels, was found to contribute almost half of the total daily naphthalene burden in human exposure studies conducted in Southern California (Lu et al., 2005), where naphthalene average hourly exposure levels were estimated at between 270 and 430 $ng.m^{-3}$ for summer and winter, respectively.

Cigarette smoking also releases small amounts of naphthalene into the air, at a rate of between 40 and 110 µg per cigarette. 10 % of naphthalene entering the environment is from coal production and distillation, and less than 1 % is from losses during naphthalene production from coal tar or petroleum (ATSDR, 2005). Naphthalene is an intermediate in the production of phthalic anhydride, which is used in the production of phthalate plasticizers, pharmaceuticals, insect repellents and other materials. Naphthalene has also been used as an intermediate in the production of other chemicals for use in leather tanning, as surfactants, and so on. Due to these sources, as well as the use of naphthalene in many consumer products, including multipurpose solvents, lubricants, charcoal lighters, degreasers and hair spray,

naphthalene indoor air concentrations of 1000 to 2200 ng.m^{-3} have been reported in various studies (Lu et al., 2005).

A range of concentrations of PAHs in air have been reported, and are summarized in Table 3.2. A strong seasonality in measured ambient concentrations is evident in many studies, which is attributed to increased emissions from combustion sources for heating during the winter, as well as enhanced degradation of PAHs by sunlight during summer. It should be noted that other meteorological conditions besides solar radiation, such as wind speed and temperature also have significant impacts on the atmospheric concentrations of PAHs (Chang et al., 2006). A negative correlation was found between wind speed and concentrations of phenanthrene and anthracene, for example (Prevedouros et al., 2004).

Table 3.2: Summary of selected reported atmospheric PAH concentrations. Note: PM_{10} refers to particulate matter of size ≤ 10 micron.

[a] Gundel et al., 1995; [b] Šišović et al., 2008; [c] Chang et al., 2006; [d] Odabasi et al., 1999; [e] Jaward et al., 2004; [f] Ohura et al., 2004a; [g] Park et al., 2002.

PAH	Average indoor air ($ng.m^{-3}$) [a]	Suburban PM_{10} PAH in summer ($ng.m^{-3}$) [b]	Suburban PM_{10} PAH in winter ($ng.m^{-3}$) [b]	Thailand traffic (gas + particle) ($ng.m^{-3}$) [c]	China traffic (particle) ($ng.m^{-3}$) [c]	Korea urban (gas + particle) ($ng.m^{-3}$) [c]	Japan traffic (particle) ($ng.m^{-3}$) [c]	Taiwan urban (gas) ($ng.m^{-3}$) [c]	Taiwan urban (particle) ($ng.m^{-3}$) [c]	Thailand traffic (gas + particle) ($ng.m^{-3}$) [c]	Average Chicago ambient air ($ng.m^{-3}$) [d]	European ambient air ($ng.m^{-3}$) [e]	Japan indoor air (summer) ($ng.m^{-3}$) [f]	Japan indoor air (winter) ($ng.m^{-3}$) [f]	Seoul ambient total ($ng.m^{-3}$) [g]
Naphthalene	338					11.2		283	10.2	9570			1130	955	11.23
Phenanthrene	23					16.5	4.2				200.3	0.24-26	28.4	8.82	16.46
Fluoranthene	6.5	0.13	4.22					53.7	5.2	154	44.1	0.012-13.2	2.57	1.11	8.10
Pyrene	3.0	0.12	4.17		0.30	12.6	42	53.3	1.2	134	24.6	0.012-7.3	1.81	0.832	12.56
Acenaphthene and acenaphthylene	8.3				0.01	3.35; 7.39		118	8.3	200	76.9		8.93	5.18	3.35; 7.39
Fluorene	8.2			0.02	0.03	6.46	25				74.8	0.1-7.3	11.2	4.17	6.46
Anthracene	0.4			0.21	0.29	2.07		105	4.1	103	14.1	<0.004 -1.2	0.739	0.185	2.70
Benz(*a*)anthracene	0.4			1.06	0.36	2.62	11	19.2	1.1	31.5	2.1	0.004-0.6	0.118	0.162	2.62
Chrysene	1.4			1.12	0.55	3.62					3.6	0.006-1.3	0.284	0.331	3.62
Benzo(*b*)fluoranthene				0.94	0.53		3.0	6.7	2.4	154	2.3		0.497	0.528	
Benzo(*a*)pyrene				1.7	0.67	2.55	11	1.8	0.9	121	1.6	<0.004 -0.25	0.240	0.343	2.55

In a Japanese study, the gaseous PAH concentrations in both indoor and outdoor air were higher in summer than in winter, whilst the opposite trend was true for particle-bound PAHs (Ohura et al., 2004a), as would be expected. The gaseous indoor PAH concentrations were mostly derived from insect repellents and heating sources, whilst that of indoor particulate PAH was a result of cigarette smoking and was also related to the age and type of wood from which the house was constructed and outdoor PAH concentrations.

Urban centres in the United Kingdom have been found to have PAH concentrations of 1-2 orders of magnitude higher than that found in rural Europe, and up to 3 orders of magnitude higher than Arctic Canada (Prevedouros et al., 2004). In a medium traffic area in Rome, a slightly decreasing trend in annual PAH mean values was noted from 1994-1998 (Menichini et al., 1999).

Semi-rural ambient concentrations of gaseous naphthalene of 13.1 - 45.2 $ng.m^{-3}$ and urban levels of 70.2 - 167.4 $ng.m^{-3}$ have been reported in France (Temime-Roussel et al., 2004), whilst in urban Greece, the most abundant PAHs (gas + particles) were phenanthrene (20.0 $ng.m^{-3}$), pyrene (6.6 $ng.m^{-3}$) and fluoranthene (6.5 $ng.m^{-3}$) (Tsapakis and Stephanou, 2005).

The overall environmental fate of PAHs in the context of different environmental compartments (air, water, soil, etc), is summarized in Figure 3.2, from which it can be seen that there are various means by which PAHs may be removed from the atmosphere including degradation, deposition and precipitation. The effect of precipitation on less volatile PAHs is greater than that on the more volatile PAHs (such as naphthalene and phenanthrene), as the less volatile PAHs tend to be associated with particles which can be washed out during precipitation (Subramanyam et al., 1994). Soil has been identified as the major repository in the UK for PAHs (Wild and Jones, 1995).

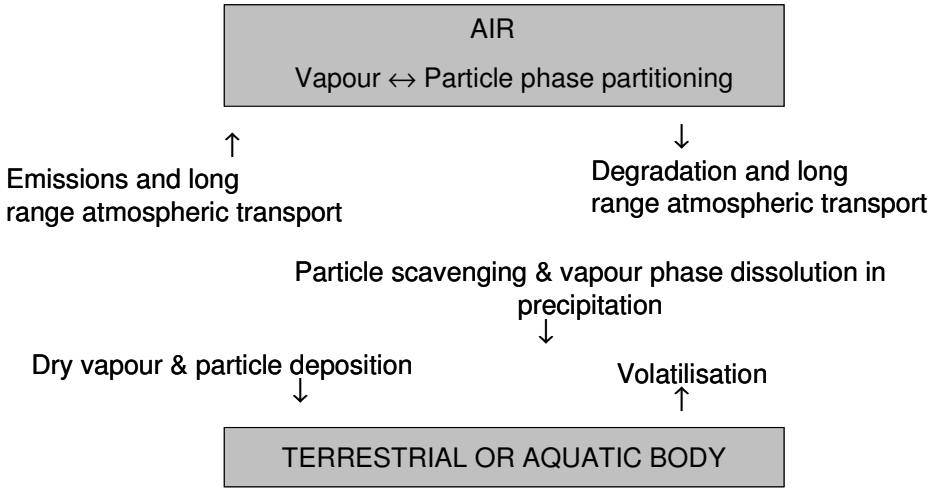

Figure 3.2: Environmental fate of PAHs (adapted from Prevedouros et al., 2004).

Gas phase PAHs present in the atmosphere may undergo various reactions with reactive species, such as the hydroxyl radical. PAHs, especially the larger ring structures, are sensitive to electrophilic substitution and to oxidation (Nikolaou et al., 1984). Reported atmospheric lifetimes of selected gas phase PAHs are summarized in Table 3.3.

Table 3.3: Atmospheric lifetimes of gas-phase PAHs, based on reaction with reactive species (USA EPA, 2002).

PAH	**OH•** at 1.6 x 10^6 molecules.cm^{-3} (12 h average)	**O_3** at 7 x 10^{11} molecules.cm^{-3} (24 h average)	**NO_3** 5 x 10^8 molecules.cm^{-3} (12 h average)
Naph	6.8 h	> 80 days	1.5 years
PhA	11.2 h	41 days	4.6 h
FlA	~2.9 h	-	~1 year
Py	~2.9 h	-	~120 days

It is evident that the hydroxyl radical is the most important species in removing these gas phase PAHs from the atmosphere, and would result in their removal in under a day. Particulate phase PAHs have been found to undergo long range transport from Asia to North America and atmospheric lifetimes of particulate phase PAHs are reported to be in the order of a week (Primbs et al., 2008).

Photodegradation of PAHs in the environment is also an important atmospheric removal process, and will be discussed under section 3.2.4.

Microbial degradation is of relevance to PAHs which have been deposited onto soil, although due to the high hydrophobicity of PAHs, they are not readily available for microbial degradation, as bacteria degrade compounds dissolved in water (Johnsen et al., 2005). This is of particular concern for high molecular weight PAHs, due to their lower water solubilities. The dense cloud of π-electrons above and below the PAH ring structures also makes them resistant to nucleophilic attack, however degradation pathways have been proposed (Zhang et al., 2006).

3.1.3 Fluorescence characteristics of PAHs

The spectroscopic features of PAHs include large absorption cross-sections and high fluorescence quantum yields (Song et al., 2003), thus fluorescence has been used as a means of detection of these compounds in applications such as HPLC for many years (for example, NIOSH methods 5506 and 5800, 1998). Enhanced sensitivity of HPLC-based PAH methods over GC-MS based methods have also been reported (Ohura et al., 2004a). Fluorescence excitation and emission wavelengths pertaining to the PAHs of interest in this study are given in Table 3.4, which are based on room temperature fluorescence of PAHs on extraction membranes.

Table 3.4: Reported fluorescence excitation and emission wavelengths for selected PAHs, with preferred wavelengths given in bold (Whitcomb et al., 2002).

PAH	Excitation wavelength (nm)	Emission wavelength (nm)
Naph	281; **292**	323; **337**
PhA	258; 279; 286; **298**	**388**; 407
FlA	292; **365**	465
Py	278; 326; **341**	386; **395**; 474

Fluorescence detection was also one of the methods used, in addition to ultraviolet (UV) and visible analysis, to determine PAHs in column chromatography derived benzene extracts of urban air particulates by Sawicki et al. in 1960, as well as for the analysis of PAHs in thin layer chromatography extracts of traffic related aerosol samples (Handa et al., 1980). The detection limits relating to HPLC fluorescence detection for the PAHs of interest in this study are included in Table 3.5, and are based on a signal to noise ratio of 2:1. Other studies have reported limits of quantitation for PAHs of < 0.1 ng.m^{-3} (Šišović et al., 2008).

Table 3.5: HPLC fluorescence detection limits of selected PAHs, based on a signal to noise ratio of 2:1 (Harrison et al., 1996).

PAH	Detection limit (ng)
Naph	0.43
PhA	0.49
FlA	0.85
Py	0.48

The aromatic rings of PAHs serve as *chromophores*, as the delocalized π-electron systems exhibit characteristic UV-visible absorption spectra. The most probable electron transitions are π → π*, which thus have the most intense absorption bands in the absorption spectra of these compounds (except for naphthalene, where such transitions are forbidden) (Schwarzenbach et al., 2003).

A *bathochromic shift* occurs as the number of aromatic rings increases, in that the absorption maximum of the lowest energy π → π* transition generally shifts to lower energies

(Schwarzenbach et al., 2003). This allows for different size classes of PAHs to be selectively detected based on their fluorescence: excitation with wavelengths < 300 nm results in fluorescence of PAHs containing 2-3 aromatic rings at 300-450 nm; whilst PAHs containing > 4 aromatic rings will tend to fluoresce at 300-700 nm, with the fluorescence maximum generally in the visible region of the spectrum (Vander Wal et al., 1997).

It should be noted, however, that not only the number of aromatic rings, but also the way in which they are fused together, influences the absorption spectrum of PAHs, as does the physical state of the PAH and the presence of solvent.

The fluorescence quantum yield is defined as the ratio of the number of photons emitted to the number of photons absorbed. Molecules with higher quantum yields may therefore be determined at lower concentrations compared to those with lower quantum yields, and the sensitivity of the method will be enhanced. Quantum yields and fluorescence lifetimes of the PAHs of interest in this study are given in Table 3.6. It is evident that naphthalene does not have as high a fluorescence quantum yield as pyrene, for example, thus it is expected that the detection limit obtained for naphthalene will not be as low as for pyrene. The fluorescence lifetimes reported are in the order of ns, with pyrene having the longest fluorescent lifetime of 450 ns.

Table 3.6: Fluorescence lifetimes and quantum yields for PAHs of interest (as reported in Kumke et al., 1995).

PAH	**Florescence lifetime (τ_F) (ns)**	**Quantum yield (Φ_F)**
Naph	96	0.23
PhA	57.5	0.13
FlA	53	0.30
Py	450	0.65

The fluorescence is affected by the presence of solvents, which may lead to redshifting, such as that found in the fluorescence spectrum of pyrene dissolved in cyclohexane as compared to that in the vapour phase, which was ascribed to solvent stabilization effects (Chi et al., 2001).

Fluorescence bandwidths in vapour phase samples tend to broaden with increase in sample temperature, due to thermal vibrational sequence congestion effects, although the fluorescence intensity of pyrene increased with increase in temperature, as a consequence of an increase in the absorption cross-section at the excitation wavelength of 337 nm at elevated temperatures (Chi et al., 2001).

3.1.4 Literature review of the use of laser induced fluorescence in the monitoring of PAHs

Quantitative analysis of vapour phase PAHs at elevated temperatures (> 150 ^{o}C) by LIF, utilizing an excitation wavelength of 337.1 nm, has been reported (Chi et al., 2001 and Allain et al., 2003). Pyrene in cigarette smoke has been determined by LIF based on fiber optics with time resolution to enhance sensitivity (Song et al., 2003), and similar systems have been developed for PAH determinations on aerosols (Panne et al., 2000) and in water (Kotzick and Niessner, 1996). Again excitation at 337 nm was utilized, due to the ease of obtaining this wavelength by means of a nitrogen laser, and the system was time-resolved. A disadvantage of fibre optic based systems is the distortion of the fluorescence spectra in the (usually long) fibres that are employed (Kotzick and Niessner, 1996). A similar fibre optic based system, which utilized a frequency doubled excimer pumped dye laser, was developed for the detection of particle-bound PAHs, which allowed for excitation wavelength tunability (Niessner et al., 1991).

Mixtures of PAHs are difficult to separate into component concentrations when analyzing at a single wavelength, thus deconvolution algorithms have been employed in this regard, although only mixtures of ≤ 3 components could be effectively treated in this manner (Kotzick and Niessner, 1996; Knorr and Harris, 1981). The technique reported here employs a number of (shorter) wavelengths, allowing for improved selectivity and the detection of two- and three-membered ring structures.

The on-line monitoring of airborne PAHs by LIF and multi-photon ionization is described by Gridin et al., 2000. Here the sample gas was bubbled through a quartz measurement chamber containing hexane and the emitted fluorescence was collected by means of an optical fiber. Detection limits of 1 mg.m^{-3} were obtained for pyrene and naphthalene.

Two-photon excitation fluorescence microscopy, where each photon contributes a portion of the energy necessary to excite the molecule, has been used to visualize the fate and behaviour of PAHs (anthracene, phenanthrene and fluoranthene) within living vegetation (Wild et al., 2005 and Wild et al., 2007). Such studies are important in the context of understanding the environmental fate of picogram amounts of PAHs, which may be taken up by vegetation from the air and soil, and may then undergo processes such as transportation and storage within the plant. This is a significant advancement on previous methods for this application, which are largely destructive or damaging to the plant. A pulsed solid state laser, which scanned over the sample, was used for excitation purposes. Fluorescence microscopy has also been employed for the qualitative analysis of PAH contaminated soils (Roper et al., 2006).

In addition, LIF coupled with fiber optics has been employed in the determination of PAHs in soils and sediments (Grundl et al., 2003). Solid-phase extraction onto octadecyl membranes has been used to monitor PAHs in aqueous solutions with LIF detection of the analytes pre-concentrated on these membranes (Whitcomb et al., 2002). Detection limits at the parts per trillion level were achieved.

Naphthalene has been detected in air using the Fluorescent Assay by Gas Expansion (FAGE) technique, where the gas phase analyte (without pre-concentration) is excited by laser pulses at 308 nm passing through a detection chamber (Martinez et al., 2004). Quenching of naphthalene fluorescence by N_2 and O_2 in the air sample was reported.

The graphite furnace has been used as a vapourisation source for laser induced fluorescence of PAHs from engine exhaust and cigarette smoke (Kirsh and Winefordner, 1987).

Commercial PDMS solid-phase microextraction (SPME) fibers have been employed in the sampling of airborne particulate matter, such as that arising from diesel vehicular exhausts, followed by GC-MS analysis (Koziel et al., 2001). SPME fibers have also been used in aqueous PAH determinations, coupled with fluorescence microscopy (Mayer et al., 2000), as well as single-particle analysis by Raman spectroscopy (Odziemkowski et al., 2001). SPME utilizing a 50 μm coating of PDMS on a glass fiber rod coupled with LIF detection has

recently been tested for PAH determinations in sediment pore water (Hawthorne et al., 2008). The larger volume of PDMS present in the sampling traps used in our study, however, allows for larger sampling volumes and therefore potential improvements to the detection limits of the method.

3.1.5 The role of screening methods in PAH analysis

Internationally accepted analytical methods for environmental monitoring are based on comprehensive techniques in order to ensure accuracy and precision of the results obtained. These methods for PAHs are based on sampling ~300 m^3 of air onto an adsorbent (typically XAD-2 resin) or a PUF cartridge and a filter, followed by solvent extraction and pre-concentration (often also incorporating sample cleanup using liquid chromatography) (Liu et al., 2007). The liquid extract is then analysed by GC-MS (USA EPA based methods), or by HPLC with UV or fluorescence detection (Japanese Ministry of the Environment based methods) (Ono-Ogasawara and Smith, 2004). There are also additional steps in the procedure, which involve the use of (isotopically-labelled) standards to check for both extraction and analytical recoveries. Extensive cleanup of the sorbent may be required prior to use due to the presence of contaminants, where naphthalene for example, has been detected at ~5 $ng.m^{-3}$ in XAD-2 resin blanks (Ohura et al., 2004a). Methods have been adapted to shorten sample preparation time such as by the use of accelerated solvent extraction (Ravindra et al., 2008), ultrasonic extraction, and supercritical fluid extraction of PAHs from sample matrices, as alternatives to traditional Soxhlet extraction.

Comprehensive methods are time consuming and costly to perform, thus screening methods which can be used to isolate samples of interest for detailed analysis using internationally accepted best practice, may find application in studies to understand the temporal and spatial variations in the concentration of PAHs, where many samples would need to be analysed. There is also a greater need for cost saving screening methods in developing countries, where access to funds and instrumentation may be limited.

In terms of screening studies for PAHs, Shekiro et al. (1988) developed a method for this purpose based on electrothermal vaporization - multiple-wavelength spectrometry, using an electrothermal atomizer usually used for atomic absorption spectroscopy and a photodiode

array detector. The vapour phase absorption of the sample was thus recorded over the 200-350 nm region. A liquid sample was injected into the device, which was then heated to remove the solvent prior to measurements being taken. This method therefore requires solvent extraction of samples prior to analysis, and the more volatile PAHs (particularly naphthalene) may be lost during the drying step. Spectral overlap is also a problem with this method, although determination limits of 0.05 μg were reported.

Other reported methods for PAH screening include those based on photoelectric aerosol sensors (Tang et al., 2001) and UV-induced photoemission (Hart et al., 1993), however these devices do not provide speciation information and do not detect vapour phase PAHs, which is of particular importance for the lower molar mass, more volatile PAHs.

Passive samplers have been developed in order to save costs and to allow for sampling in remote areas away from a power supply. These samplers include SPME devices made from PDMS (Liu et al., 2007) and the use of PUF disks, which sample PAHs at ~3-4 m^3 of air per day (Jaward et al., 2004). In the latter study, samplers were exposed for a six week period in 22 European countries, which allowed for an understanding of the long range transport of these chemicals.

A recent review article on analytical methods for PAHs in airborne particulates (Liu et al., 2007) noted the following areas as being important for further method development:

- Avoidance of volatilization and loss of PAHs during sampling
- Prevention of the reaction of PAHs and other compounds and redistribution of PAHs between different particle sizes
- Development of a noiseless and lower-volume sampler
- Removal of the need for sample pretreatment in a cost effective manner.

The method developed in this study sought to address a number of these needs.

3.1.6 Choice of PAHs to be studied

The choice of PAHs on which to focus this work was based on the concentrations at which they are emitted from sources, as well as their ubiquity in the environment (refer to

section 3.1.2), and the environmental concerns associated with them. It was important that the chosen analytes would be present at concentrations which could be measurable by the proposed LIF screening method, and they could thus be used as indicators for those PAHs usually present at far lower concentrations which are also of environmental concern. Good correlations have been found, for example, between phenanthrene concentrations (which averaged at 200 $ng.m^{-3}$) and the concentrations of PAHs with molecular masses between 154 and 202 (average concentrations ranged from 6 to 77 $ng.m^{-3}$) (Odabasi et al., 1999).

Although the lighter PAHs have lower carcinogenic properties than benzo(*a*)pyrene, for example, which has a toxic equivalency factor of 1 as compared to that of 0.001 for naphthalene, fluoranthene, phenanthrene and pyrene (Nisbet and LaGoy, 1992), they are the most abundant PAHs in the urban atmosphere and they may react with other pollutants to form more toxic derivatives (Odabasi et al., 1999). It has been found in some studies that the carcinogenicity of indoor air is dominated by naphthalene, and that this PAH was the most abundant in all samples (summer and winter), reaching 1100 $ng.m^{-3}$ in summer (Ohura et al., 2004a). Ohura also suggested the use of naphthalene as a surrogate compound for PAH mixtures in indoor air, and others have also reported the importance of naphthalene as a marker for PAH contamination (Wauters et al., 2008). The use of fluoranthene as an indicator compound for more toxic PAHs has similarly been recommended (Boström et al., 2002).

It has been noted in previous studies that there is a serious lack of data on low molecular weight PAHs and vapour phase emissions from some combustion sources, which may lead to significant underestimations of inputs of PAHs into the environment (Wild et al., 1995).

Naphthalene (Naph), phenanthrene (PhA), fluoranthene (FlA) and pyrene (Py) were therefore identified from the USA EPA list of 16 priority PAHs as suitable test analytes. An additional consideration for focusing primarily on naphthalene, was due to the analytical challenges it presents as the most volatile PAH.

3.1.7 Multi-channel silicone rubber traps

Due to the generally low environmental levels of organic air pollutants, pre-concentration of the analytes prior to analysis is necessary. This can be achieved during

sampling by means of traps which extract the analytes of interest from the sample air stream by adsorption or sorption processes (Baltussen et al., 1998). Common adsorptive traps are based on Tenax TA (a polymer of 2,6-diphenyl-*p*-phenylene oxide), XAD-2 and polyurethane foam (PUF), for example, whilst polydimethylsiloxane (PDMS) has been used in various configurations in sorptive samplers, including the use of mixed bed traps containing PDMS foam, PDMS particles and Tenax TA for the sampling of PAHs in air (Wauters et al., 2008). Adsorptive traps have the disadvantages of artifact formation, high background concentrations (therefore cleaning prior to usage is necessary) and irreversible analyte loading, although they generally have high capacities. Sorptive samplers are based on the reversible transfer of the analyte into the sorptive medium (PDMS), therefore breakthrough volumes are an important consideration in the utilization of these traps (Baltussen et al., 1997). Silicone degradation products are usually evident in the chromatograms obtained upon sample analysis, and can be easily identified by mass spectrometry.

Multi-channel silicone rubber traps, as first described by Ortner (1994), were utilized in this study, which comprised 22 parallel PDMS tubes of 0.3 mm i.d. housed in a quartz tube (refer to section 3.2.1.2b). Quartz was used due to its well known transparency in the UV-visible region. PDMS was found to absorb at wavelengths below 300 nm, which may impact on the excitation process but should not affect the sensitivity of the method as fluorescence emission wavelengths longer than this can be selected for the PAHs of interest.

The operation of the trap can be viewed as a gas chromatography column, where the gas phase organic analyte partitions between the stationary phase (PDMS) and the air flowing through the trap. The breakthrough volume (V_b) of the trap may be defined as the sample volume at a particular flow rate, at which 10 % of the total concentration of analyte which is entering the trap is exiting the trap at the outlet. The breakthrough volume will be smaller for higher sampling flow rates, due to the smaller number of theoretical plates (N) generated under these conditions, whilst V_b will be larger at low flow rates (refer to equation 3.1). The retention volume (V_R) is, however, independent of the flow rate.

$$V_b = V_R\left(1-\frac{2}{\sqrt{N}}\right) \qquad \text{Equation 3.1}$$

The more volatile analytes, such as naphthalene, will also have lower V_b than the less volatile compounds, such as pyrene. The determination of breakthrough volumes is discussed under section 3.2.3.

3.2 DEVELOPMENT OF THE LIF METHOD

3.2.1 Initial method development

3.2.1.1 Background

The first series of experiments which were conducted to provide an indication of the viability of the use of LIF to monitor PAHs sampled onto quartz multi-channel silicone rubber traps, were based on liquid injections of PAH standards onto these traps. Initially benzo(*a*)pyrene was used, but due to the toxicity of this compound, and for reasons discussed in section 3.1.6, naphthalene was subsequently used for method development. This section describes the initial experiments conducted and the results obtained, as well as the laser system used. In later experiments, gas phase standards were provided by diffusion tubes and gas chromatographic fraction collection, as described in Chapter 2.

3.2.1.2 Experimental method

a) Liquid standards

Benzo(*a*)pyrene (ChemService, > 95 % purity) and naphthalene (Fluka, 99.8 % purity, GC grade) PAH standards were prepared in AR grade toluene (99 % purity, Merck). These standards were loaded onto the silicone rubber traps by liquid injection; or by evaporation from a bulk liquid holding vessel of the liquid naphthalene standard (for qualitative experiments), where a portable GilAir pump was used to draw the analyte-loaded air through the trap at a pre-determined flow rate (measured by means of a bubble flowmeter).

b) Multi-channel silicone rubber traps

Multi-channel silicone rubber traps were prepared in 178 mm long quartz tubes of 4 mm i.d. and 6 mm o.d., according to the method described by Ortner (1996). This involved

folding a length of PDMS tubing the required number of times and then threading it through the quartz tube using a hairpin shaped wire. The looped ends of the tubing were then cut through using a scalpel. In these experiments, each trap contained twenty two 55 mm polydimethylsiloxane channels (0.64 mm o.d., 0.3 mm i.d., Sil-Tec, Technical Products, USA) (and one trap contained sixteen 90 mm long PDMS tubes denoted as a "long trap"). Some of the traps were prepared by the author and the remainder were prepared by a supervised laboratory technician at the University of Pretoria. The traps were conditioned before use by heating in a GC oven at 300 ^{o}C for ~24 hrs with a hydrogen carrier gas flow of ~60 mℓ.min^{-1}. After use, the traps were re-conditioned at 250 ^{o}C under nitrogen gas flow for 2 hours in a Gerstel Tube Conditioner (TC1).

c) Laser setup

An excimer laser (Lambda Physik EMG201) was used to optically pump a dye laser (LC6200 dye for benzo(*a*)pyrene and Rhodamine 6G dye for naphthalene, both dyes were supplied by Lambda Physik). Rhodamine 6G is *o*-(6-ethylamino-3-ethylimino-2,7-dimethyl-3H-xanthen-9-yl) benzoic acid ethylester, as shown in Figure 3.3.

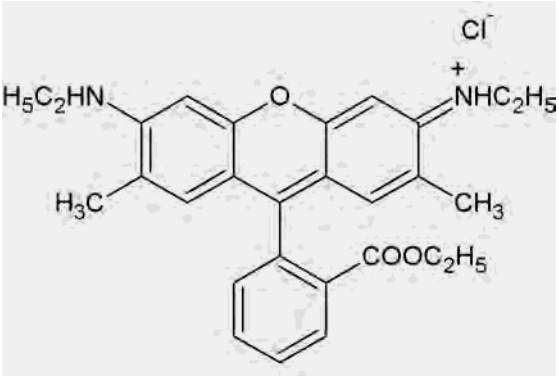

Figure 3.3: Chemical structure of Rhodamine 6G.

An intra-cavity grating allowed for wavelength tuneability over the gain bandwidth of the dye, and ensured a narrow bandwidth output (0.1 cm^{-1} at 495 nm). In the case of naphthalene, the 584 nm output beam was frequency doubled through second harmonic generation in a non-linear crystal (beta barium borate (BBO)), resulting in the desired 292 nm excitation laser wavelength (302 nm was obtained for benzo(*a*)pyrene). The unconverted

pump wavelength was filtered out using a prism arrangement. The 292 nm laser beam had a pulse energy of roughly 500 μJ in a 30 ns pulse. This laser beam was directed onto the silicone rubber trap without any focusing elements resulting in a roughly 5 mm diameter spot at the trap. The resulting fluorescence was optically collected with a plano-convex lens (f = 75 mm), and resolved with a scanning double monochromator (Kratos, Schoeffel Instruments) equipped with a photomultiplier tube (PMT). Results were recorded on a PC linked to an oscilloscope (Tektronix TDS 360).

The initial experimental setup is shown graphically in Figure 3.4. The layout of the system was later optimized and the final configuration is shown in Figure 3.5. It should be noted that for later experiments, the pinhole diaphragm was removed, and both a folding prism and an enhanced UV coated aluminium mirror were placed between the Pelin Broker crystal and the silicone rubber trap. These adjustments were needed due to other experiments being conducted in the laser laboratory, which were in the original path of the laser beam.

Similar experiments were attempted for naphthalene using the frequency doubled output from an Optically Pumped Parametric Oscillator (OPPO) laser (Lambda Physik Scanmate), which was pumped with a 10 Hz Continuum laser. Less than 100 μJ of energy reached the sample, which proved to be insufficient and therefore experiments were resumed using the dye laser system.

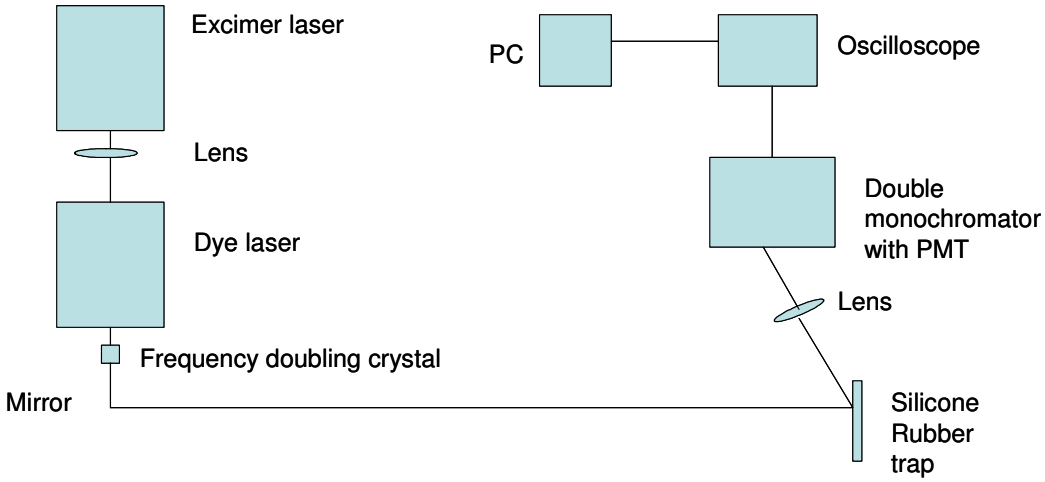

Figure 3.4: Initial experimental setup for the dye laser system.

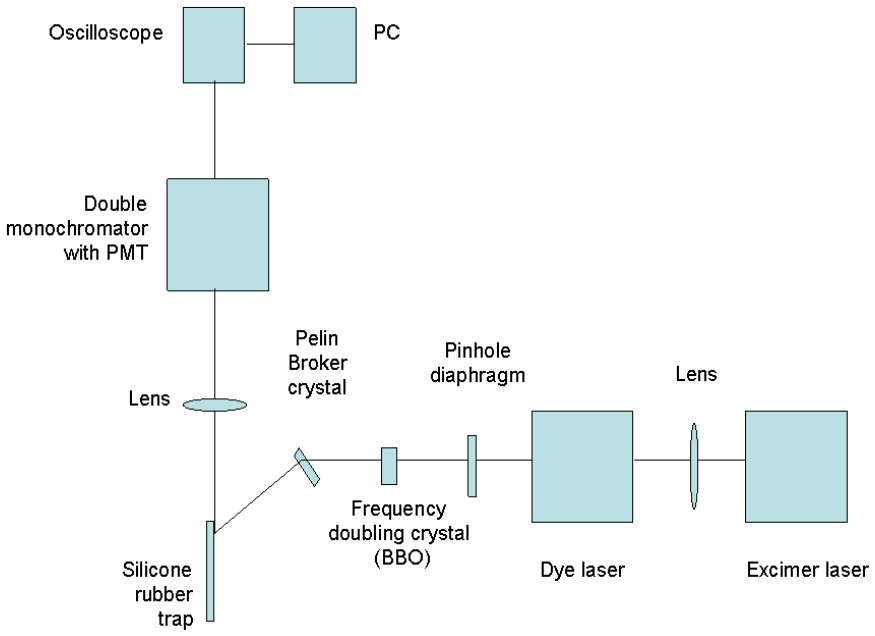

Figure 3.5: Final experimental setup for the dye laser system.

3.2.1.3 Results and discussion

The spectra obtained by liquid injection of standards onto the trap provided a first approximation of the detection limits of the method. These were in the order of 30 ng for both benzo(*a*)pyrene and naphthalene (for a signal-to-noise ratio of 3:1), as shown in Figures 3.6 and 3.7.

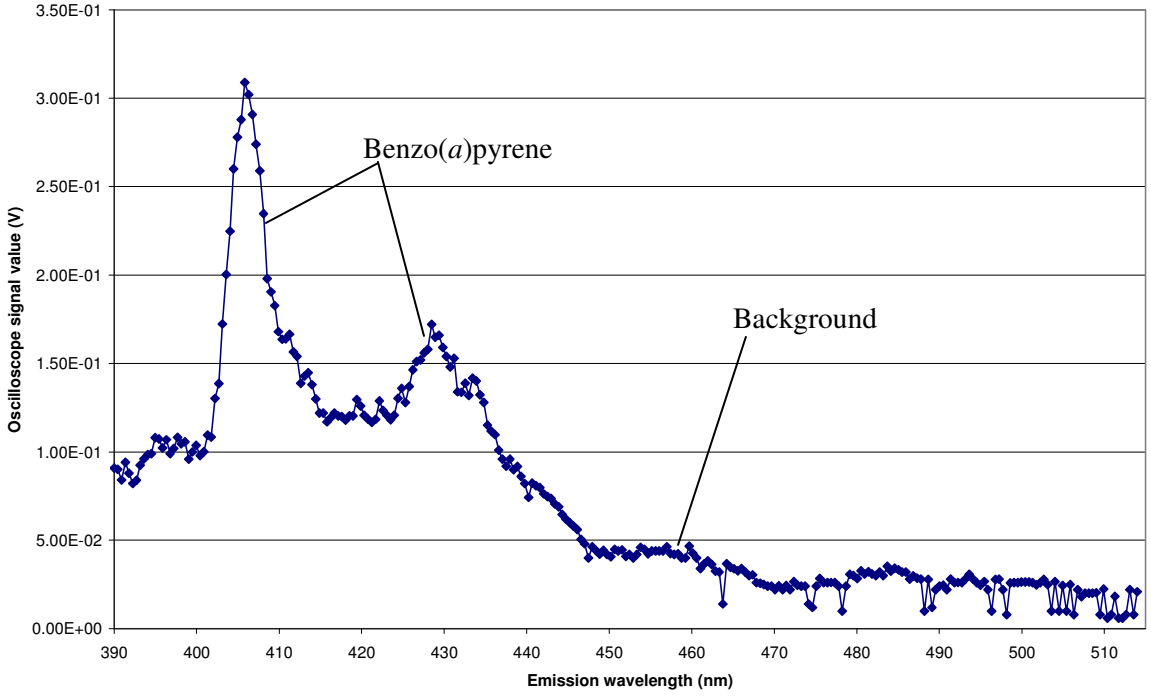

Figure 3.6: Fluorescence spectrum obtained for 27 ng of benzo(*a*)pyrene on a quartz multi-channel silicone rubber trap, with 302 nm excitation.

The well-documented fluorescence maximum of benzo(*a*)pyrene at 406 nm is clearly evident from Figure 3.6, which was obtained upon the injection of 1 μℓ of a liquid standard onto a silicone rubber trap.

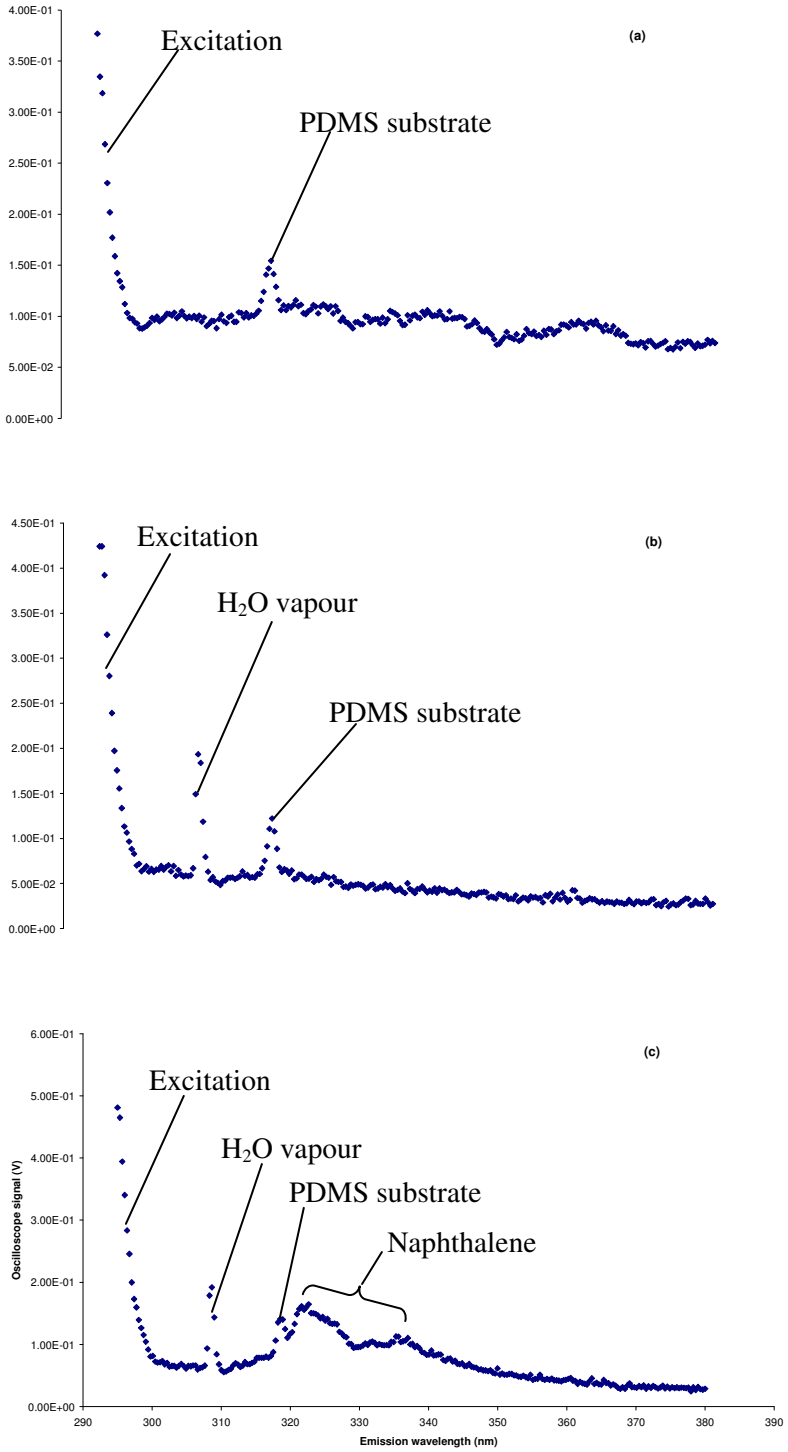

Figure 3.7: Fluorescence spectrum of (a) a blank quartz silicone rubber trap; (b) a quartz silicone rubber trap with laboratory air flowing through it at 580 mℓ.min^{-1}; and (c) a quartz silicone rubber trap containing 30 ng of naphthalene (added as a liquid standard). All spectra were obtained with the dye laser system operating at an excitation wavelength of 292 nm.

Similarly, 30 ng of naphthalene (injected onto a trap as 1 μℓ of liquid standard in toluene) was detected by means of excitation at 292 nm, with a characteristic emission around 323 nm evident (Figure 3.7). The signal-to-noise ratio was not as good as in the case of benzo(*a*)pyrene, possibly due to the smaller absorption cross-section of PAHs containing fewer aromatic rings. Volatilisation of naphthalene from the trap during analysis is also possible due to its lower vapour pressure, leading to sample loss.

The spectra of the blank trap and that of laboratory air flowing though the trap are included in Figure 3.7. It is evident from these that the peak at 319 nm most likely arose from the PDMS substrate, whilst that at 309 nm was due to humidity in the ambient laboratory air.

Experiments conducted with the introduction of naphthalene onto the trap in the gas phase via volatilization of liquid standard placed in a glass vessel upstream of the sample trap, whilst drawing air through the system at approximately 100 mℓ.min^{-1}, indicated that the solvent was not impacting significantly on the results.

3.2.1.4 Conclusion

These initial experiments indicated that this LIF method had potential for use as a screening tool for atmospheric PAH monitoring, and an approximate limit of detection of 30 ng was obtained for benzo(*a*)pyrene and naphthalene in this unoptimised system. It was also shown that the solvent did not have a significant impact on the fluorescence results when liquid PAH injections were performed. Due to the intended use of the method for atmospheric monitoring, however, a more accurate and quantitative means of achieving gas phase introduction of the PAHs was needed, and therefore naphthalene diffusion tubes were used in future experiments, as described in Chapter 2.

3.2.2 Repeatability of the method

3.2.2.1 Background

The repeatability of an analytical method is important to ensure that samples containing the same concentration of an analyte yield the same response from the detector, and that the

extent of any variation is quantified. In the case of the LIF method developed in this study, it was also important to determine the variation in detector signals obtained for different blank traps, as this has an impact on the detection limit of the method, which is covered in section 3.2.3. The effect of slight variations in loaded trap positioning in the LIF system was also explored.

3.2.2.2 Experimental method

a) *Diffusion tube loading repeatability: GC-MS experiment*

In order to determine the contribution of variations in diffusion tube loading of naphthalene to the amount detected by LIF in repeat experiments, TD-GC-MS analyses were first conducted on repeatedly loaded traps.

The silicone rubber traps were thermally desorbed using a thermal desorber system (TDS) (Gerstel TDS 3) and the desorbed naphthalene was cryogenically focused via a cooled injection system (CIS). The traps were desorbed from 0 °C (0.2 min) to 270 °C (2 min) at 120 °C.min^{-1} in the solvent vent mode (100 mℓ.min^{-1} until 0.1 min). Cryo-focusing of the PAHs was achieved using liquid nitrogen at -40 °C followed by rapid heating at 12 °C. s^{-1} to 300 °C (1 min). The GC-MS system was an Agilent GC 7890A coupled to a Hewlett Packard 5975 inert XL EI/CI mass selective detector (MSD). The GC inlet was in the split mode with helium (Ultra High Purity, Afrox) as the inlet gas. An Agilent HP5 (30 m x 250 µm x 0.25 µm) GC column was used and the column head pressure was 68.8 kPa using helium as the carrier gas. The total flow rate of the gas was 40.3 mℓ.min^{-1} for a split ratio of 30:1, where the split flow was 39 mℓ.min^{-1}, thus the flow rate through the column was 1.3 mℓ.min^{-1} at 40 °C. The GC oven was temperature programmed from 40 °C (1.5 min) at 20 °C.min^{-1} to 150 °C (0 min) and at 50 °C.min^{-1} to 300 °C (0 min). The GC-MS transfer line was at 300 °C, the mass scan range was 80-250 atomic mass units (amu), the solvent delay 6.8 minutes, and the electron multiplier voltage ~1070 V.

It should be noted that for the later analyses of traps containing other PAHs (such as pyrene and phenanthrene), this TD-GC-MS method was adjusted slightly in that the desorption was from 0 °C (0.2 min) to 270 °C (1.5 min) at 120 °C.min^{-1} in the solvent vent mode (100 mℓ.min^{-1} until 0.2 min). Cryo-focusing of the PAHs was achieved using liquid nitrogen

at -40 °C followed by rapid heating at 12 °C.s $^{-1}$ to 300 °C (10 min). The GC oven was temperature programmed from 40 °C (10.5 min) at 20 °C.min $^{-1}$ to 150 °C (0 min) and at 30 °C.min^{-1} to 300 °C (1 min).

After a blank TD-GC-MS analysis had been performed on a conditioned multi-channel silicone rubber trap, it was loaded with naphthalene from a diffusion tube (as discussed in Chapter 2) for a period of 5 minutes, at a flow rate of 493 mℓ.min^{-1}. The trap was then analysed by TD-GC-MS using a CIS split ratio of 30:1 with the TDS in solvent vent mode. The gas phase loading of naphthalene was repeated three times; and the experiment was then repeated three times with another trap.

After the first TD-GC-MS analysis of the gas phase loaded trap, it was analysed again which proved that no naphthalene remained on the trap after analysis (it was equivalent to a blank), thus a second desorption analysis was deemed unnecessary and was not repeated.

The GC-MS laboratory room air was also sampled onto a trap for 5 and 60 minutes, respectively, at 477 mℓ.min^{-1}, and laser laboratory room air was similarly sampled onto a clean trap for 85 min in order to verify that all the naphthalene present on loaded traps originated from the diffusion tube, as described in section 2.3 of Chapter 2.

b) *LIF experiments*

i) Variations in detector response to blank trap signals

Fluorescence spectra of seven blank multi-channel silicone rubber traps were recorded from 290 to 470 nm, with 292 nm excitation, and the energy of the incident beam at the trap location was measured by means of a Gentec energy meter. These experiments were conducted over two days, with one trap being analysed on both days for comparative purposes.

ii) Variations in detector response to similarly loaded traps

A conditioned multi-channel silicone rubber trap was loaded with naphthalene from a diffusion tube, by the method previously described, for a period of 5 minutes, at a flow rate of 484 mℓ.min^{-1}. The diffusion tube was disconnected from the trap, which was then positioned in the LIF excitation beam. The resulting fluorescence at 323 nm was recorded for 60 s. The

energy of the incident radiation was then measured at the trap location using a Gentec energy meter. This experiment was repeated with two other conditioned traps.

iii) Variations in detector response due to slight variations in positioning a loaded trap

A multi-channel silicone rubber trap, which had previously been loaded with naphthalene from a diffusion tube for 900 s prior to a photodegradation experiment (refer to section 3.2.4), was loaded again for 30 seconds, at a flow rate of 514 mℓ.min^{-1}. The diffusion tube was disconnected from the trap which was then positioned in the LIF excitation beam after the energy had been measured at the trap location using a Gentec energy meter. The oscilloscope signal was recorded at 323 nm for 60 s, and the trap was then removed from the laser beam (which continued to fire) for a period of approximately 60 s. The trap was then re-positioned in the laser beam and measurements were resumed for approximately 60 s. This process of measurement and re-positioning was repeated a number of times. The experiment was repeated using a different trap and with re-loading from the naphthalene diffusion tube during out-of-beam periods, in order to compensate for any volatilization or photodegradation losses.

3.2.2.3 Results and discussion

a) *Diffusion tube loading repeatability: GC-MS experiment*

The results of these experiments are presented in Table 3.7, from which the variability in diffusion tube loading of ~ 14 % was determined. This was deemed acceptable for the purposes of this study. As mentioned in section 2.3 of Chapter 2, the GC –MS laboratory air loading experiments yielded concentrations of < 1 ng naphthalene for 5 minute loading, and ~ 1 ng for 60 minute loading periods, whilst 10 ng of naphthalene was detected in the laser laboratory air sample. It was therefore deemed unnecessary to pre-clean laboratory air prior to its passage through the diffusion tube.

Table 3.7: TD-GC-MS results of repeated 5 minute diffusion tube loading of naphthalene onto two different traps.

Run #	Trap 1 (P1) Naphthalene peak area	Trap 2 (P4) Naphthalene peak area
1	1 689 582	1 519 977
2	1 584 184	1 773 389
3	1 317 746	1 345 629
Average	1 530 504	1 546 332
Standard deviation	191 642	215 094
% RSD	13	14

b) *LIF experiments*

i) Variations in detector response signals to blank traps

The fluorescence spectra of the blank traps are presented in Figure 3.8, and the repeat measurements of trap P11 are shown more clearly in Figure 3.9. The emission signal obtained at 323 nm for each trap is given in Table 3.8, as this is of interest with respect to naphthalene analyses (each oscilloscope reading is an average response over eight laser pulses).

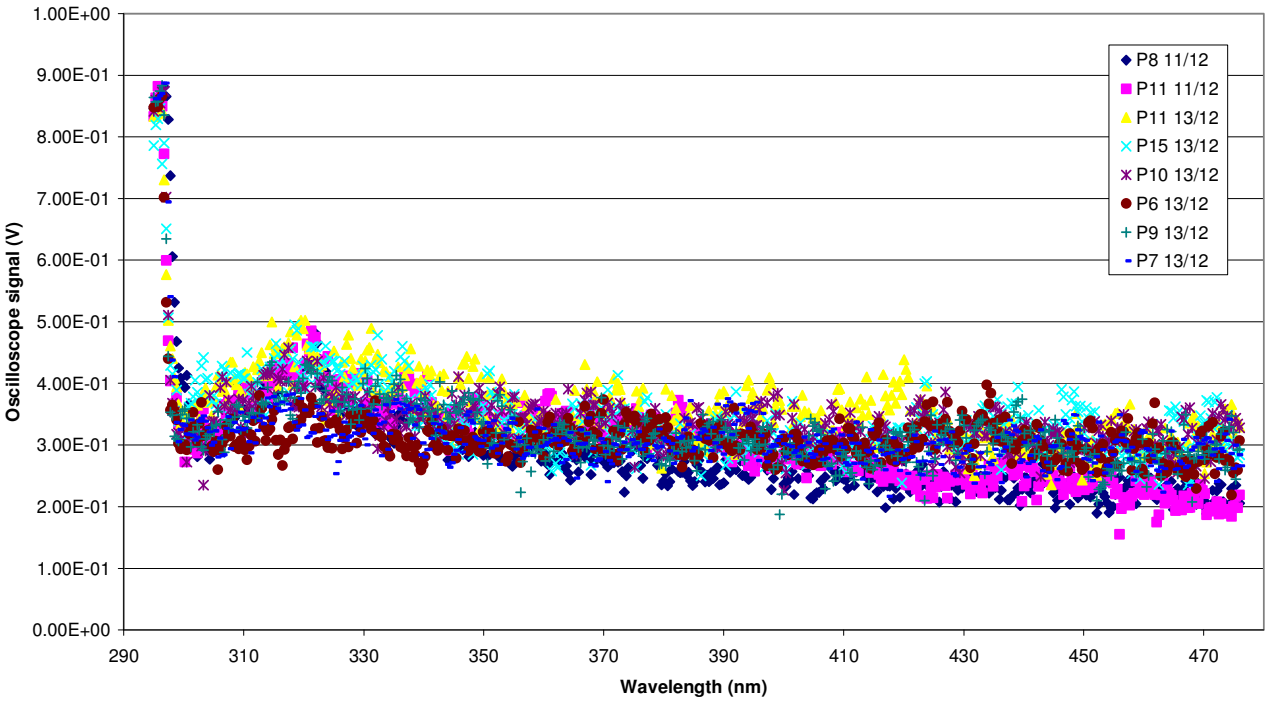

Figure 3.8: Blank trap fluorescence spectra for various traps with 292 nm excitation.

From the results in Table 3.8, it is evident that the variation in detector response was less than that of the incident laser energy (9.3 % RSD as compared to 14.7 %), which would indicate that the incident energy would dominate the variation in blank fluorescence signals more than the variations in fluorescence signals between traps.

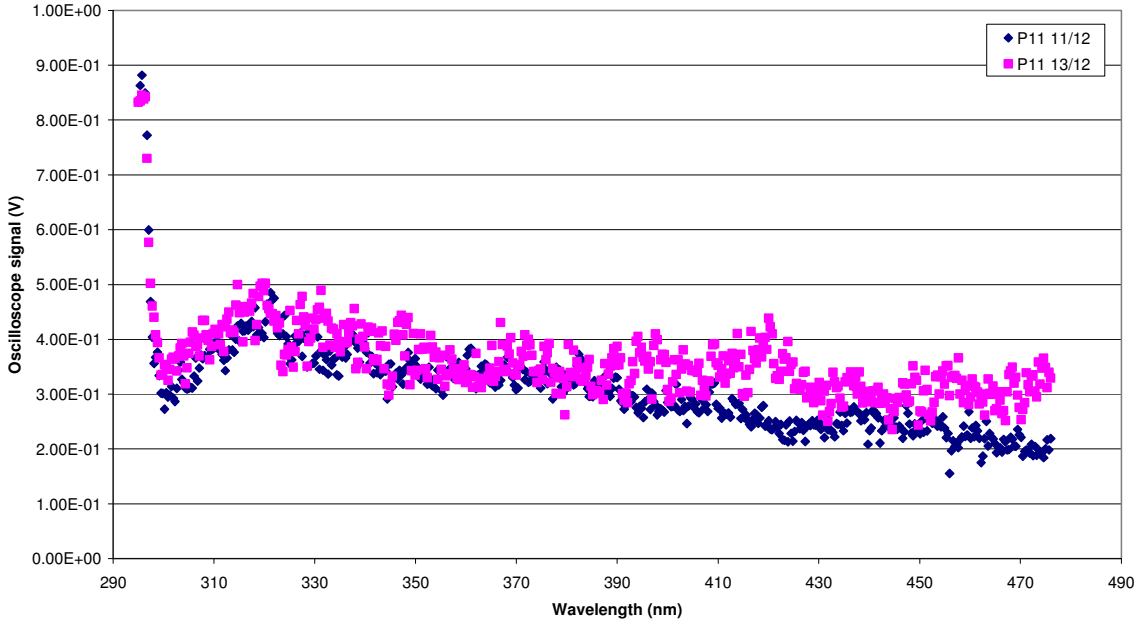

Figure 3.9: Comparison of the fluorescence spectra of blank trap P11, recorded on different days, with different laser incident energies.

Table 3.8: Variations in detector response at 323 nm for blank traps, with incident laser energies.

Trap	Oscilloscope signal at 323 nm (V)	Incident laser energy (µJ)
P8	0.395	576
P11	0.407	576
P11	0.430	657
P15	0.433	851
P10	0.361	678
P6	0.346	624
P9	0.373	622
P7	0.342	554
Average	**0.386**	**642**
Standard deviation	**0.036**	**94.4**
% RSD	**9.3**	**14.7**

ii) Variations in detector response to similarly loaded traps

It was evident that the incident laser energy decreased during the experiment, which impacted on the oscilloscope signal for the three sets of results, as shown in Figure 3.10 and Table 3.9, although the % RSD in the oscilloscope results was less than that of the incident energy. The second trap was loaded for 15 s longer than the other two traps, hence slightly more naphthalene was loaded in this case at a diffusion rate of 1.88 ng.s^{-1}, as indicated in Table 3.9. The top 5 mm portion of each trap, which was analysed in these LIF experiments, would most likely have been loaded to equilibrium conditions, as determined in later experiments.

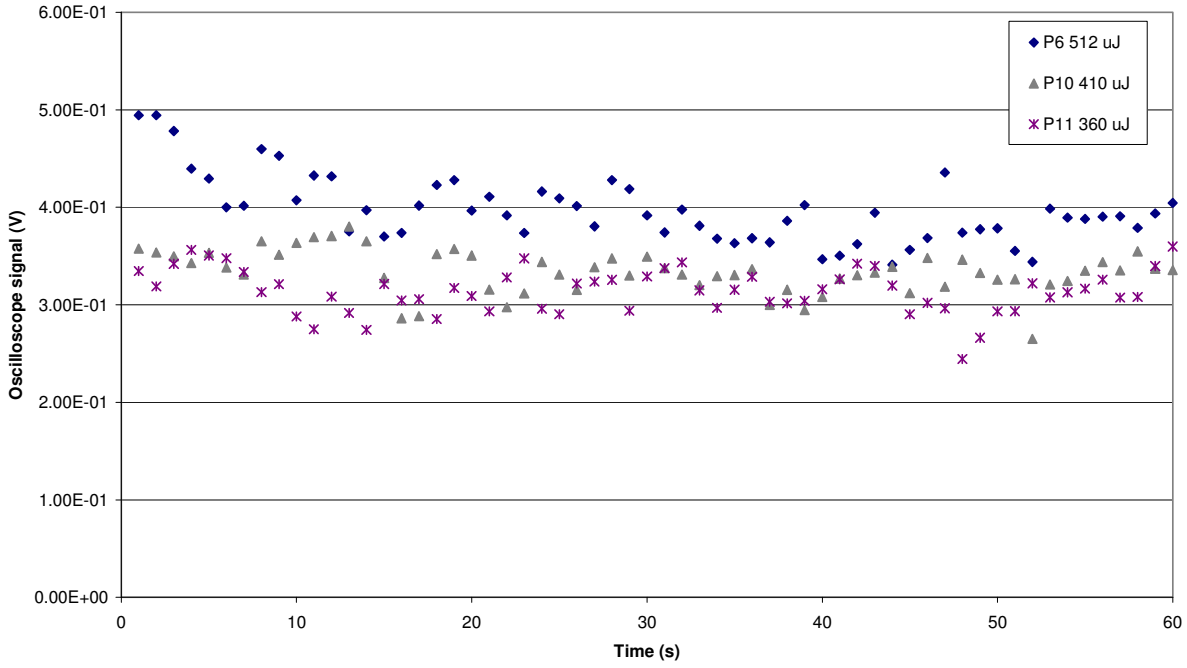

Figure 3.10: Naphthalene fluorescence signal at 323 nm after diffusion tube loading onto three different traps in the same manner.

Table 3.9: Average oscilloscope signals over 60 s for naphthalene loaded onto different multi-channel silicone rubber traps.

Sample number	Incident energy (µJ)	Naphthalene loading (ng)	Average oscilloscope signal (V)
1	512	564	0.397
2	410	592	0.334
3	360	564	0.314
Overall average	**427**	**573**	**0.348**
Overall standard deviation	**77.5**	**16.2**	**0.043**
Overall % RSD	**18.1**	**2.8**	**12.4**

It would appear that variations between different traps as well as variations in loading are small in comparison to the variations in oscilloscope response brought about by changes in the laser incident energy. Incident energy considerations were therefore investigated in more detail under section 3.2.5.

iii) Variations in detector response due to slight variations in positioning a loaded trap

The results of these experiments are presented in Figures 3.11 and 3.12. In the first experiment, where no re-loading was performed during the experiment, the in-beam detector signal varied less (4.5 % RSD) than in the second experiment (13.5 % RSD), although the energy varied less in the second experiment (2.9 % RSD as compared to 14.8 % RSD in the first experiment).

The increase in oscilloscope signal over time in the second experiment (even with a decrease in incident energy) could have been as a consequence of the trap not having reached equilibrium loading conditions at the start of the experiment, thus additional (and not just replacement) naphthalene was loaded during the re-loading periods, which resulted in an elevated detector response.

The slight decrease in oscilloscope signal towards the end of the first experiment would most likely have arisen from volatilization and photodegradation losses of naphthalene

from the trap. The decrease in incident energy would also have contributed to the lower oscilloscope signal.

Slight variations in the positioning of the trap therefore did not appear to result in significant variations in the oscilloscope signal when the analyte was evenly distributed over the silicone surfaces.

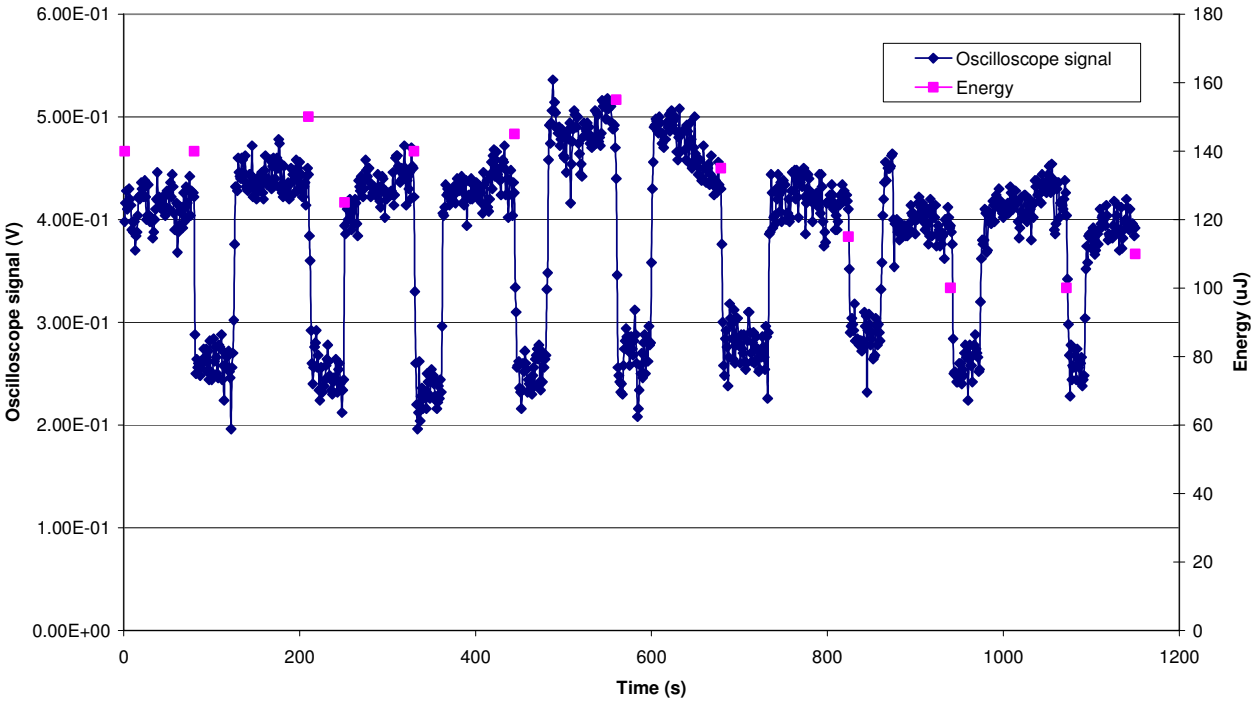

Figure 3.11: Naphthalene repeatability experiment to determine the effect of slight variations in trap positioning, showing consecutive in- and out-of-beam periods. Oscilloscope signal measured at 323 nm. No re-loading of the trap during out-of-beam periods was performed.

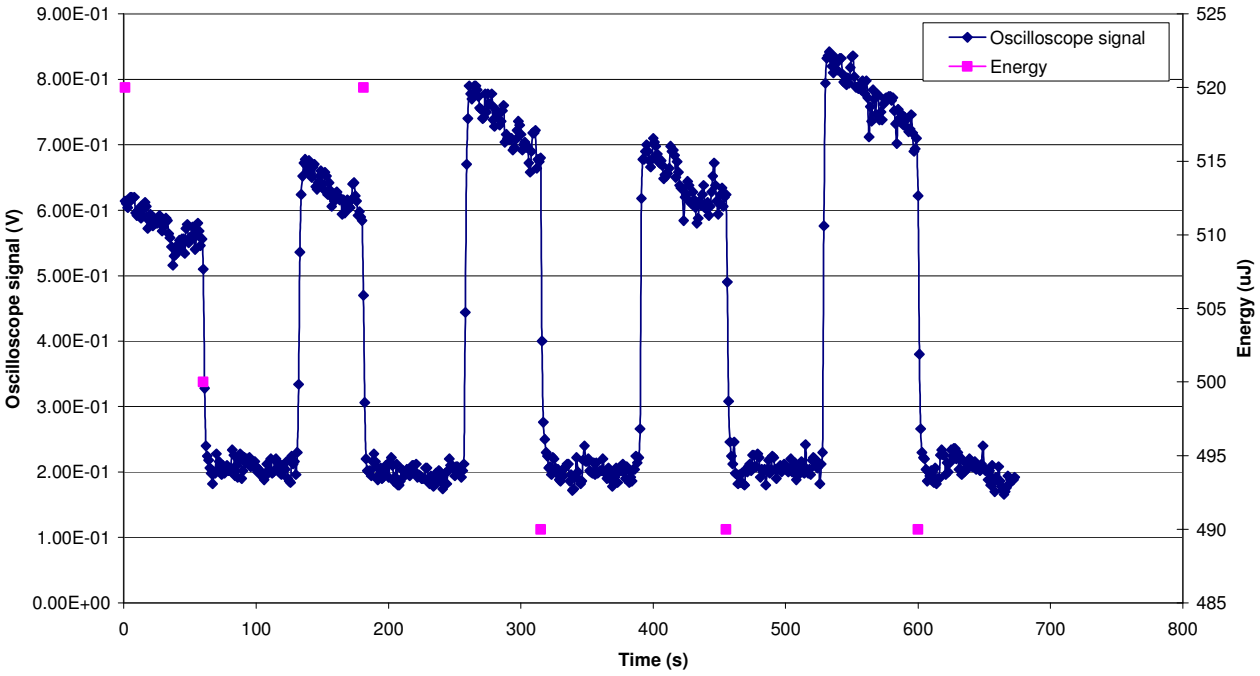

Figure 3.12: Second naphthalene repeatability experiment to determine the effect of slight variations in trap positioning, showing consecutive in- and out-of-beam periods. The trap was re-loaded with naphthalene from the diffusion tube during out-of-beam periods. Oscilloscope signal measured at 323 nm.

3.2.2.4 Conclusion

From these experiments it would appear that the incident laser energy had the most impact on the detector response, and that variations in blank trap fluorescence, detector response to similarly loaded traps (and differences in this loading), as well as slight variations in trap positioning, were of minor importance in this experimental setup. The effect of variations in incident laser energy was therefore investigated in more detail, as discussed under section 3.2.5. Even with fluctuations in incident energy, the % RSD of the oscilloscope response did not exceed 15 % in these experiments, which was deemed acceptable for a screening method.

3.2.3 Sensitivity of the method

3.2.3.1 Background

In order for a monitoring method to find practical application, it is important that it is sufficiently sensitive to enable detection of the relevant analyte(s) at application specific levels. The levels at which environmental effects occur, primarily human health effects, are also important considerations, as the limit of detection (or quantitation) of a monitoring method should be below any legislated limits of these pollutants. Depending on the application, occupational exposure limits, industrial emission limits, or maximum permissible ambient air concentrations may have relevance.

In terms of occupational exposure, the United States National Institute for Occupational Safety and Health (NIOSH) has set a recommended occupational exposure limit, based on a time-weighted average for a 10-hour workday within a 40-hour workweek, of 0.1 $mg.m^{-3}$ for PAHs arising from coal tar products. The American Conference of Governmental Industrial Hygienists (ACGIH) recommends an occupational exposure limit of 0.2 $mg.m^{-3}$ for coal tar products (based on an 8-hour day and 40-hour workweek) and the Occupational Safety and Health Administration (OSHA) has legally enforced this limit over an 8-hour exposure period (ATSDR, 1995).

Concentrations of PAHs in ambient air are presented in Table 3.2, however, concentrations in air near sources of PAHs are expected to be higher than general ambient levels.

The OSHA, ACGIH and NIOSH occupational exposure limit for naphthalene is 10 ppm (50 $mg.m^{-3}$) over an 8-hour workday, and 15 ppm (75 $mg.m^{-3}$) for short term exposures (ATSDR, 2005). In addition, NIOSH have an Immediately Dangerous to Life and Health (IDLH) limit for naphthalene of 250 ppm (1250 $mg.m^{-3}$).

Phenanthrene and pyrene both have OSHA exposure limits of 0.2 $mg.m^{-3}$ (NIOSH, Method 5506, 1998). In our study we investigated whether these PAHs could also be detected using the 292 nm excitation wavelength, which is optimal for naphthalene, in order to simplify the proposed method without losing a significant amount of selectivity.

The low breakthrough volume of the more volatile PAHs, particularly naphthalene, with the multi-channel silicone rubber traps hinders significant pre-concentration of these analytes, which thus necessitates low analytical detection limits, or else precludes the monitoring of low concentrations of these analytes. Fortunately the more volatile species are usually emitted from sources at higher concentrations than the less volatile PAHs, as previously discussed. The breakthrough volume for naphthalene was determined in this study by means of both a GC-MS and a LIF-based method, in order to assess V_B for the traps used in this study, which were of a different configuration to those used for previous V_B determinations, where a value of ~500 cm^3 was found (Ortner, 1994).

The minimum detectable concentrations of the atmospheric analytes of interest are also limited by the instrument or method detection limit (LIF), the variability in blank values, and by the sample volume (Rosenberg et al., 1988).

The LIF method presented here is for use as a screening tool for PAHs near possible source emissions, thus comparisons of limits of detection to concentrations in impacted environments is appropriate. Comparisons are therefore made to occupational exposure limits rather than ambient background levels, for which there are no South African limit values.

In terms of the limits of detection (LOD) and limits of quantitation (LOQ) of PAH methods, the NIOSH method 5506 provides a useful comparison. This method is used to analyse atmospheric PAH samples which have been adsorbed onto XAD-2, and is based on the detection of the PAHs by HPLC either with fluorescence (fluoranthene and pyrene with 340 nm excitation and 425 nm emission) or UV detection (naphthalene and phenanthrene at 254 nm). LODs and LOQs of method 5506 for the PAHs of interest in our study are presented in Table 3.10.

Table 3.10: NIOSH method 5506, LOD and LOQ values for PAHs (NIOSH, 1998).

PAH	LOD (µg per sample)	LOQ (µg per sample)
Naph	0.20 – 0.80	0.39 – 2.6
PhA	0.0070 – 0.060	0.023 – 0.19
FlA	0.0020 – 0.090	0.0066 – 0.30
Py	0.0010 – 0.30	0.0036 – 0.99

3.2.3.2 Experimental method

a) Analytical detection limits

i) Background signal

This parameter has been covered under section 3.2.2, although these experiments also have relevance to the determination of the analytical detection limits of our method.

ii) LIF derived limit of detection

A silicone rubber trap was positioned in the laser system, as described under section 3.2.1, and it was then loaded with naphthalene from a diffusion tube (as discussed in Chapter 2) at a flow rate of 486 mℓ.min^{-1}, until equilibrium had been reached (at 50 seconds) at the sample spot (the entrance end of the silicone tubes). Irradiation was at 292 nm, and the fluorescence was recorded at 323 nm via the PC linked to the oscilloscope.

b) Breakthrough volume

i) LIF experiments

Two multi-channel silicone rubber traps were placed in series (primary and secondary or backup trap). A portable Gilair pump was used to draw air at 387 mℓ.min^{-1} through the naphthalene diffusion tube and then through the two traps. The excitation beam (at 292 nm) was focused on the inlet side of the secondary trap (5 mm spot size), and fluorescence emission from the secondary trap was collected by the monochromator at 323 nm for detection purposes. The experimental setup is shown in Figure 3.13. After 900 s, the pump was

switched off, and an emission spectrum was obtained of the secondary trap. The trap side of the experimental setup was then dismantled and an emission spectrum was obtained of the primary trap. Both traps were then capped and refrigerated prior to analysis by TD-GC-MS (standards: 30, 50, 100 and 200 ng).

This experiment was repeated using a diffusion tube loading flow rate of 480 mℓ.min^{-1}, and loading was conducted for 1 hour (incident laser energy = 180 μJ). LIF scans were then recorded for both traps, and the profile of naphthalene loading through the primary trap was investigated by recording LIF scans along the length of the trap. 50, 100, 200 and 500 ng TD-GC-MS standards were used.

In a third experiment, diffusion tube loading was conducted for 2 hours at a flow rate of 495 mℓ.min^{-1}. 50, 250, 500 and 2000 ng TD-GC-MS standards were used.

The impact of flow rate on the breakthrough volume profile was then investigated by conducting similar experiments at flow rates of 1276 mℓ.min^{-1} and 200 mℓ.min^{-1}.

ii) TD-GC-MS experiments

In order to determine the breakthrough volume of naphthalene on the traps by TD-GC-MS a series of experiments was conducted. A trap was loaded with naphthalene from a diffusion tube (as discussed in Chapter 2) for a period of 5 minutes, at a flow rate of ~475 mℓ.min^{-1}. The trap was then analysed by TD-GC-MS using a suitable CIS split ratio (refer to Table 3.11) with the TDS in solvent vent mode. The instrument was calibrated by injection of liquid standards in toluene onto traps (100, 200 and 300 ng of naphthalene ranging from 1 to 6 μℓ), followed by TD-GC-MS analysis. The experiment was repeated with another trap, as well as for increased loading times up to 60 minutes, at 10 minute intervals.

Figure 3.13: Experimental setup for the LIF breakthrough experiments. The naphthalene diffusion tube is mounted on two multi-channel silicone rubber traps in series, which are connected to a portable sampling pump. The monochromator is shown in the background.

This experiment was again repeated in order to determine naphthalene TD-GC-MS peak areas for lower sampling volumes ranging from 500 to 4933 mℓ with a sampling flow rate of 370 mℓ.min^{-1} (the CIS split ratio used ranged from 100:1 to 400:1).

In another series of experiments, a trap was loaded with naphthalene from a diffusion tube for 5 min at increasing flow rates from 492 to 775 mℓ.min^{-1}. Experiments were also repeated using another trap for comparison.

c) Excitation of other PAHs of interest utilizing 292 nm excitation

i) Pyrene

Three multi-channel silicone rubber traps were loaded with pyrene by means of the gas chromatographic fraction collection method described in Chapter 2. Correction was made to the concentration of PAH injected into the GC system, based on the average recoveries obtained with the optimized method so that the final amount of pyrene on each trap was ~100, 150 and 200 ng, respectively. After loading, the traps were end-capped, wrapped in aluminium foil and refrigerated prior to use.

LIF analysis of each loaded trap was performed in the same manner as for naphthalene, with 292 nm incident radiation focused as a spot on the top of the trap. The fluorescence spectrum was recorded from 295 – 465 nm. The traps were then end-capped, wrapped in aluminium foil and refrigerated prior to TD-GC-MS analysis, using the method described under section 3.2.2.2, with injection of 1 μℓ of 100 and 200 ng standards onto multi-channel silicone rubber traps for calibration purposes.

ii) Phenanthrene

Three multi-channel silicone rubber traps containing ~100, 150 and 200 ng phenanthrene respectively, were prepared and analysed in the same manner as for pyrene. In this case, the fluorescence scan was recorded from 295 – 480 nm.

3.2.3.3 Results and discussion

a) Analytical detection limits

i) Background signal

The analytical detection limit has been defined as 3x the standard deviation of repeated 100 μℓ, 1 μg.mℓ$^{-1}$ standard injections (which equates to 100 ng loading) by Rosenberg et al. (1988), whilst blank tube values were defined as the mean value of 10 determinations. For this LIF method, the average blank trap detector response at 323 nm with 292 nm excitation irradiation was found to be 0.386V (n = 8) (refer to Table 3.8).

ii) LIF derived limit of detection

Figure 3.14 shows the 323 nm fluorescence emission which was recorded over a period of time as naphthalene was drawn into the short trap from the diffusion tube (diffusion rate ~2 ng.s^{-1}). A mass detection limit of ~20 ng can be calculated using a signal:noise ratio of 3:1, and equilibrium conditions were obtained for the analysed sample spot within ~16 s (each data point is an average over 8 laser pulses).

The noise (0.001 V) was calculated from the root mean square (RMS) value of the data points post equilibrium, as there were statistically insufficient data points in the region prior to the signal increase, and it was found that the RMS values were in fact the same for both regions. The voltage at equilibrium averaged 0.873 V, thus the signal:noise ratio was 873:1 for a diffusion rate of ~2 ng.s^{-1} and operation at ~500 mℓ.min^{-1}. For a signal:noise ratio of 3:1, a diffusion rate of ~7 pg.s^{-1} at this flow rate could therefore be used, which equates to a limit of detection of ~1 µg.m^{-3}, which is suitable for impacted environments, including workplace exposure.

b) Breakthrough volume

i) LIF experiments

No increase in emission signal at 323 nm was observed on the secondary trap throughout the 900 s loading period, as shown in Figure 3.15, thus the quantity of naphthalene present in the irradiated portion of the trap was below the LOD of the method, which was confirmed by the emission spectrum for this trap which did not differ from that of the blank trap at the wavelength of interest (Figure 3.16). A significant emission was found on the primary trap, however, indicating extensive loading of naphthalene.

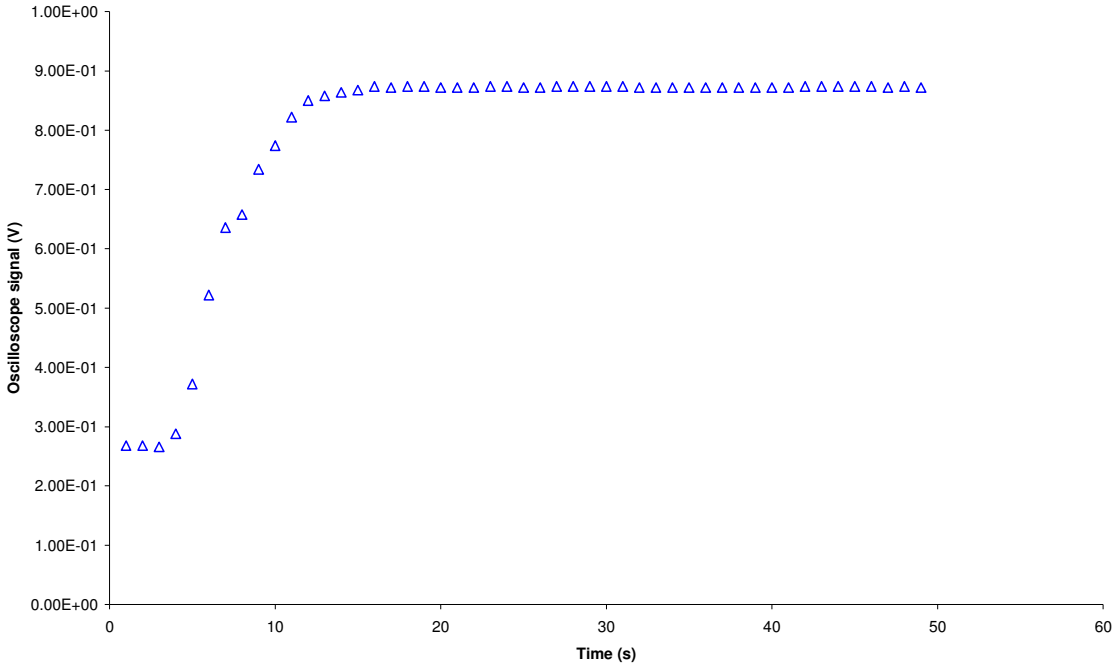

Figure 3.14: Fluorescence signal at 323 nm (naphthalene emission) obtained with 292 nm excitation as a function of time at a sample spot at the entrance of the trap. Loading of naphthalene vapour was from a diffusion tube onto a short trap.

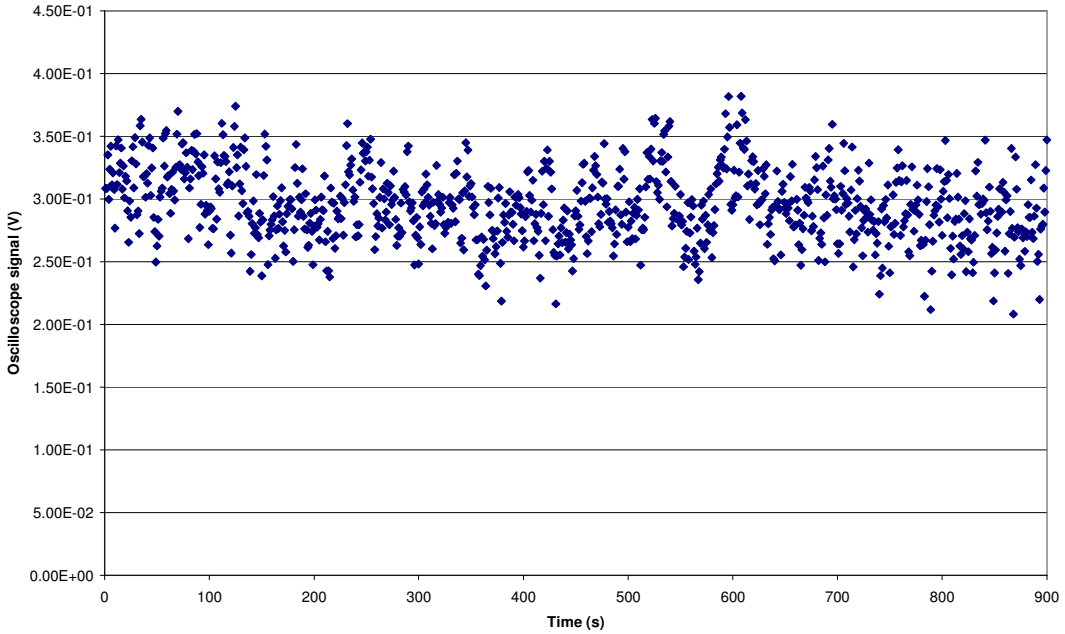

Figure 3.15: Secondary trap fluorescence at 323 nm during the loading phase of a breakthrough experiment for naphthalene, using a diffusion tube (900 s at 387 mℓ.min^{-1}).

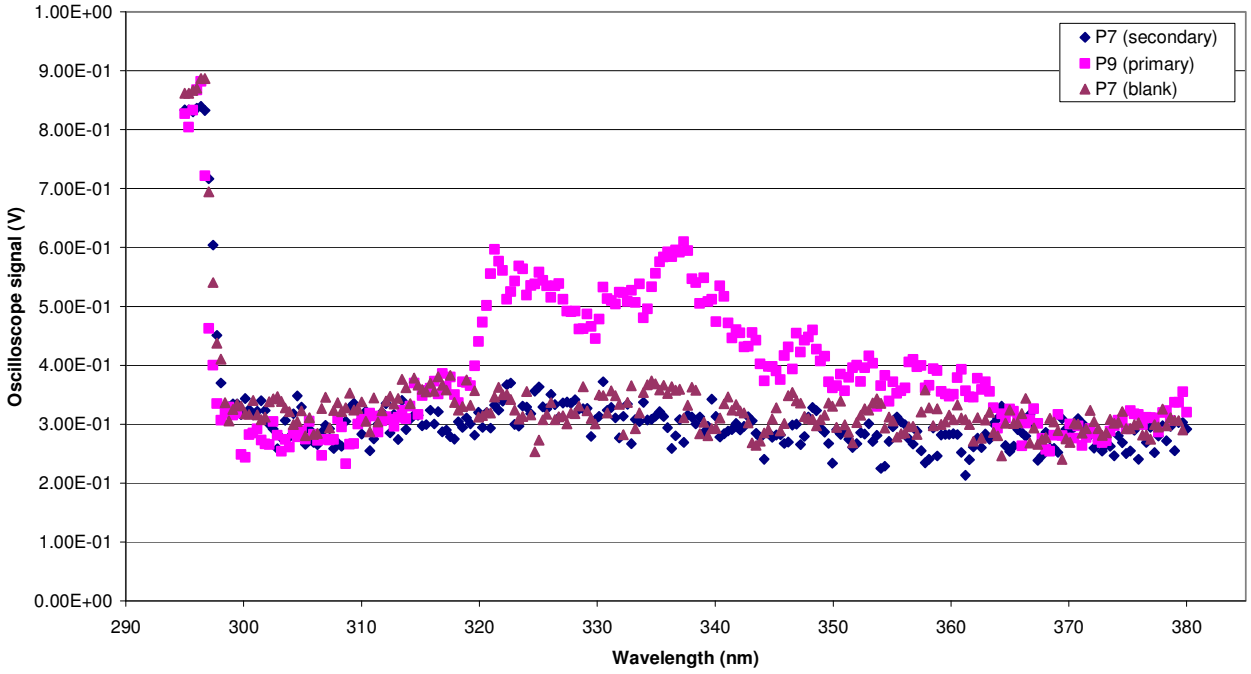

Figure 3.16: Primary, secondary and blank trap spectra obtained after a breakthrough loading experiment using a naphthalene diffusion tube and 292 nm excitation (900 s loading at 387 mℓ.min^{-1}).

Subsequent TD-GC-MS analysis of the two traps indicated that the primary trap contained >300 ng of naphthalene, whilst the secondary trap contained ~200 ng (using a calibration curve of y = 6.262 x 10^3x with r^2 = 0.995). These results are semi-quantitative, as the samples were over the calibration range.

As the silicone rubber portion of the trap was 55 mm long, and the irradiated area was 5 mm in length, the trap may be considered as containing 11 sections or plates. For the primary trap, this would relate to ~27 ng of naphthalene per plate, which is above the LOD of ~20 ng, whilst the secondary trap would contain ~18 ng per plate, which is below the LOD, thus there was no detectable increase in LIF signal.

The trap contained ~300 ng naphthalene when equilibrium conditions had been established at a diffusion tube loading rate of 1.88 ng.s^{-1} (ie, breakthrough sampling conditions

had been established). Equilibrium conditions were reached in the first plate after loading of ~27 ng of naphthalene. This would occur after ~14.5 s at a diffusion rate of 1.88 $ng.s^{-1}$, which compares well to that determined during the LIF limit of detection experiment reported under portion (a) of this section (equilibrium after ~16 s).

Similar results were obtained for the hour long loading experiment, in that no increase in fluorescence intensity at 323 nm at the top of the second trap was evident, although a significant decrease in incident energy occurred during the course of the experiment (the energy decreased from 180 μJ at the start of the experiment to 25 μJ at the end).

A low concentration of naphthalene was found on the secondary trap by TD-GC-MS analysis (75 ng) post LIF, which would relate to < 7 ng of naphthalene on the top spot of the trap (using a calibration curve of $y = 1.852 \times 10^{3}x$ with $r^2 = 0.986$, a 10:1 CIS split was used in the case of the secondary trap, whilst a 100:1 split was used for the standards and primary trap). This accounts for the lack of detection by the LIF method. The primary trap was found to contain 6 794 ng of naphthalene by TD-GC-MS and its distribution through the trap is shown in Figure 3.17. A slight decrease in naphthalene concentration is evident through the trap upon comparison of the oscilloscope signals at 323 nm. The total mass of naphthalene found on both traps by TD-GC-MS would relate to a diffusion rate of 1.9 $ng.s^{-1}$, which agrees with the experimentally derived diffusion rate (refer to Chapter 2).

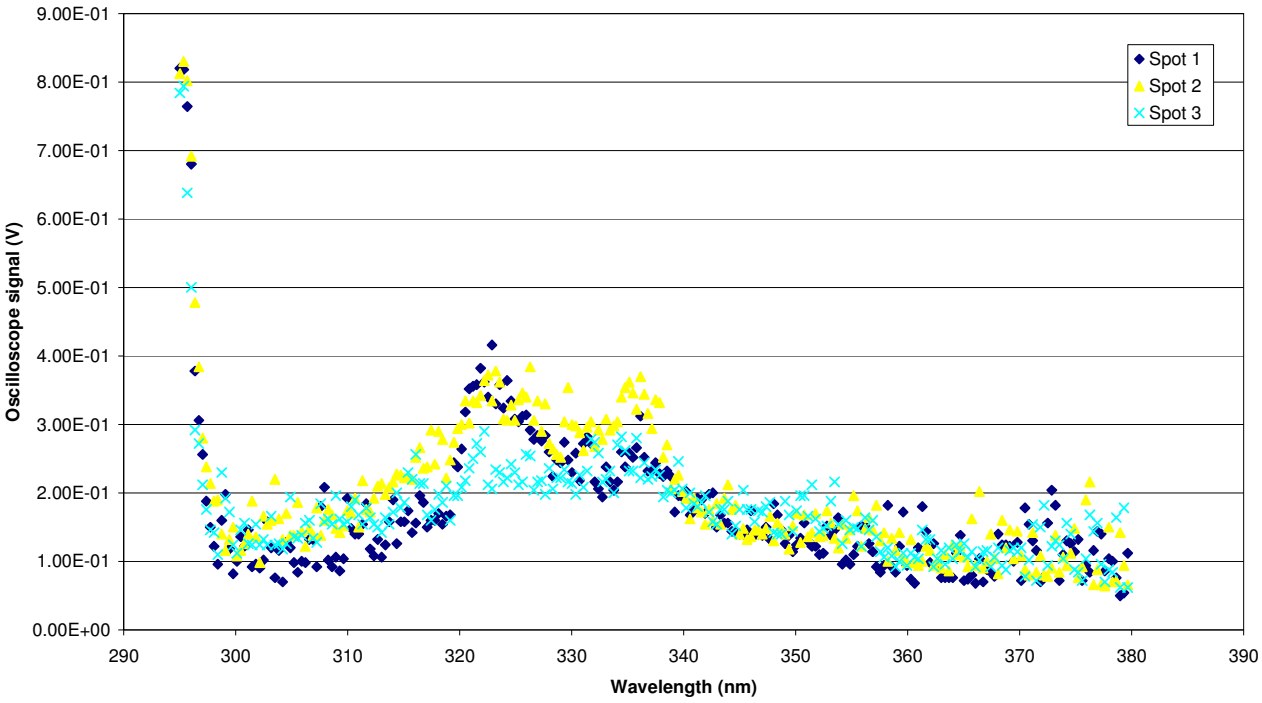

Figure 3.17: LIF scans of the primary trap after 1 h naphthalene diffusion tube loading at 480 mℓ.min^{-1}, where spot 1 is at the top of the trap and spots 2 and 3 are below this.

The naphthalene TD-GC-MS results for the 2 h loading experiment were 9 507 ng for the primary trap and 9 245 ng for the secondary trap, which indicates that the secondary trap had also nearly reached equilibrium conditions (using a naphthalene m/z 127 calibration curve of y = 5.02 x 10^2x with r^2 = 0.998, as the naphthalene m/z 128 results were over range). The LIF scans of the primary and secondary traps post loading also indicated similar naphthalene concentrations (emission at 323 nm, refer to Figure 3.18). A total of 14 400 ng of naphthalene was expected on the traps, using a diffusion rate of 2 ng.s^{-1}, which is lower than the total concentration obtained by TD-GC-MS (18 752 ng, which would relate to a diffusion rate of 2.6 ng.s^{-1}). This may have been due to a higher diffusion rate, variations in the pump flow rate, or as a result of the utilization of liquid standards for TD-GC-MS calibration purposes.

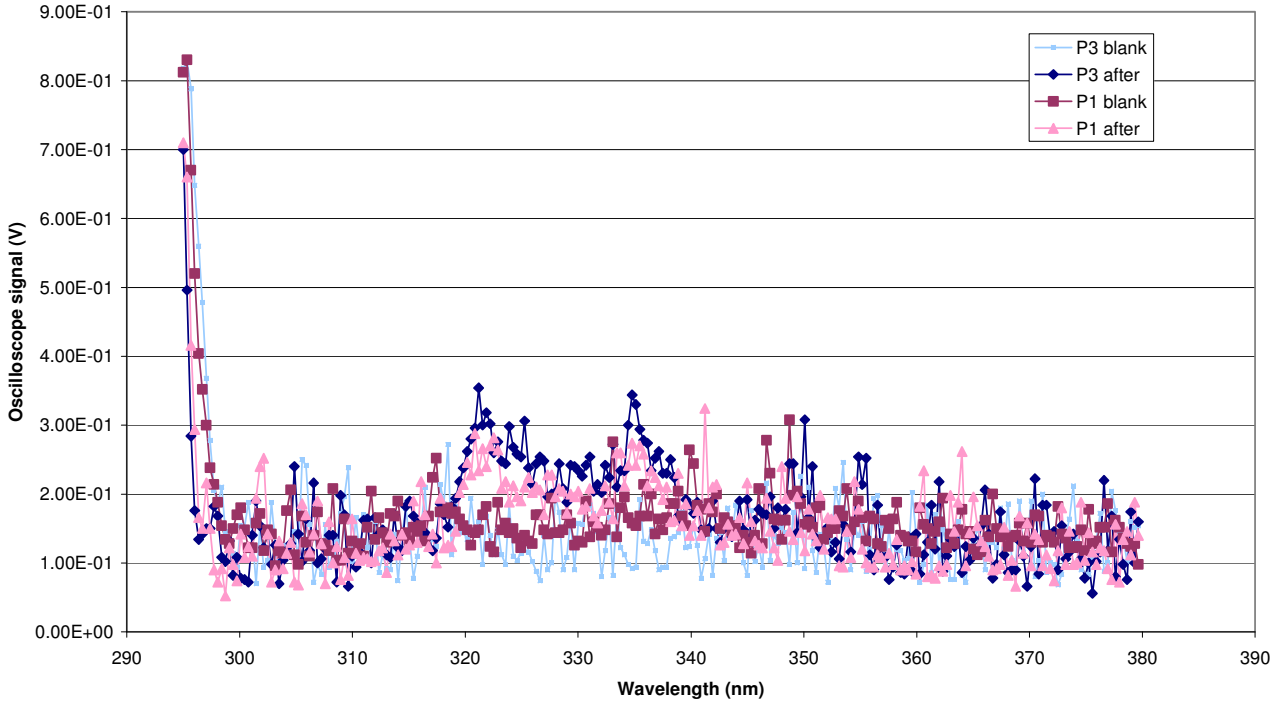

Figure 3.18: LIF scans, showing similar concentrations of naphthalene in the primary (P1) and secondary (P3) traps after 2 hours of diffusion tube loading at 495 mℓ.min^{-1}.

The fluorescence emission at 323 nm of a spot at the top of the secondary trap obtained during diffusion tube loading over 2 hours is shown in Figure 3.19. 59 ℓ of air was drawn through the system of traps during this experiment. The incident energy decreased from 100 µJ to 30 µJ over the 2 hour period, and the excimer laser tripped after ~30 minutes and had to be re-started.

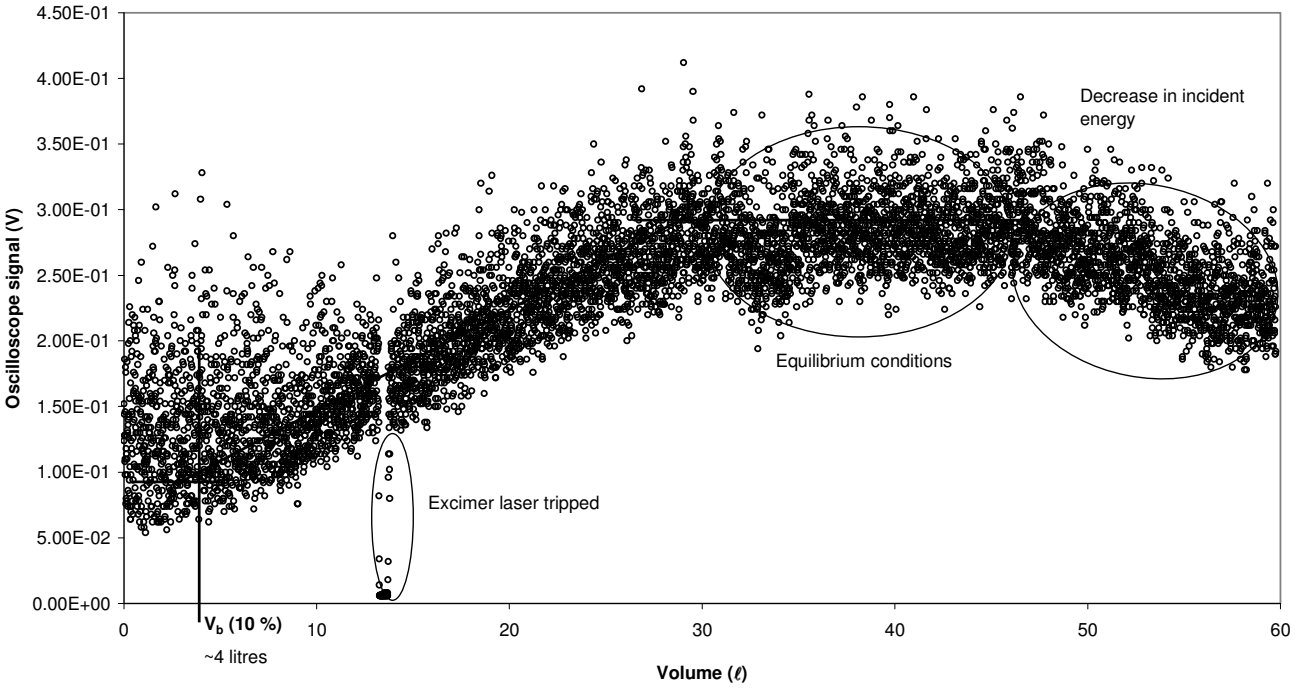

Figure 3.19: Fluorescence at 323 nm of the top portion of the secondary trap during 2 hour naphthalene diffusion tube loading at 495 mℓ.min^{-1}.

A breakthrough volume of ~4 ℓ was estimated for 10 % breakthrough of naphthalene, which relates to a sampling interval of ~8 min at 500 mℓ.min^{-1}. The GC-MS can detect 1 pg with a signal to noise ratio of 400:1 in total ion current (TIC) chromatogram mode, according to the instrument specifications, which would equate to a detection limit of ~0.3 ng.m^{-3} for this breakthrough volume. The breakthrough volume for naphthalene determined in our experiments is significantly higher than that reported previously (0.5 ℓ, Ortner, 1994), which is feasible as the traps used in our study contained twenty two, 55 mm long channels, whilst those used previously contained eight, 105 mm long channels and the PDMS was obtained from different suppliers. The flow rates used also differed, in that Ortner utilized a much lower flow rate of 14 mℓ.min^{-1}.

The loading profile at the top of the secondary trap obtained at a flow rate of 1276 mℓ.min^{-1} is shown in Figure 3.20. It is evident that the excimer laser did not perform well during this experiment, as it tripped twice and the energy dropped from 470 to 348 μJ over the 53 min experiment. In addition there was significant noise in the measurements. A breakthrough volume of ~500 mℓ was roughly estimated from the profile, based on the volume at which the initial fluorescence signal (~0.076 V) had increased by 10 % of the difference between the maximum fluorescence signal (~0.140 V) and the initial fluorescence signal. The diffusion rate may not have been constant over the course of the experiment, as turbulent conditions are expected in the naphthalene diffusion tube at this elevated flow rate. This was tested by varying the flow rate through the diffusion tube holder from ~500 mℓ.min^{-1} to ~700 mℓ.min^{-1} in a separate series of experiments, and it was found upon TD-GC-MS analysis of each of the traps thus loaded for 5 min, that the naphthalene diffusion rate had increased for flow rates > 500 mℓ.min^{-1}.

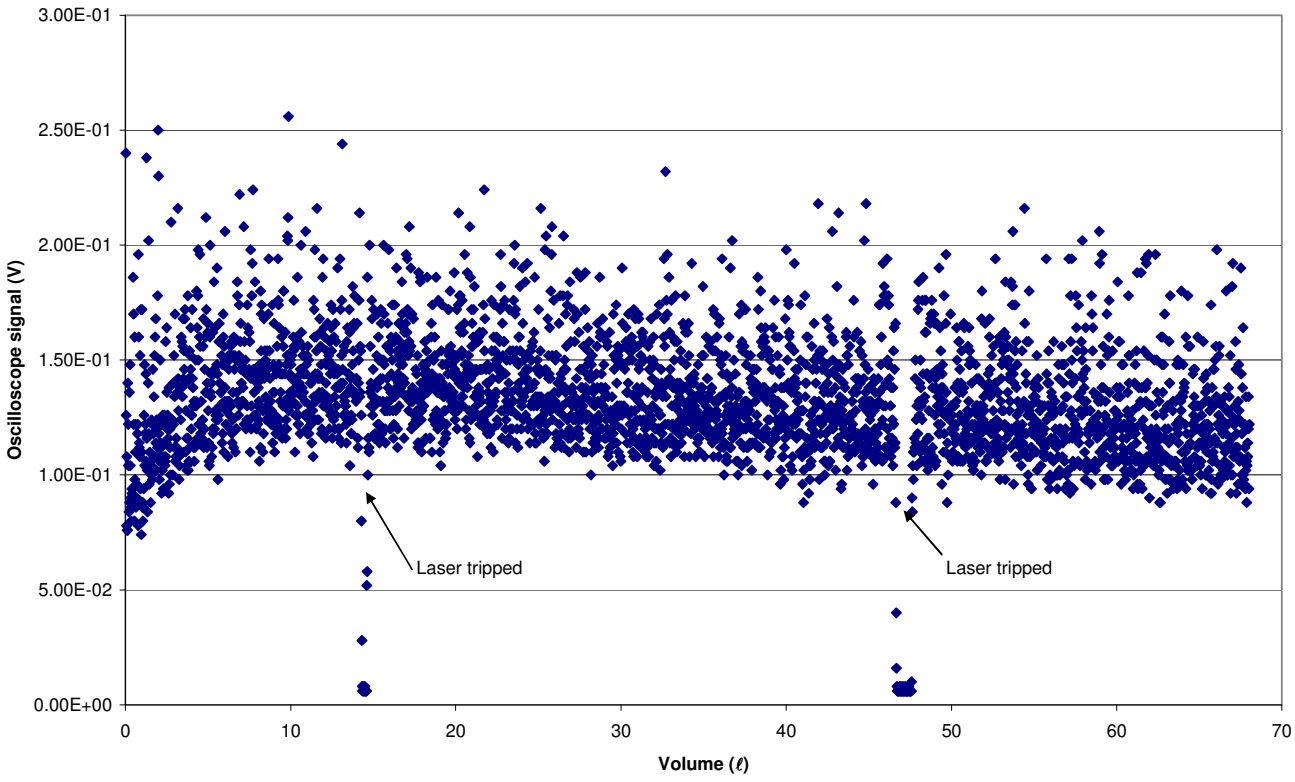

Figure 3:20: Loading profile at the top of the secondary trap with diffusion tube loading at 1276 mℓ.min^{-1} for 53 min (fluorescence at 323 nm).

The experiment at 200 mℓ.min^{-1} was unsuccessful, as the laser energy dropped significantly (to ~100 μJ), therefore an increase in fluorescence signal at the top of the secondary trap was not evident over the 1.5 h duration of the experiment. It was not possible to repeat this low flow rate experiment, as the laser was too unstable over the long time interval required.

ii) TD-GC-MS experiments

The results of the experiment involving variations in diffusion tube loading times are presented in Table 3.11 and Figure 3.21 (TD-GC-MS results are based on a calibration curve of $y = 3.17 \times 10^3 x$ with $r^2 = 0.981$). They should be regarded as semi-quantitative, as many of the results were over the range of the calibration). The diffusion rate was ~3 ng.s^{-1} during these experiments, due to higher room temperatures during the summer months.

Table 3.11: TD-GC-MS results of diffusion tube loading of naphthalene onto two traps for different time intervals.

Parameter	5 min	10 min	20 min	30 min	40 min	60 min
Sampling flow rate (mℓ.min^{-1})	492	473	473	473	478	478
Sample volume (mℓ)	2460	4730	9460	14190	19120	28680
CIS split ratio	30:1	60:1/30:1	100:1	100:1	200:1	200:1
Trap P1 (ng)	826.3	2946	4100	-	5120	-
Trap P4 (ng)	835.1	4608	3720	8470	-	7120
TD-GC-MS average (ng)	851.9	3777	3910	8470	5120	7120
Calculated loading (diffusion rate of 3 ng.s^{-1})	900	1800	3600	5400	7200	10800
Difference (calculated less TD-GC-MS average)	48	(1977)	(310)	(3070)	2080	3680

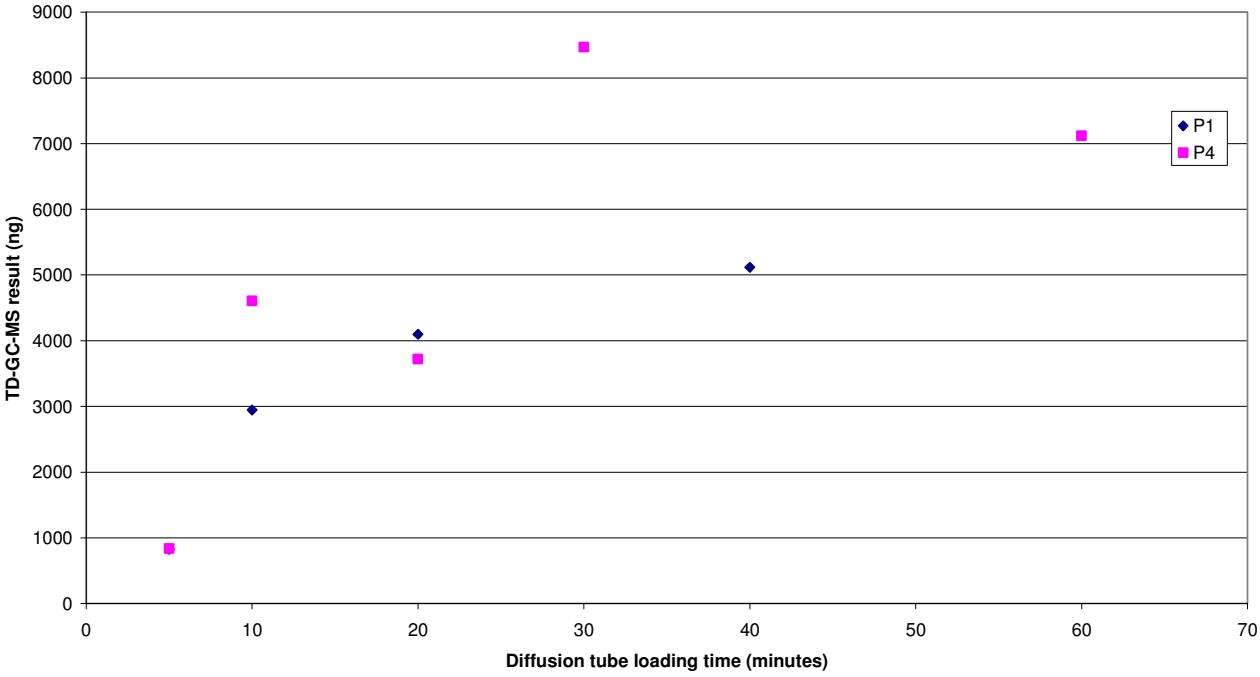

Figure 3.21: TD-GC-MS results for traps loaded with naphthalene from a diffusion tube for different time periods.

From these results, it is evident that the trap continued to accumulate naphthalene throughout the sampling interval (up to 60 min), at which stage the increasing trend appeared to be flattening. From the loading trends in Figure 3.21, it may be estimated that breakthrough occurred at sample volumes > 4730 mℓ (ie: after ~10 min of sampling), although this is not clear from the difference between the amount of analyte which should have loaded from the diffusion tube based on the diffusion rate, and the concentration determined by TD-GC-MS, however it must be borne in mind that the TD-GC-MS results should be regarded as semi-quantitative, as previously mentioned.

The results of the second series of experiments are shown in Figure 3.22, from which a breakthrough volume of ~4 ℓ is also evident.

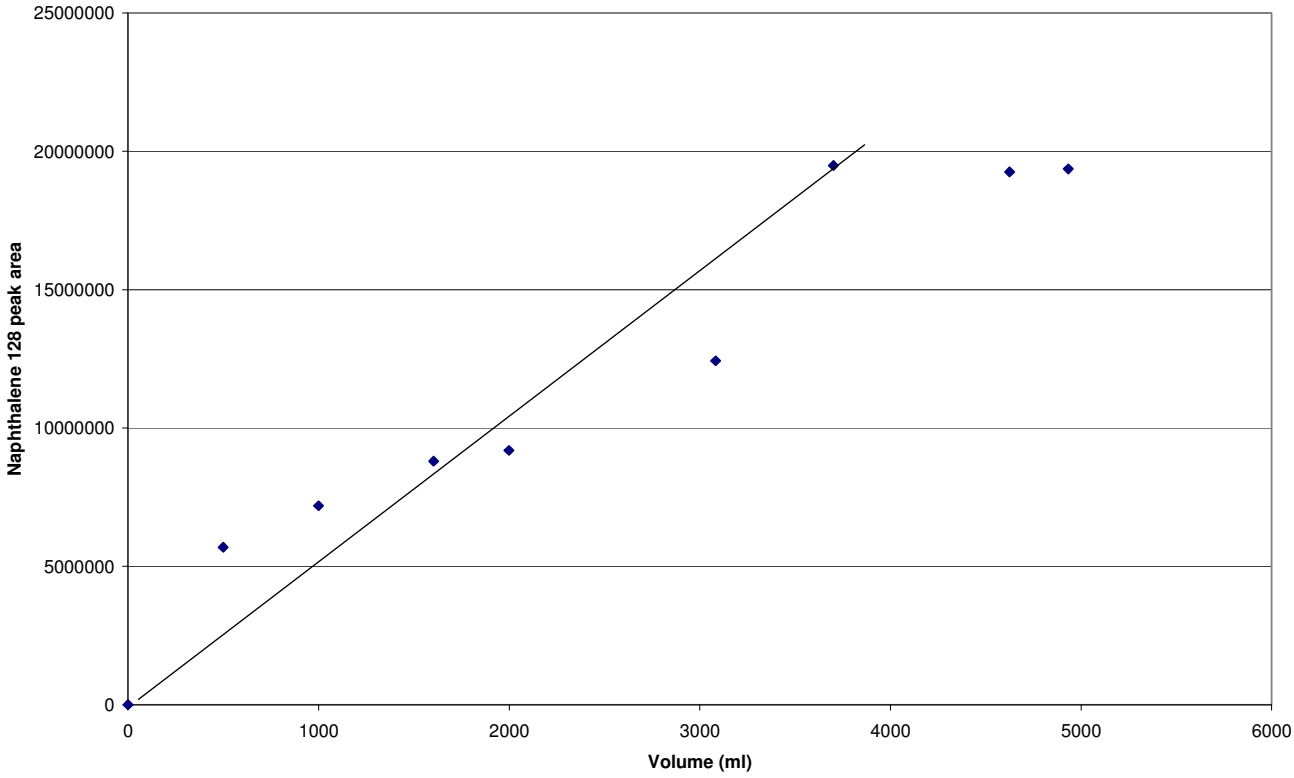

Figure 3.22: TD-GC-MS peak areas for traps loaded with naphthalene from a diffusion tube for different time periods at 370 mℓ.min^{-1}.

The results of the different diffusion tube loading rate experiments are presented in Table 3.12. In these flow rate studies, the impact of faster flow rates on the establishment of equilibrium conditions between the gas and PDMS phases in the sampling trap could be probed. They also allowed for an evaluation of the impact of a faster sampling rate (turbulent conditions) on the rate of diffusion from the diffusion tube.

From the results in Table 3.12, it is evident that there was an over-recovery of naphthalene in all cases, except in the case of ~500 mℓ.min^{-1}. This can be attributed to turbulent conditions in the diffusion tube holder as a result of the higher flow rates, which caused higher rates of loss of naphthalene from the diffusion tube.

Table 3.12: Experimental results obtained for different diffusion tube loading flow rates.

Parameter	Test A	Test B	Test C	Test D
Sampling flow rate (mℓ.min^{-1})	492	641	704	775
Sample volume (mℓ)	2460	3205	3520	3875
CIS split ratio	30:1	30:1	30:1	30:1
Trap P1 (ng)	826	1296	1971	-
Trap P4 (ng)	835	1329	-	1182
TD-GC-MS average (ng)	831	1313	1971	1182
Calculated loading (diffusion rate of 3 ng.s^{-1})	900	900	900	900
Difference (calculated less TD-GC-MS average)	69	(413)	(1071)	(282)

The variation in injection volume for trap calibration purposes was also not ideal, however, due to variations in detector response with changes in solvent volumes during TD-GC-MS analyses, as previously mentioned, which would have contributed to the difference between calculated naphthalene loading and that found by TD-GC-MS analysis.

c) Excitation of other PAHs of interest utilizing 292 nm excitation

i) Pyrene

None of the fluorescence spectra shown in Figure 3.23 contained the characteristic pyrene fluorescence emission peaks (refer to Table 3.4), although slightly elevated oscilloscope signals were obtained at 370 – 390 nm for the 200 ng pyrene sample. The TD-GC-MS results obtained after LIF analysis are summarized in Table 3.13 (using a calibration curve of $y = 4.112 \times 10^{3}x$ with $r^2 = 1.0$). It is evident that conservative loading recoveries were used in determining loading correction factors, thus actual concentrations were ~25 % higher than expected. This variation was consistent between the different concentrations loaded (Table 3.13).

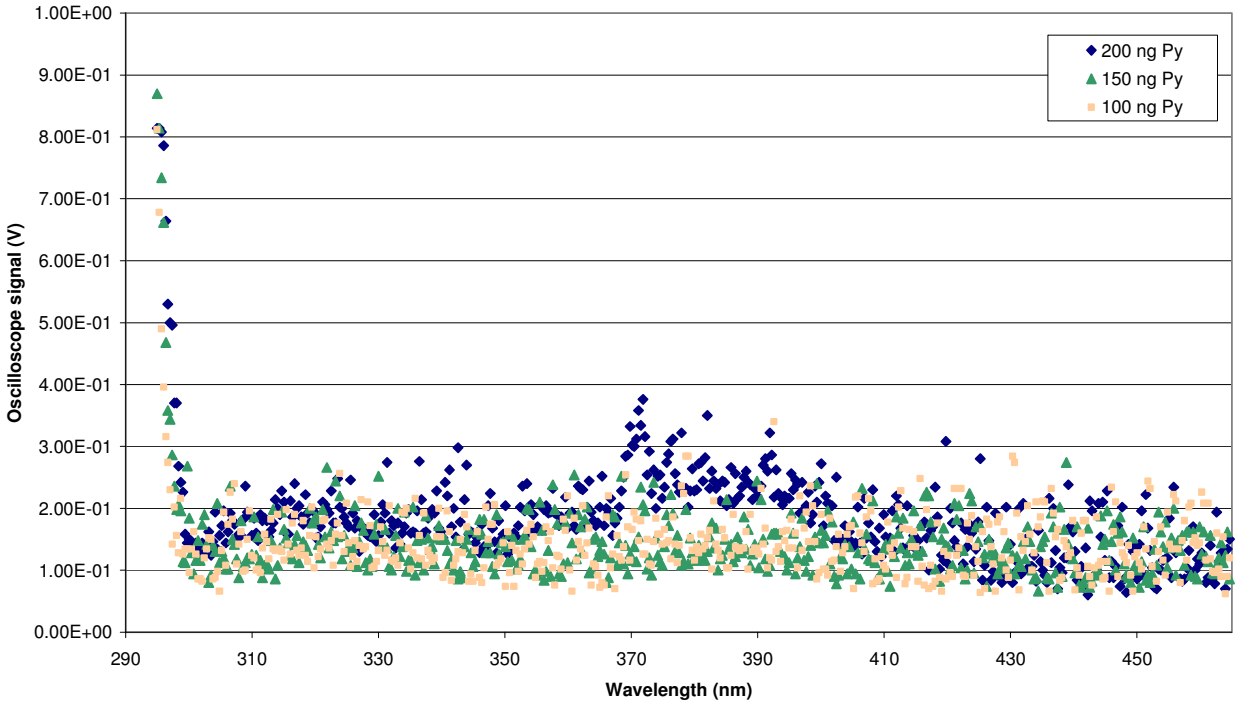

Figure 3.23: Fluorescence spectra of multi-channel silicone rubber traps containing pyrene loaded via gas chromatographic fraction collection, with 292 nm incident radiation (100 µJ in each case).

Table 3.13: Comparison of expected versus actual pyrene concentrations on multi-channel silicone rubber traps loaded via gas chromatographic fraction collection.

Expected pyrene concentration (ng)	**TD-GC-MS pyrene concentration post LIF analysis (ng)**	**% variation**
200	246	23
150	186	24
100	126	26

From the results it is evident that 292 nm is not a suitable excitation wavelength for pyrene, and a longer wavelength would be desirable for this analyte (refer to Table 3.4), although a higher incident energy may also have improved the response obtained.

ii) Phenanthrene

A well resolved fluorescence emission spectrum was obtained when a trap containing 200 ng of phenanthrene was excited with 292 nm radiation, which was characteristic of this PAH (Figure 3.24). The response was much poorer for 150 and 100 ng. The incident energy was lower for the 150 ng trap and it is also possible that channeling occurred through a small number of silicone tubes during gas chromatographic loading of the 150 ng trap, which resulted in the poor response (the laser could have been focused on other silicone tubes to those through which the analyte had preferentially passed). The total amount of phenanthrene loaded onto the trap via gas chromatographic fraction collection would of course be distributed throughout the length of the trap, and not just on the LIF sampling spot, which would contain ~20 ng if 200 ng of analyte is evenly distributed throughout the length of the trap. The profile of phenanthrene through the ~200 ng loaded trap was confirmed qualitatively upon moving the trap slowly upwards in the laser beam, and observing the gradual decrease in oscilloscope signal (and therefore fluorescence emission). A repeat loading and analysis of 100 ng of phenanthrene gave improved results, although the signal to noise ratio of the peaks was still poor, which would impact on detection limits.

There appeared to be some naphthalene contamination of the 150 ng trap, as can be seen by the elevated emission at 323 nm, which was most likely due to carryover during gas chromatographic loading of the trap. Baking out of the gas chromatographic system between trap loading runs may therefore be advisable. TD-GC-MS results of traps post-LIF analysis are presented in Table 3.14 (using a calibration curve of $y = 3.593 \times 10^3 x$ with $r^2 = 1.0$). The amount of phenanthrene loaded onto the traps was higher in the case of the 150 ng loaded trap, and lower for the 100 ng loaded trap, both by 20 %.

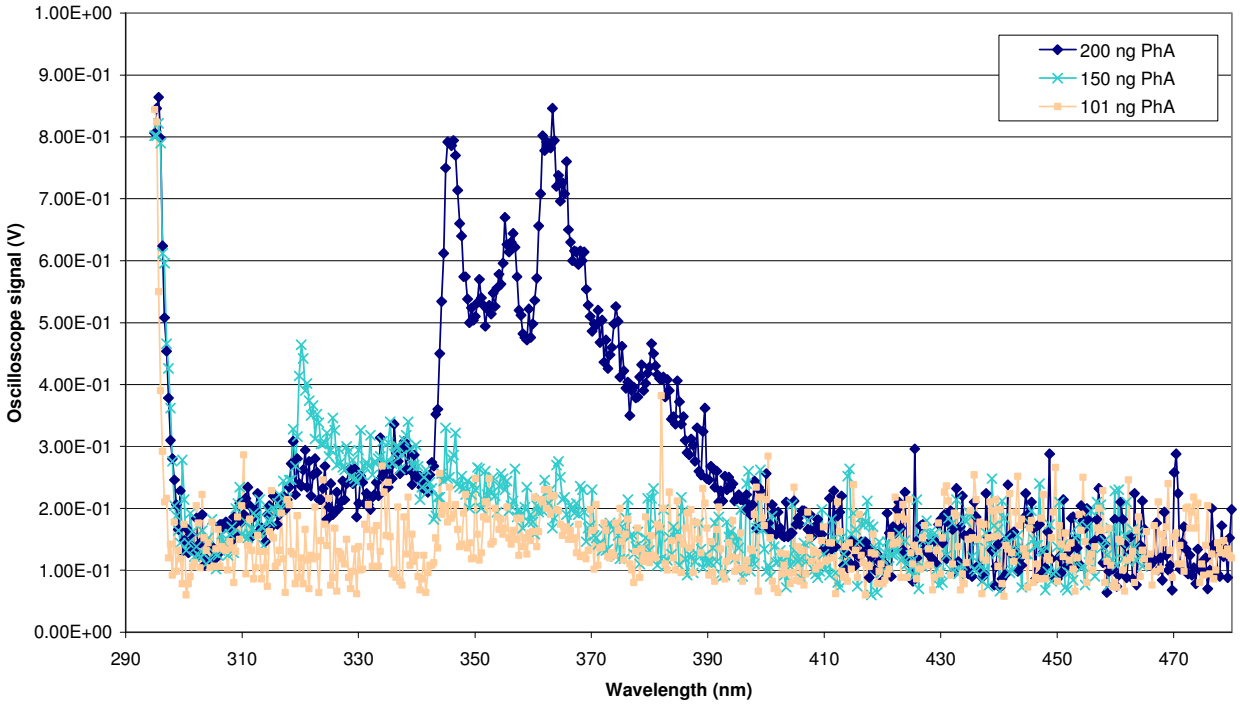

Figure 3.24: Fluorescence spectra of multi-channel silicone rubber traps containing phenanthrene loaded using the gas chromatographic fraction collection method, with 292 nm incident radiation (140 µJ for 200 and 100 ng PhA, 100 µJ for 150 ng PhA).

Table 3.14: Comparison of expected versus actual phenanthrene concentrations on multi-channel silicone rubber traps loaded via gas chromatographic fraction collection (na = not available, as this trap was used for a photodegradation study).

Expected phenanthrene concentration (ng)	**TD-GC-MS phenanthrene concentration post LIF analysis (ng)**	**% variation**
200	na	na
150	180	20
100	80	(20)

3.2.3.4 Conclusion

The LIF method LOD was found to be ~20 ng for a signal to noise ratio of 3:1, and the breakthrough volume (10 %) of the traps was estimated to be in the order of 4 ℓ for

naphthalene based on both LIF and TD-GC-MS experiments. This relates to a sampling interval of ~8 min at 500 mℓ.min^{-1}, and as the GC-MS can detect 1 pg with a signal to noise ratio of 400:1 in total ion current (TIC) chromatogram mode, a detection limit of ~0.3 ng.m^{-3} can be calculated for this breakthrough volume.

Turbulent conditions were established in the diffusion tube holder when sampling flow rates higher than ~500 mℓ.min^{-1} were employed. As flow rates below 500 mℓ.min^{-1} were utilized for all experiments in which the diffusion tubes were used, this was not a cause for concern.

The 292 nm excitation radiation did not prove successful in the case of pyrene fluorescence, which would require longer wavelength excitation radiation. Phenanthrene was successfully detected at this wavelength, however, after ~200 ng was loaded onto a trap via gas chromatographic fraction collection (which would distribute the analyte along the length of the trap). The incident energy will contribute to the sensitivities observed, thus optimization of the LIF system to increase incident energies may improve the results obtained.

Excitation radiation of 292 nm may therefore also be useful for the analysis of phenanthrene in addition to naphthalene, whilst selectivity can be provided by the monochromator for samples containing mixtures of PAHs.

3.2.4 PAH photodegradation

3.2.4.1 Background

PAHs are known to photodegrade under environmental conditions (Kamens et al., 1990), although the rate of this photodegradation is dependent on many factors. Naphthalene, for example, is been reported to photodegrade in the air within a day under moist conditions (ATSDR, 2005). On the other hand, photodegradation of PAHs bound to diesel particulates has been found to be slow under average light intensities, after deposition to ground (Matsuzawa et al., 2001). Photodegradation rates were also found to be minimal for a number of PAHs, including phenanthrene and fluoranthene, adsorbed onto coal fly ash particles

(Korfmacher et al., 1980a and b). It was noted that the photosensitivity of PAHs is strongly dependent upon the nature of the surface onto which they are adsorbed (Korfmacher et al., 1980b).

In terms of photodegradation, PAHs become excited after absorption of photons (ie, by direct photolysis, whilst indirect photolysis occurs when energy is transferred to the target analyte from another excited species). The molecules return to the ground state upon dissipation of the excess energy by means of chemical reactions or by energy transfer processes. The latter may lead to the formation of singlet state oxygen upon energy transfer to oxygen. This product may then attack molecular PAHs via addition reactions (Wang et al., 2005). Singlet oxygen attack and hydrogen abstraction-initiated radical reactions have been proposed as possible mechanisms for the decomposition of PAHs present in atmospheric particulate matter, yielding highly oxygenated compounds (such as dicarboxylic acids; phthalic acid has been observed from naphthalene adsorbed on silica surfaces), polymeric products or hydro-substituted PAHs (Jang and McDow, 1997).

A good correlation was found between the half-life of individual PAHs adsorbed onto particles and their Dewar reactivity number, which is the energy required to remove a π electron at a specific carbon centre from the remaining π system (Behymer and Hites, 1985). Enhanced photodegradation was noted for substrates which had larger surface areas, due to greater PAH dispersion and darker substrates, such as carbon black, were also found to absorb more of the incident light, which reduced the rate of PAH photodegradation (Yokley et al., 1986).

Studies on the influence of UV-B radiation (280 to 320 nm) and temperature on the photodegradation of PAHs dissolved in tetradecane, have indicated that the half-life is dependent on the molecular mass of the PAH concerned, with faster degradation evident for lower molar mass PAHs (Nadal et al., 2006) and similar results were obtained for particle bound PAHs (Ohura et al., 2004b). The degradation rates of PAHs in tetradecane were of the order: naphthalene > pyrene > fluoranthene, although fluoranthene was degraded more slowly than pyrene at low UV-B doses, but faster than pyrene at high temperatures and high UV-B doses (Nadal et al., 2006). The rate of photodegradation of PAHs adsorbed onto wood smoke

particles, which were exposed to midday sun, was strongly influenced by temperature (Kamens et al., 1986). This would result in higher concentrations of PAHs in winter than in summer.

Photolysis of PAHs sorbed onto pine needles showed first order kinetics when exposed to sunlight, with photolysis half-lives ($t_{1/2}$) ranging from 12.9 hours for naphthalene to 51.0 hours for phenanthrene (Wang et al., 2005), as presented in Table 3.15 along with other published PAH $t_{1/2}$ values. The cuticular waxes of the pine needles stabilized the PAHs with respect to photolysis, and it was concluded that the photochemical behaviour of PAHs is dependent on the physical-chemical properties of the substrate onto which they are adsorbed, in addition to the molecular structure of the PAHs (Wang et al., 2005).

Real-time visualization and quantification of PAH photodegradation on and within plant leaves by means of two-photon excitation microscopy revealed that degradation was greater for PAHs at the surface of the leaf as compared to that within epidermal cells of maize leaves (*Zea mays*) (Wild et al., 2005).

Studies investigating the effect of UV-B radiation on the degradation of PAHs sorbed onto the surface of 1-year old spruce needles also yielded first order kinetics (Niu et al., 2003) (refer to Table 3.15 for the $t_{1/2}$ values), with direct photolysis being the most important means of photodegradation (Niu et al., 2004). Similarly, first order rate constants were found in the case of PAHs collected onto filters from residential wood smoke and internal gasoline combustion emissions, where half lives of the order of 1 hour were found under moderate temperature and humidity conditions, with higher decay under higher humidity conditions (Kamens et al., 1988).

Faster photodegradation rates were observed in aqueous solutions ($t_{1/2}$ of the order of 12 min for pyrene), which followed first order reaction kinetics (Lehto et al., 2000). Low et al. (1987) also reported first order reaction kinetics for photodegradation of PAHs in various organic solvents, where benzo(*a*)anthracene, for example, had a $t_{1/2}$ of less than 2 minutes in a number of solvents including acetone and dichloromethane. It was noted that faster degradation occured in more polar solvents, most likely due to the formation of radical cation intermediates (except for phenanthrene which did not show detectable decomposition). The photodegradation products indicated that solvent-induced photodegradation had occurred, and

the rate of photodegradation was found to be higher when irradiation was at wavelengths below 300 nm.

It was concluded that polar solvents should not be used in the extraction of PAHs for analysis, unless light can be excluded. This is another reason why analytical methods for PAHs which do not require solvent extraction steps are preferable.

In the case of the silicone rubber traps, the substrate (i.e. the PDMS) absorbed a very small portion of the incident laser light, thus "filtering" of incident light by the substrate would not occur to any significant extent. This, accompanied by the high intensity of the laser light and the fact that this light is at the maximum PAH absorption wavelength, should result in shorter $t_{1/2}$ values when compared to those of other studies. The fact that PDMS is non-polar may mitigate these effects to some extent.

The products of photodegradation of PAHs have been identified in a number of studies. Naphthalene, for example, was studied when adsorbed onto titanium dioxide, ferric oxide, muscovite (a natural silicoaluminate) and fly ash (Guillard et al., 1993). Naphthalene was chosen for this study, as it is one of the PAHs with the highest atmospheric concentrations. Direct photolysis was prevented by using incident light of $\lambda > 340$ nm. Photocatalysed degradation products were thus noted, particularly with respect to TiO_2 surfaces, in the presence of oxygen, whilst water vapour increased the degradation rate. Products such as 1,4-naphthoquinone (the main intermediate product); 2-naphthol; phthalide; phthaldialdehyde; phthalic acid; acetophenone; benzaldehyde; and benzoic acid were identified. Depending on the volatility of these compounds, some were transferred to the gas phase, whilst others were adsorbed onto the solid surface and underwent further reactions.

Table 3.15: Photolytic half-lives (in hours) of the PAHs of interest, including the light intensity.
Naphthalene was excluded from these studies, as it volatilizes too quickly to be effectively retained on the surface of the spruce needles (Niu et al., 2003).

PAH	Spruce needles (Niu et al., 2004) UV-A 11-16 W.m^{-2}	Tetradecane (Nadal, et al. 2006), UV-B (280 – 320 nm) 20 °C & 22.5 KJ.m^{-2}.day^{-1} (0.26 W.m^{-2})	Spruce needles (Niu et al., 2003) Sunlight 620±50 W.m^{-2}	Maize leaves (Wild et al., 2005) 355-375 nm, 25°C & < 24 W.m^{-2}	Particles (Behymer and Hites, 1985) 300 – 410 nm, 18 W.m^{-2}				Pine needles (Wang et al., 2005) Sunlight, 450 W.m^{-2}	Diesel particulate matter (Matsuzawa et al., 2001) Simulated sunlight, 925 W.m^{-2}	Spruce needles (Niu et al., 2004) UV-A + UV-B 11.43-16.53 W.m^{-2}
					Silica gel	Alumina	Fly ash	Carbon black			
Naph	#	12 – 17	#						12.9		#
PhA	231		75	0.46 (surface)	150	45	49	>1000	51.0	60.63±1.33	158
FlA	182	136 – 201	26	0.09 (surface) 0.24 (cellular)	74	23	44	>1000	25.6	22.16±0.77	151
Py	120	155 – 250	37		21	31	46	>1000	26.1	737.55±124.49	105

The aim of this series of experiments was therefore to determine whether the excitation light provided by the laser system resulted in photodegradation of the PAHs dissolved in the silicone rubber traps. The extent of such photodegradation over a defined time interval was also to be determined, should such degradation be evident, and degradation products were to be identified. These experiments are important in terms of quantitation of PAHs. In addition, it is necessary to determine the photodegradation products so that these are not mistakenly ascribed to the original gas sample. Naphthalene served as a worst case scenario, due to its high volatility and reportedly fast rate of photodegradation (Nadal et al., 2006).

3.2.4.2 Experimental method

a) Photodegradation of naphthalene as determined by LIF

Naphthalene was introduced in the gas phase onto a silicone rubber trap by means of a diffusion tube, after a blank trap fluorescence spectrum had been recorded. The sampling pump was switched off after equilibrium conditions (constant [PAH]) had been established on the sample spot at the top of the trap, as evidenced by a stable oscilloscope signal, which was obtained with the monochromator set to 323 nm (the trap was not end-capped). The laser continued to provide excitation radiation, and the consequent change in oscilloscope signal (and thus [PAH]) was recorded for a period of at least 10 minutes. The laser light intensity was approximately 204 $W.m^{-2}$ (assuming operation at 8 Hz, 500 μJ and a 5 mm spot diameter). Sunlight, by comparison, varies significantly, but was in the order of 450 $W.m^{-2}$ in the pine needle study (Wang et al., 2005). Wild et al. (2005) noted that environmental UV-A intensities average a few $W.m^{-2}$ in temperate latitudes and may reach >10 $W.m^{-2}$ under the most intense tropical conditions.

The experiment was conducted on different days, with different silicone rubber traps and slightly different incident laser pulse energies.

b) Photodegradation of phenanthrene as determined by LIF

Approximately 200 ng of phenanthrene was introduced in the vapour phase onto a silicone rubber trap by means of gas chromatographic fraction collection loading. A LIF scan was recorded of the loaded trap from 295 to 480 nm with 292 nm excitation, after the laser energy had been determined with an energy meter. The laser continued to provide excitation radiation, and the consequent change in oscilloscope signal at 364 nm (and thus [PAH]) was recorded over 30 minutes. The laser light intensity was approximately 41 $W.m^{-2}$ (assuming operation at 8 Hz, 100 μJ and a 5 mm spot diameter).

A LIF scan was recorded again after the 30 minute interval after the laser energy had been determined with a Gentec energy meter.

c) Identification of photodegradation products

Traps were end-capped after the LIF experiments, wrapped in aluminium foil, and were stored in the dark under cool conditions (< 5 ^{o}C) prior to analysis by TD-GC-MS in order to tentatively identify photodegradation products by means of National Institute of Standards and Technology (NIST) library searches. No comparison to standards or quantitation was performed. Six traps which contained naphthalene, three traps loaded with phenanthrene, three traps which contained pyrene, and one trap loaded with both phenanthrene and pyrene were analysed by TD-GC-MS after LIF exposure for various time periods and at different incident energies. TD-GC-MS conditions as described under section 3.2.2.2 were employed. The CIS split ratio was varied between 10:1 and 100:1, depending on the concentration of analytes loaded onto the trap. The mass spectra of ions which were extracted from the total ion chromatogram were compared to those contained in the NIST library. GC peaks which were significantly above the background signal, and target ions from literature were examined.

3.2.4.3 Results and discussion

a) Photodegradation of naphthalene as determined by LIF

Equilibrium conditions were reached in the sample spot at the top of the traps after a loading period of 2 minutes, on average, which related to a total of approximately 240 ng of naphthalene over the trap (based on a diffusion rate of 2 ng.s^{-1}).

A decrease in oscilloscope signal upon continued irradiation, and thus [PAH] was evident from the various repeat experiments conducted, as shown in Figures 3.25, 3.26 and 3.27, with a decrease in oscilloscope signal (and thus [PAH]) of around 12 % over 10 minutes (refer to Table 3.16). The timescale of typical PAH scanning analyses, as detailed under section 3.2.1 was under 5 minutes, which would relate to a decrease in signal of approximately 9 % over this time interval.

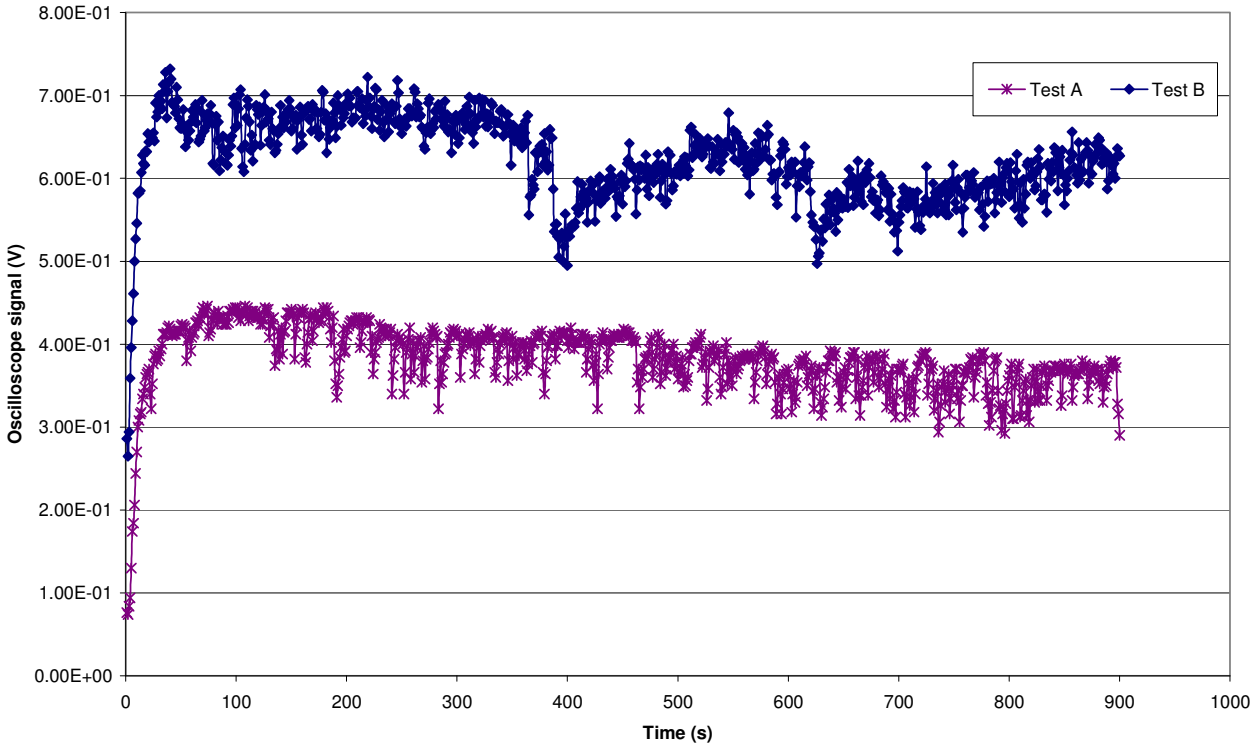

Figure 3.25: Naphthalene 323 nm fluorescence signal upon continued laser irradiation (Test A and B).

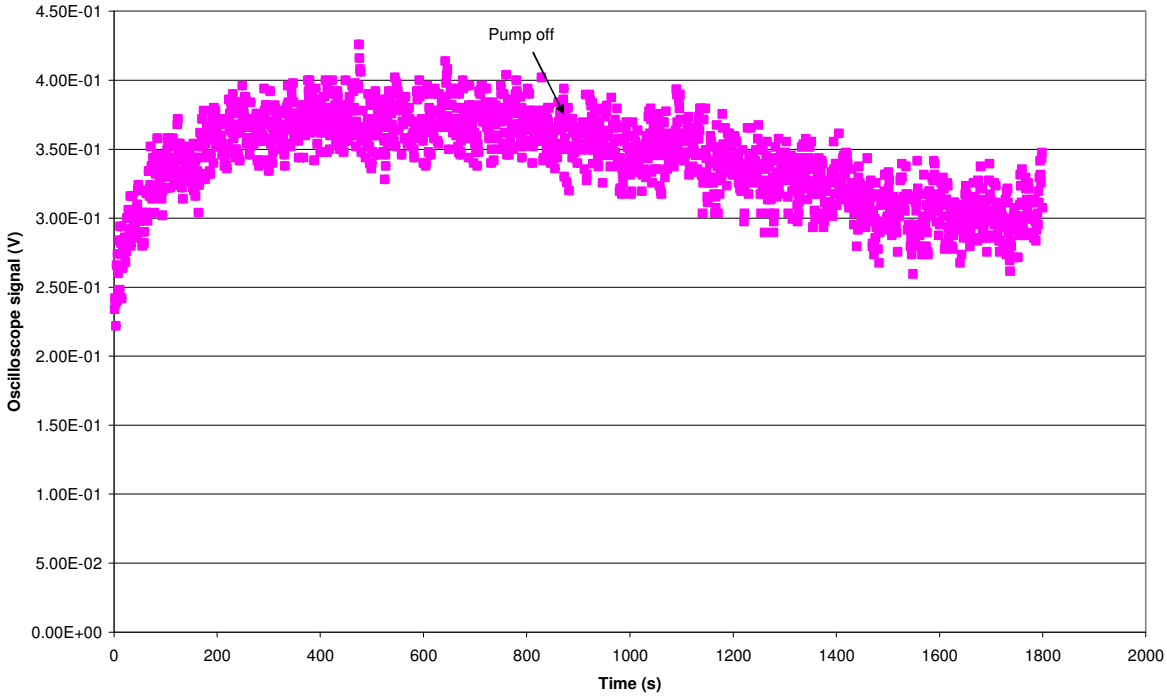

Figure 3.26: Naphthalene 323 nm fluorescence signal upon continued laser irradiation (Test C).

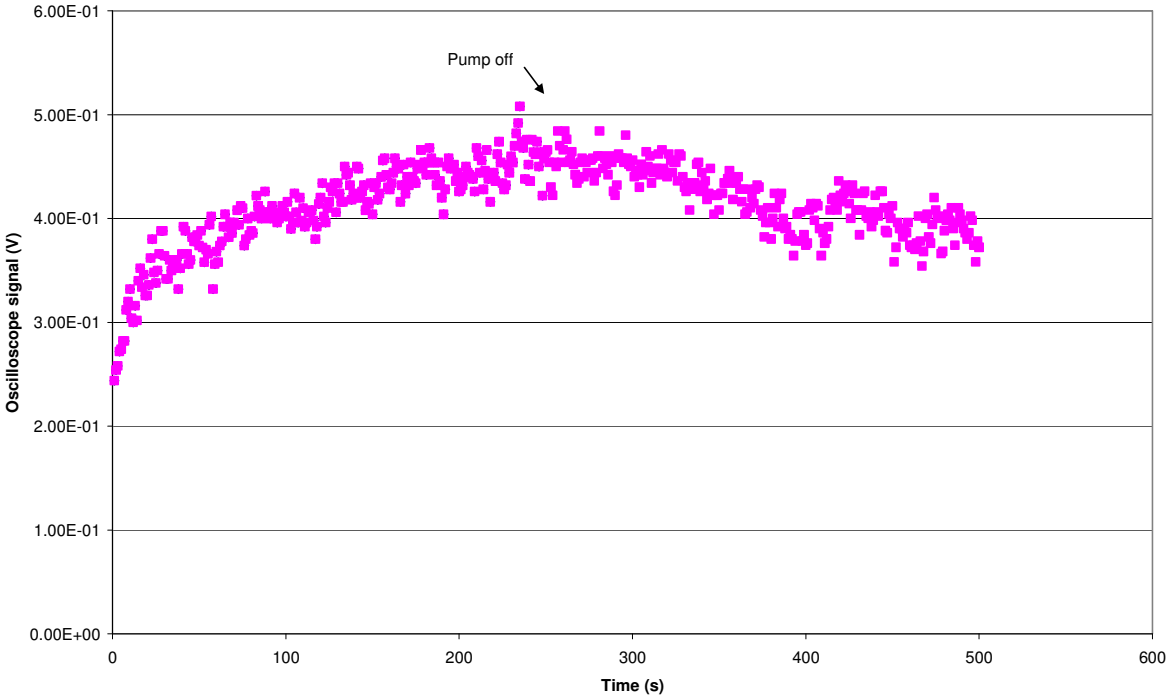

Figure 3.27: Naphthalene 323 nm fluorescence signal upon continued laser irradiation (Test D).

Table 3.16: Naphthalene LIF photodegradation data with estimated fluorescence signal decreases post equilibration.

Test	Energy (µJ)	Loading time (s)	Total irradiation time (s)	Equilibrium oscilloscope signal (V)	% decrease after 5 min	% decrease after 10 min
A	150	110	900	0.444	7 (0.412 V)	14 (0.382 V)
B	386	110	900	0.695	7 (0.648 V)	10 (0.584 V)
C	120	900	1800	0.362	7 (0.338 V)	12 (0.318 V)
D	520	250	500	0.466	14 (0.402 V)	Not available

Similar photodegradation rates were noted in each experiment, although a higher degradation rate was noted in Test D, which could have been due to the relatively high energy of the incident radiation (520 µJ); increased volatilization losses during this experiment; or even due to increased degradation of naphthalene due to the presence of active sites, moisture, or particles in the trap used for this experiment. The cyclic effect in oscilloscope signal observed in Test B was likely to have been caused by laser effects (variations in laser energy).

The time interval over which the experiment was conducted was insufficient to determine the reaction order accurately, as these experiments were conducted over a maximum of 15 minutes, whilst studies in the literature extended over more than 250 hours (Wang et al., 2005; Niu et al., 2003). Upon assuming a first order reaction, as reported in the literature, k can be determined from the equation:

$$\ln \frac{[A]}{[A]_0} = -kt \qquad \text{Equation 3.2}$$

In this case, $[A] \propto V$, where V is the oscilloscope signal. Thus k may be determined from the slope of $ln\ (V_t / V_0)$ versus t. In this manner, $k = 0.0004$ was determined for Test A, although the fit was very poor ($r^2 = 0.4$). The half-life for naphthalene was then calculated to be 29 minutes from the following equation (based on first order kinetics):

$$t_{1/2} = \frac{0.693}{k} \qquad \text{Equation 3.3}$$

The results from each of the datasets are included in Table 3.17. The $t_{1/2}$ for Test D was found to be shorter than the others, possibly due to the reasons previously described, whilst the longest $t_{1/2}$ was determined for Test C, where the incident laser energy was the lowest. An overall average $t_{1/2}$ for naphthalene of approximately 35 minutes was thus calculated. It should be noted that this refers to an overall or total half-life, which incorporates both photodegradation and any volatilization losses.

Table 3.17: Half-life of naphthalene calculated from the LIF experimental data and first order reaction kinetics.

Test	**ln (V_t/V_0) vs t**		
	r^2	**k**	**$t_{1/2}$ (min)**
A	0.4	0.0004	29
B	0.3	0.0003	39
C	0.6	0.0002	58
D	0.7	0.0008	14

b) Photodegradation of phenanthrene as determined by LIF

A decrease in the fluorescence signal of phenanthrene was evident during the 30 min irradiation period, as shown in Figure 3.28. A decrease in phenanthrene fluorescence was also noted upon comparison of the LIF scans obtained before and after the 30 minute irradiation period (Figure 3.29). First order reaction kinetics were assumed, and a photodegradation rate was determined as shown in Figure 3.30.

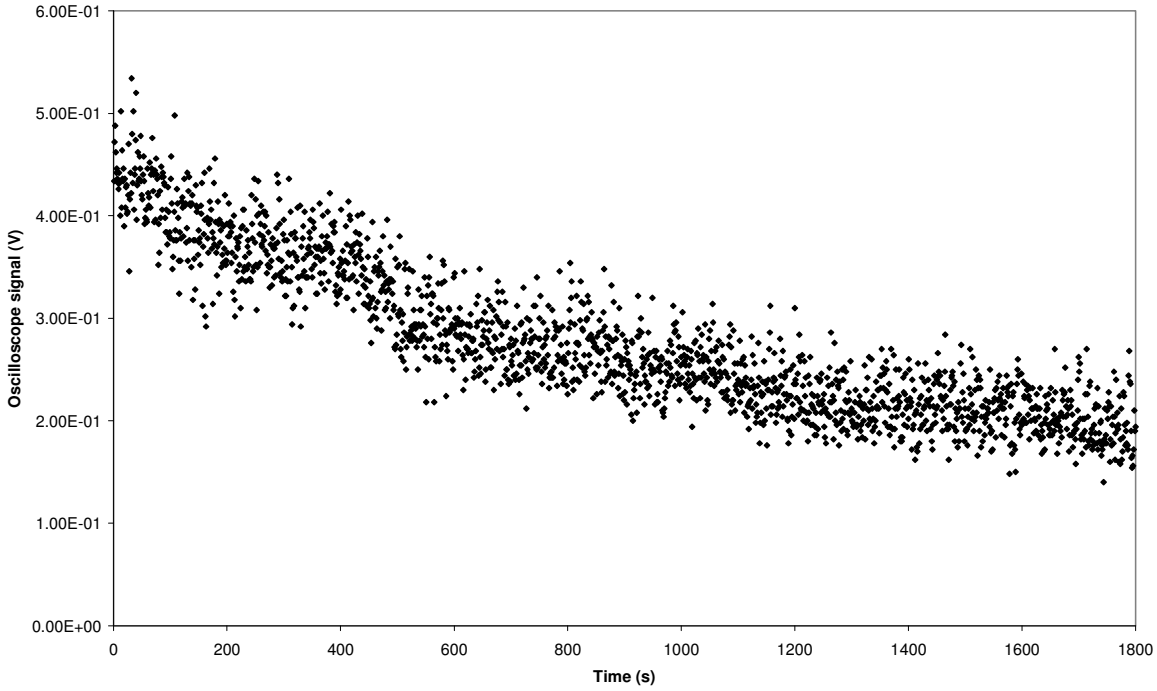

Figure 3.28: Phenanthrene 364 nm fluorescence signal upon continued laser irradiation (200 ng loaded using the gas chromatographic fraction collection method).

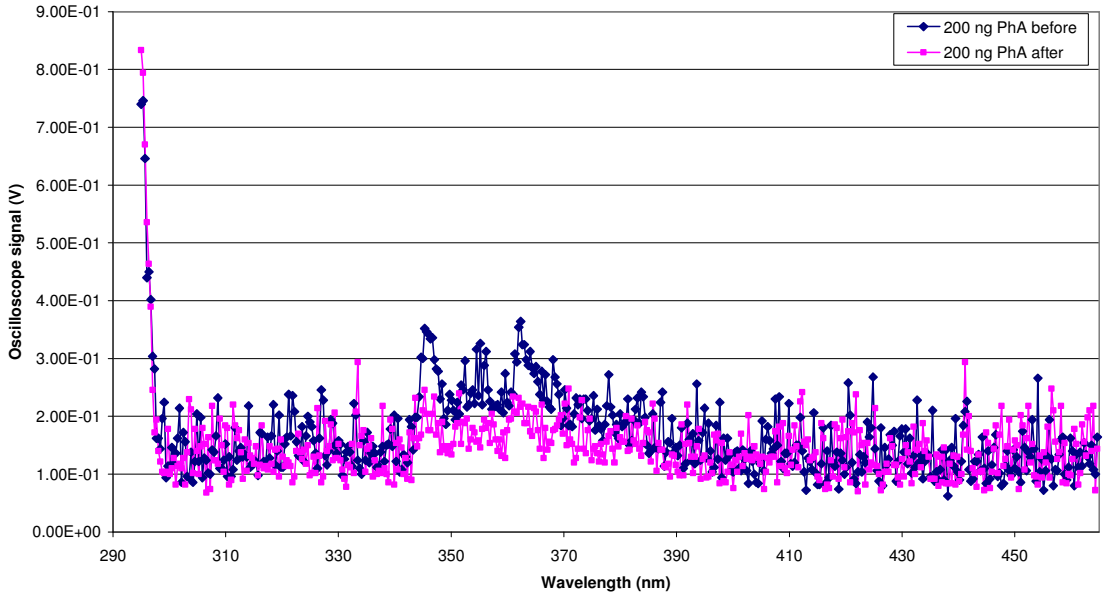

Figure 3.29: LIF scans of phenanthrene before and after 30 minutes of irradiation at 292 nm (200 ng loaded using the gas chromatographic fraction collection method).

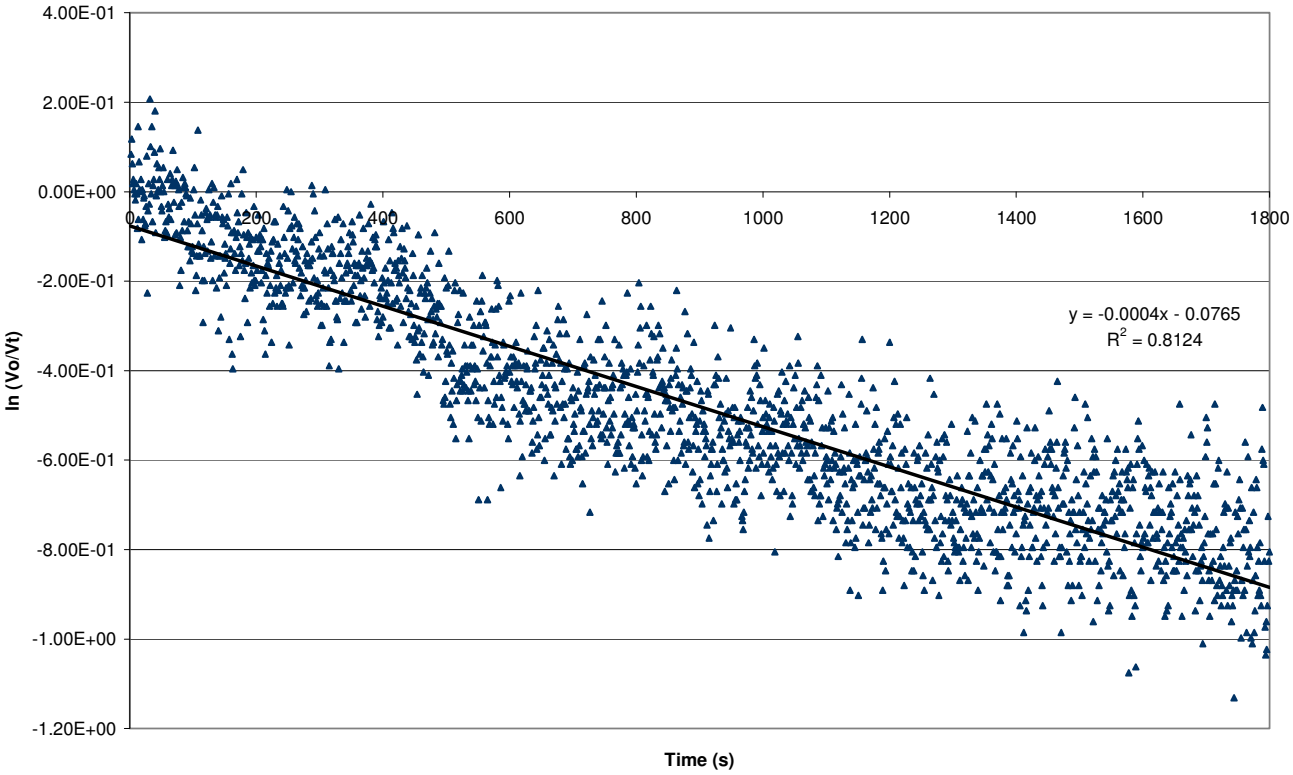

Figure 3.30: First order photodegradation kinetics of 200 ng phenanthrene (loaded using the gas chromatographic fraction collection method) with 292 nm excitation.

The laser energy at the sample position was found to be 100 μJ both before and after the photodegradation experiment was conducted. 117 ng of phenanthrene was found to be present on the trap after the photodegradation experiment by TD-GC-MS analysis. This relates roughly to a 42 % loss after 30 minutes of irradiation, assuming that there was indeed 200 ng of phenanthrene loaded on the trap at the start of the experiment. The oscilloscope signal at 364 nm obtained from the LIF scans also decreased by 44 % after the 30 min irradiation period (refer to Figure 3.28).

A 17 % decrease in oscilloscope signal for a 5 minute LIF scan and a 23 % loss over a 10 minute scan may be estimated from Figure 3.28. A half life of 29 min is obtained from the slope of the kinetics graph (k = 0.0004), which compares favourably to the decrease in oscilloscope signal measured after the 30 minute irradiation period (which is basically equivalent to the half life) and to the TD-GC-MS results.

c) Identification of photodegradation products

The qualitative results of the NIST library searches are presented in Table 3.18, including the laser incident energies and exposure periods for each sample. The photodegradation products were generally present at very low levels, thus the library matches were not very good in some cases, however, they do provide an indication of possible breakdown products.

Five of the six traps which had been loaded with naphthalene were found to contain phenol, whilst four contained both benzyl alcohol and phthalic anhydride. Benzaldehyde, benzoic acid, and benzyl formate were each found on one trap. No breakdown products were found in the naphthalene trap which had only been irradiated for 5 minutes, even though it contained a high concentration of naphthalene, and the laser energy was comparable to that of other LIF analyses where degradation products were detected.

Benzyl alcohol and phthalic anhydride were present on two of the three phenanthrene containing traps, whilst benzyl formate and phenol were present on one of the traps.

Fewer degradation products were generally found in the traps loaded with pyrene, although exposure times were all relatively short (10 minutes). Benzyl alcohol was present on two of the traps, whilst acetophenone, benzyl formate, and phthalic anhydride were each found on one trap.

Phenol, benzaldehyde, and benzyl alcohol were identified on the trap which had been loaded with both phenanthrene and pyrene.

Generally better matches were obtained for traps which had been irradiated for longer or contained more analyte, which would have generated higher concentrations of the breakdown products. The naphthalene trap which was irradiated for the shortest time (5 min) did not contain any detectable concentrations of the breakdown products, therefore such products should not interfere with TD-GC-MS analyses of traps post LIF analysis, as LIF scans are completed in < 5 min. No effect of the variation in laser incident energy on the production of photodegradation products was evident for the range of energies included in this study (12 – 200 μJ). The effect of the photodegradation products (particularly the organic

acids) was also visible in subsequent TD-GC-MS analysis, in that column bleed was evident in the chromatograms (Figure 3.31), due to breakdown of the stationary phase by these acidic compounds.

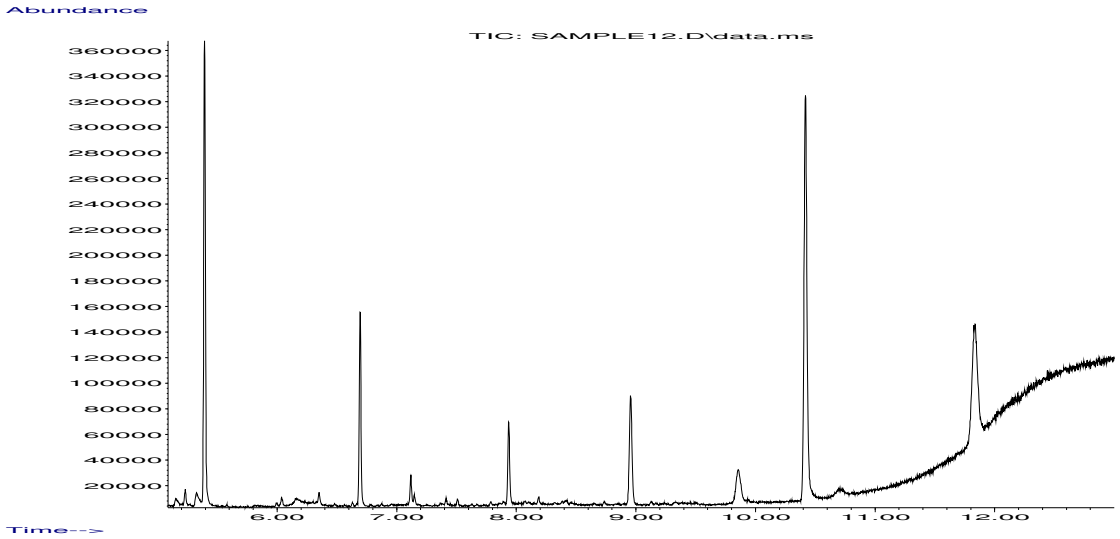

Figure 3.31: Increase in the chromatogram baseline upon the analysis of a sample containing photodegradation products (a mixture of 138 ng of phenanthrene and 100 ng of pyrene irradiated for 10 min at 70 μJ).

Table 3.18: Photodegradation products of naphthalene, phenanthrene and pyrene, as determined by NIST library comparisons.

NOTE: Numbers in brackets reflect the quality of the match between the mass spectrum of the sample to that of the library. Analyte concentrations were determined by TD-GC-MS after LIF analysis. *Naphthalene contamination evident.

Compound	**m/z**	**R_t (min)**	**Trap 1: Naph**	**Trap 2: Naph**	**Trap 3: Naph**	**Trap 4: Naph**	**Trap 5: Naph**	**Trap 6: Naph**	**Trap 1: PhA**	**Trap 2: PhA**	**Trap 3: PhA**	**Trap 1: Py**	**Trap 2: Py**	**Trap 3: Py**	**Trap 1: PhA + Py**
Laser energy at 292 nm (µJ)			160	200	12	25	100	100	140	100	100	100	100	100	70
Approximate irradiation time (min)			15	55	15	80	120	5	10	30	10	10	10	10	10
Analyte concentration post irradiation (ng)			968	31.5	75	6794	9245	9507	80	117	180*	126	246	186	138 (PhA) 100 (Py)
Benzaldehyde	106	5.2	√ (Q7)												√ (Q87)
Phenol	94	5.3	√ (Q5)	√ (Q38)	√ (Q49)	√ (Q49)	√ (Q42)				√ (Q38)				√ (Q80)
Benzyl alcohol	108	5.8	√ (Q86)	√ (Q64)		√ (Q46)	√ (Q52)		√ (Q68)	√ (Q35)			√ (Q64)	√ (Q42)	√ (Q64)
Acetophenone	120	6.1												√ (Q38)	
Benzyl formate	136	6.2	√ (Q91)							√ (Q90)				√ (Q60)	
Benzoic acid	122	6.8				√ (Q43)									
Phthalic anhydride	148	8.0		√ (Q49)	√ (Q49)	√ (Q72)	√ (Q53)			√ (Q83)	√ (Q74)	√ (Q27)			

3.2.4.4 Conclusion

Due to the fact that the silicone rubber traps sample gaseous analytes, and that they effectively serve as denuders, with particles (and thus particle bound analytes) passing through them as discussed in Chapter 4; the presence of solids arising from the sample, which could catalyse the photodegradation reactions, should not be a major consideration.

It was evident that the oscilloscope signal decreased upon laser irradiation of naphthalene and phenanthrene samples, which indicated that the incident laser light was causing photodegradation of these analytes. The overall combined photodegradation and volatilisation rate determined here for naphthalene was of the order of 10 % over the time interval of a scanning LIF analysis (5 min), and would be significantly less for single fluorescence wavelength analyses, which are obtained within the order of seconds. This effect should not have a significantly negative impact on subsequent quantitation by TD-GC-MS, due to the sensitivity of this technique. A half life for naphthalene of ~35 min was determined from first order reaction kinetics. The photodegradation of phenanthrene was slightly more rapid than for naphthalene with 292 nm excitation (17 % decrease in oscilloscope signal over 5 min and $t_{1/2}$ of ~30 min). The LIF photodegradation rates were higher than that reported in most other studies, such as that of PAHs adsorbed onto pine needles, where photolytic half-lives were > 12 h with 450 $W.m^{-2}$ irradiation by sunlight (Wang et al., 2005). This is to be expected as LIF involves single wavelength irradiation at or close to the absorption maximum of the analyte. Shorter half-lives (for example, 28 min for phenanthrene) have been reported for PAHs adsorbed onto maize leaves at < 24 $W.m^{-2}$ with 355 – 375 nm irradiation (Wild et al., 2005).

Once the LIF photodegradation rate has been determined for the target PAH(s) at the experimental wavelength concerned, it is possible to correct for the resulting decrease in analyte concentration upon subsequent quantitative analysis of samples by TD-GC-MS.

Similar oxidative photodegradation products were found in traps loaded with naphthalene and phenanthrene after extended LIF irradiation, primarily phenol, benzyl alcohol, and phthalic anhydride. These compounds were not detected on a naphthalene trap, however, which was irradiated for 5 min, which is the time typically required for a LIF scan.

3.2.5 Energy experiments

3.2.5.1 Background

The laser system utilized in these experiments displayed temporal variability in the pulse energy at the target. This was noted from energy meter measurements at the target site at intervals during experimental runs. Such fluctuations may arise for a number of reasons, including degradation of the laser dye, degradation of the excimer gas, and loss of alignment of optics due to heating effects during experimental runs.

In terms of the degradation of the Rhodamine 6G laser dye, suppliers have published photochemical stability specifications of 316 W.h at 590 nm (the centre of the emission spectrum) when the dye is pumped with an excimer laser (Brackmann, 1986).

$$Eft = P_t \qquad \text{Equation 3.4}$$

Where E is the energy of the excimer laser output in J; f is the repetition rate in Hz; t is the operation time in hours and P_t is 316 W.h.

Thus at 8 Hz and 300 mJ per pulse, the energy of the dye laser output would decrease to 50 % of its initial value after 132 hours of operation (which relates to 3.8 x 10^6 pulses, as $n = 3600.f.t$). This effect should therefore be minimal over the time interval of the experiments, but needs consideration in the long term operation of the laser system.

A series of experiments were therefore conducted in order to quantify the instability of the laser energy in the experimental system, so that the potential impact of this effect could be understood. The relationship between the energy of the excitation radiation and the fluorescence intensity of the analyte (as measured by the oscilloscope signal) was also investigated by means of energy attenuation experiments, in order to determine the relationship between the analyte concentration (oscilloscope voltage) and the incident energy.

3.2.5.2 Experimental method

a) *Laser stability*

Two experiments were conducted with the aid of a Gentec PRJ-M Energy and Power Monitor with the laser system operating at 292 nm and 8 Hz. In the first experiment, the energy at the target was measured, whilst the second experiment focused on the energy of the light exiting the dye laser before it passed through any optics. In this manner, the contribution of the optical path to the energy instability could be determined.

Each experiment was conducted over the period of an hour. The maximum, minimum, and mean energies, as well as the standard deviation were recorded over 100 pulses in each minute (thus sampling over a 12.5 s interval at 8 Hz).

Based on the results of these experiments, further investigations were conducted in order to determine whether the decrease in energy of the dye laser output was due to a decrease in energy of the excimer laser output, which was used to pump the dye laser system. For these experiments, a Molectron Energy Meter (2.13 $V.J^{-1}$; 50 mm diameter) linked to a Tektronix TDS 520A oscilloscope (set at 100 mV and 2 ms per division respectively; and on peak-to-peak averaging over 100 pulses) was used at the exit of the excimer laser, which was operating at 8 Hz and a high voltage setting of 28. The average energy at 248 nm was recorded from the oscilloscope every minute over a period of an hour. The shutter of the laser was closed between readings, in order to minimize thermal effects on the energy meter. The excimer laser had been equipped with fresh chlorine gas and was conditioned a few hours prior to the experiment, and the system was connected to a chiller unit during the course of these experiments.

Two days later, this experiment was repeated at the exit of the dye laser, with an RJ 7610 Energy Radiometer (Laser Precision Corporation) equipped with a Laser Probe Option RQ, which was linked to the same oscilloscope. A high voltage setting of 29 was set on the excimer laser, and measurements were taken over a period of an hour. Immediately following this experiment, measurements were taken over a 15 minute period at the exit of the excimer laser, using the previous method (Molectron Energy Meter).

The RJ 7610 Energy Radiometer was also used to determine the energy stability at the dye laser outlet after the laser system had been further optimized (new gas for the excimer laser and methanol was added to the oscillator of the dye laser to replace that which had evaporated over time).

b) *Relationship between excitation energy and fluorescence emission*

Possible means of attenuating the incident beam were investigated, such as the use of a Brewster crystal; and cover slips of various materials (such as quartz, silica glass, etc). No attenuation of the beam was found when the Brewster crystal was positioned for attenuation of both a vertically or horizontally polarized beam, which indicated that the beam was circularly polarized. Brewster crystals were therefore not effective in attenuating the beam. Glass cover slips (Corning) were also not suitable, as the beam was fully attenuated when two cover slips were placed in the path of the incident light.

Borosilicate glass plates (20 mm x 20 mm x 3.30 mm thick, Glassblowing Industries) were found to be suitable for attenuation of the 292 nm incident beam. A glass plate was thus held in the path of the incident light to a trap which was loaded with naphthalene and the decrease in voltage (fluorescence emission) was recorded. This was repeated with two and three plates in the path of the beam.

The analyte was loaded from a naphthalene diffusion tube at 489 $m\ell.min^{-1}$ for 820 s to ensure equilibrium had been reached in the sample spot at the top of the trap prior to oscilloscope measurements. Loading continued throughout the course of this experiment, in order to prevent variations due to loss of analyte by volatilization or photodegradation.

The trap was then removed from the LIF system and the energy at the trap location was determined by means of an energy meter. The decrease in energy was also recorded when borosilicate glass plates were sequentially placed in the path of the incident beam.

3.2.5.3 Results and discussion

a) *Laser stability*

The results of the first two experimental runs are presented in Figure 3.32, where a decrease in pulse energy over time is evident in both cases.

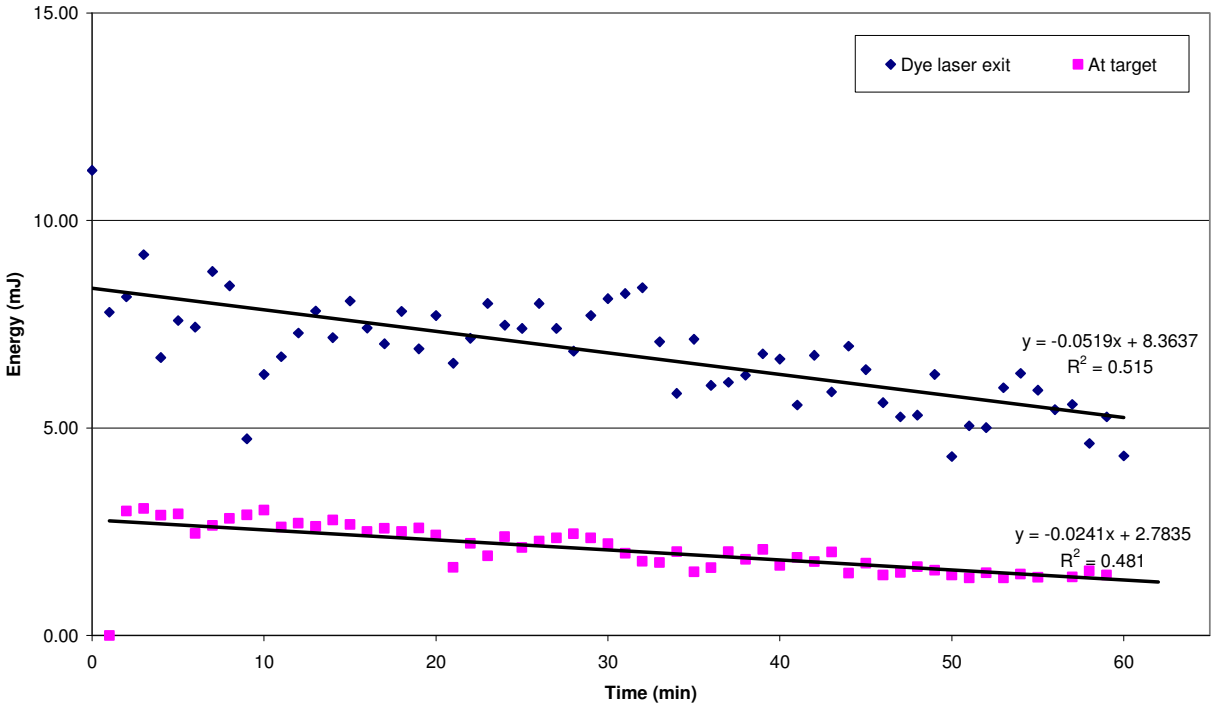

Figure 3.32: Variation in laser energy over time and at various points throughout the system.

The energy exiting the dye laser decreased by approximately 40 % over the period of an hour, whilst the decrease at the target was approximately 50 % over the same time interval. The additional loss in the later case can be attributed to the optics and the effect of heating thereon.

As the timescale of typical PAH LIF scan runs is 5 minutes, the corresponding decreases in energy over this time interval are 3 % and 5 %, respectively.

The results of the second series of experiments are presented in Figure 3.33.

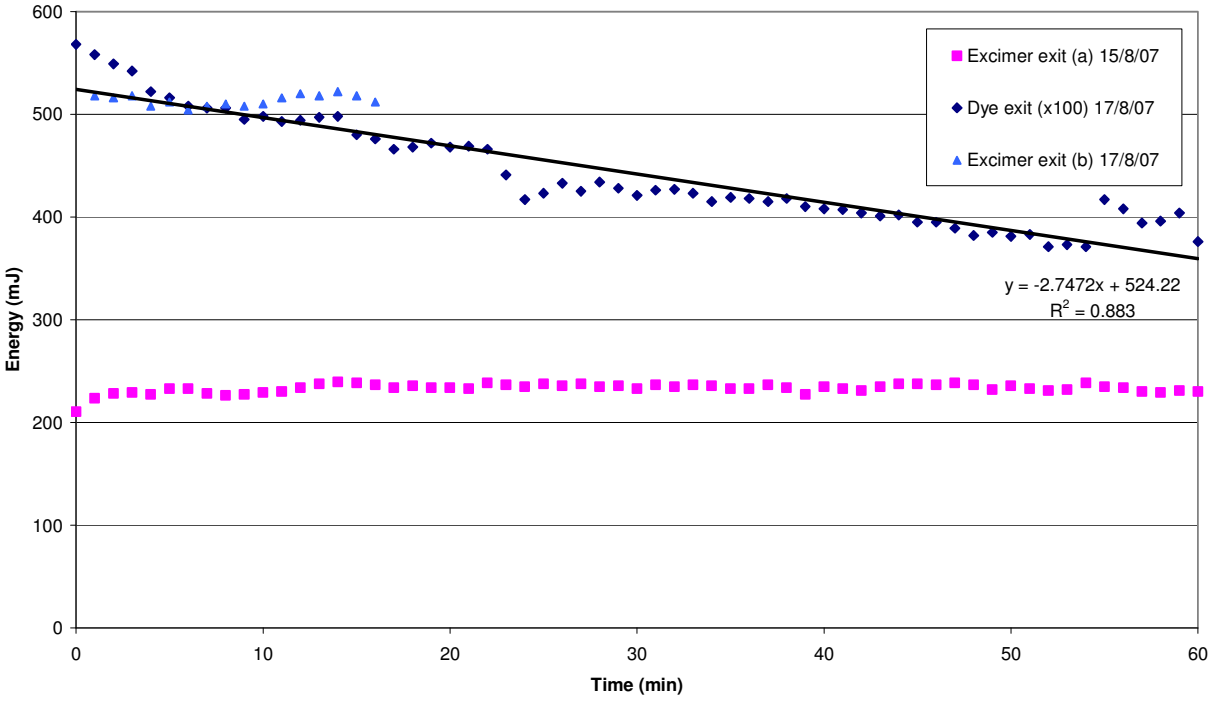

Figure 3.33: Repeat experiment: variation in laser energy over time and at various points throughout the system.

It is evident from these results that the energy of the excimer output was stable over the period of an hour (the higher energy obtained for the second experiment at the excimer exit can be attributed to the increased high voltage, and a longer time for conditioning of the excimer gas). The energy at the dye output decreased by approximately 30 % over an hour (2 % over a 5 min LIF run). There was some improvement in stability over the previous series of experiments (where the decrease was 40 % over an hour), although the energy was slightly lower. It was therefore concluded that the energy fluctuations in the system were mainly due to the dye laser, which thus required optimization.

After optimization, the same energy trend was observed, as shown in Figure 3.34 below. Once again, the energy at the dye output decreased by approximately 30 % over an hour and 2 % over a 5 min LIF run. These losses thus appear to be reproducible.

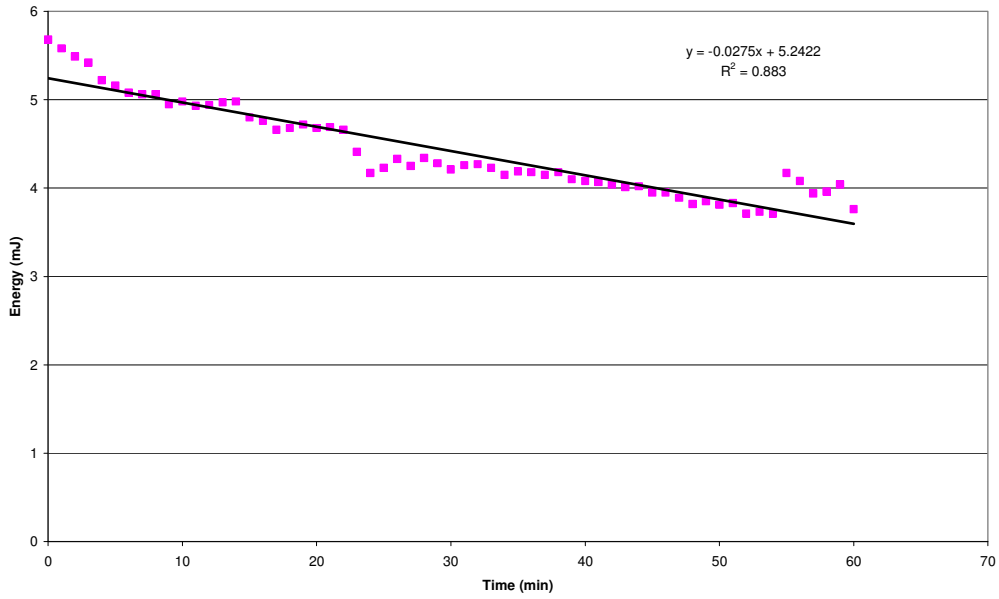

Figure 3.34: Energy at the exit of the dye laser after optimization.

b) *Relationship between excitation energy and fluorescence emission*

The loading of the trap from the naphthalene diffusion tube is shown in Figure 3.35.

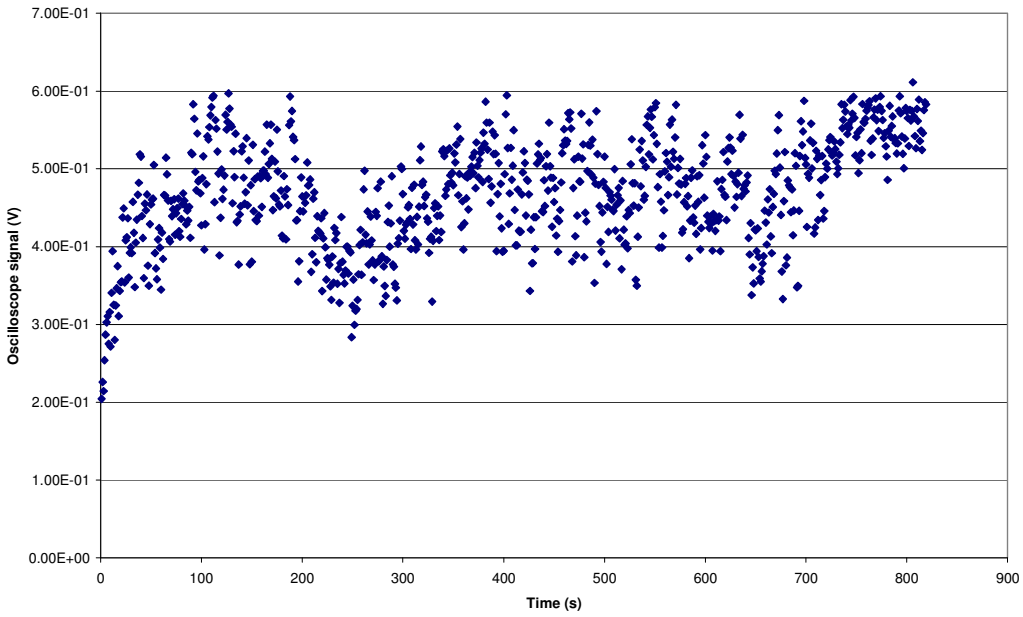

Figure 3.35: Loading of naphthalene onto a silicone rubber trap, prior to energy attenuation experiments.

The decrease in oscilloscope signal with the sequential introduction of borosilicate glass plates in the incident beam is shown in Figure 3.36 and Table 3.19. The measurements taken in between each energy attenuation step indicate that there was no detected change in concentration of naphthalene loaded on the trap during the experiment.

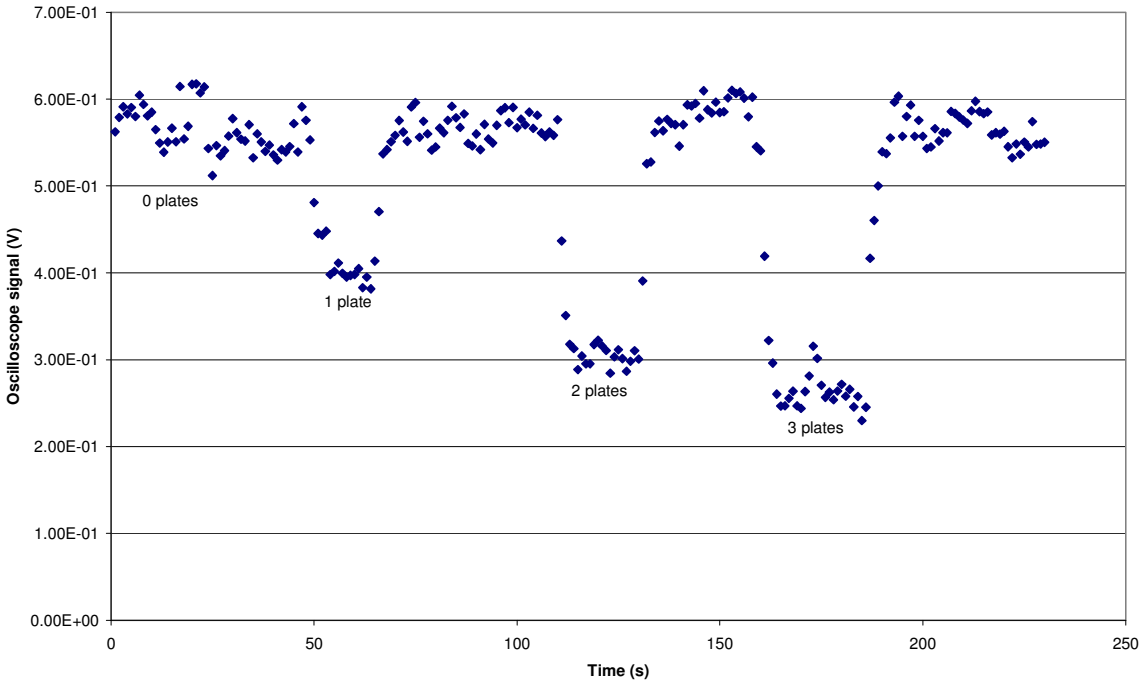

Figure 3.36: Energy attenuation for naphthalene, with n = 0 – 3 (where n represents the number of borosilicate glass plates in the path of the incident beam).

Table 3.19: Energy attenuation by borosilicate glass plates.

Number of borosilicate glass plates in the path of the beam	Average energy at the sample trap location (µJ)	Decrease in energy per plate (%)	Fluorescence signal (V)
0	630	-	0.531586
1	303	52	0.407766
2	182	40	0.306771
3	87	52	0.265053

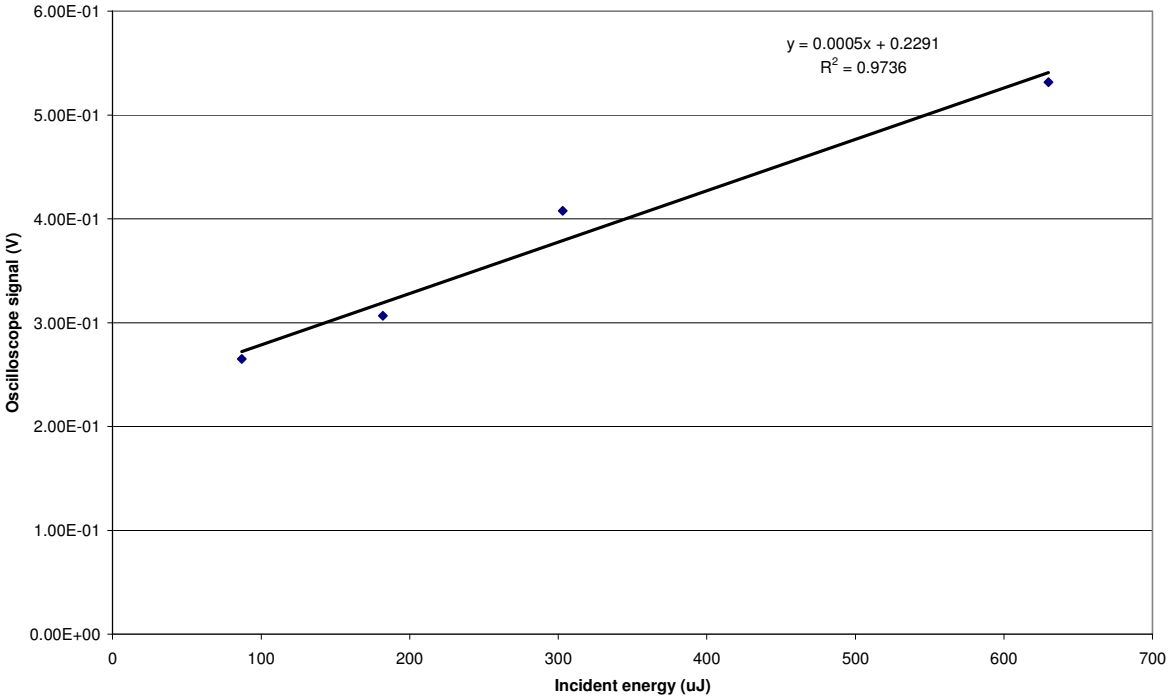

Figure 3.37: Variation in fluorescence signal with changing incident energy.

Some variation in energy attenuation is evident from the decrease in energy signals shown in Table 3.19, and from Figure 3.37. This is probably due to optical imperfections in the plates used.

Due to variations in the system from day to day including the incident energy, slight variations in positioning of the traps, detector response, optical alignment, and so on, the relationship between incident energy, fluorescence signal and concentration would not be constant. This can best be overcome by frequent incident energy measurements throughout analytical runs, as well as by calibration of the system with standard samples of known concentration each day (or more frequently if the measured incident energy fluctuates significantly) and the analysis of quality control samples (of known concentration) in amongst unknowns, as is good laboratory practice.

3.2.5.4 Conclusion

The decrease in energy at the target is largely due to the decrease in pulse energy exiting the dye laser, and there is a smaller contribution due to the optics employed. This decrease will have an impact on the sensitivity of the analytical method, thus the laser system should be carefully optimized to reduce these effects. The contribution of the decrease in energy over time to the results obtained in the photodegradation experiments discussed under section 3.2.4 is also of relevance, as the decreases in oscilloscope signals may not have been only due to photodegradation effects.

The relationship between incident energy, fluorescence signal and concentration is not a simple one, and moreover would not be constant due to concomitant fluctuations in other analytical (system) parameters. This is best overcome by frequent incident energy measurements, and the use of standards to calibrate the system at regular intervals throughout sample analytical runs.

3.2.6 Substrate optimization

3.2.6.1 Background

It is important for the background fluorescence signal obtained from unloaded (blank) traps to be as low as possible, in order to enhance the sensitivity (i.e. to reduce the detection limit) of the experimental method. Silicone rubber is manufactured from liquid silicones by cross-linking induced by an organic peroxide. Background fluorescence experiments were conducted on various silicone rubber substrates, which had been prepared differently; for example by using various monomeric reagents, different cross linking agents, and by employing different post-polymerization product rinsing methods. A number of commercial silicone products, for example that which is sold for household bathroom applications, were also tested.

It is important to note that a concurrent aim of the experiments involving preparation of silicone rubbers, was that the product be useable for air sampling in silicone rubber traps. The

silicone rubber product therefore needed to be non-sticky, easily removed from the preparation plate, as well as non-brittle and elastic, to allow the product to be rolled up for insertion into a quartz tube.

Various stoichiometries were tested in order to determine the effects of increased peroxide content on the properties of the final product.

3.2.6.2 Experimental method and results

a) Preparation of silicones

Stock solutions of various silicone monomers were made by dissolving ~2 g of the silicones (obtained from Alltech Associates (SE-52 and SE-54) and Chromatography Research Supplies Inc. (SE-30)) in 100 mℓ methylene chloride (Merck) (dissolution was assisted by means of ultrasonification).

A measured volume of a stock solution was then mixed with a weighed amount of benzoyl peroxide (The British Drug Houses Inc.) (Figure 3.38) or bis(α,α-dimethylbenzylperoxide) (Merck, 97 % purity), spread on a glass, stainless steel or Teflon plate, and then cured in an oven.

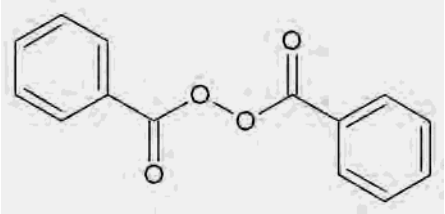

Figure 3.38: Molecular structure of benzoyl peroxide.

The properties of the silicone rubber sheets thus produced were evaluated qualitatively after the silicone rubber had cooled down.

Details of the individual experiments are summarized in Table 3.20.

Table 3.20: Variations in silicone rubber manufacture, where silicone A refers to SE-30, silicone B refers to SE-52 and silicone C refers to SE-54.

Experiment No.	Silicone	Peroxide	Curing conditions	Comments
1	6 mℓ silicone A	10 mg benzoyl peroxide	200 °C for 1 hour on stainless steel	Sticky and broke up into clumps upon removal from the plate.
2	6.5 mℓ silicone A	5.15 mg benzoyl peroxide	200 °C for 1 hour on glass	Stuck to the glass.
3	6 mℓ silicone A	5.40 mg benzoyl peroxide	100 °C for 1 hour then 200 °C for ½ hour, on Teflon	Light brown colour, slightly sticky and was removed from the plate as a sheet.
4	6 mℓ silicone A	11 mg benzoyl peroxide	200 °C for 1 hour on Teflon	Light brown discoloration, brittle, non-sticky product.
5	6 mℓ silicone A	10 mg bis(α,α-dimethylbenzylperoxide)	200 °C for 1 hour on Teflon	Slightly sticky, elastic product.
6	6 mℓ silicone A	19 mg bis(α,α-dimethylbenzylperoxide)	200 °C for 1 hour on Teflon	Sticky, clear product.
7	6 mℓ silicone A	15 mg bis(α,α-dimethylbenzylperoxide)	200 °C for 1 hour on Teflon	Sticky product.
8	25 mℓ silicone A	40 mg bis(α,α-dimethylbenzylperoxide)	200 °C for 1 hour on a larger scale Teflon plate	Clear, thin sheet which was sticky, and gel-like. Was difficult to remove from the plate.
9	6 mℓ silicone B	63 mg bis(α,α-dimethylbenzylperoxide)	200 °C for 1 hour on Teflon	Yellow-brown discoloration, non-sticky.
10	6 mℓ silicone B	40 mg bis(α,α-dimethylbenzylperoxide)	200 °C for 1 hour on Teflon	Slight yellow discoloration, non-sticky.
11	6 mℓ silicone B	35 mg bis(α,α-dimethylbenzylperoxide)	200 °C for 1 hour on Teflon	Clear, non-sticky, slightly elastic. Did not peel off from the plate entirely.
12	6 mℓ silicone B	30 mg bis(α,α-dimethylbenzylperoxide)	200 °C for 1 hour on Teflon	Clear, non-sticky, slightly elastic. Easier to peel off the plate.
13	6 mℓ silicone C	30 mg bis(α,α-dimethylbenzylperoxide)	200 °C for 1 hour on Teflon	Uneven brown discoloration. Easy to remove from the plate. Non-sticky.
14	6 mℓ silicone B	25 mg bis(α,α-dimethylbenzylperoxide)	200 °C for 1 hour on Teflon	Clear, non-sticky. Easy to remove from the plate as a sheet.
15	69 mℓ silicone B	287 mg bis(α,α-dimethylbenzylperoxide)	200 °C for 1 hour on a larger scale Teflon plate	Clear, thin, sticky. Easy to remove from the plate but broke readily. Gel-like.

Different product rinsing solvents were also tested on the SE-30 based silicone rubber, as this step is important in removing any remaining peroxide (in this case bis(α,α-dimethylbenzylperoxide)) or uncross-linked silicone from the final product. It is important that the solvents used do not cause extensive swelling of the PDMS, as this may render the polymer fragile and difficult to handle (Rusina et al., 2007). The experimental conditions and observations pertaining thereto are summarized in Table 3.21 below.

Table 3.21: Effects of solvent rinsing on silicone rubber product, where DCM denotes dichloromethane).

Experiment No.	Solvents	Observations
1	Hexane & acetone, 1:1	Transparent whilst submerged, cloudy upon removal.
2	Hexane	Transparent whilst submerged, sticky and gel-like upon removal and reduced in size.
3	DCM	Translucent whilst submerged, sticky upon removal and became cloudy.
4	Acetone	Appeared to shrink in the solvent and became cloudy.
5	Hexane & DCM, 1:1	Swelled after submersion and was slippery after removal from the solvent.
6	Hexane & DCM, 2:1	Appeared to have shrunk and was slightly cloudy.
7	Hexane & DCM, 1:2	Neither sticky nor cloudy.

b) LIF evaluation

The various silicone rubbers (and silicone monomers) were placed inside a quartz tube (the same dimensions as that used for the multi-channel silicone rubber traps), in the form of a plug, or a rolled sheet, as appropriate. The trap was then placed at the sample target position of the LIF system, as described under section 3.2.1. Various incident wavelengths were used and the resulting fluorescence spectra were recorded over a fairly wide emission wavelength range, in order to cover the range of fluorescence maxima of different PAHs.

The results obtained with 302 nm excitation (suitable for benzo(*a*)pyrene) are presented in Figure 3.39, whilst those with 292 nm excitation (suitable for naphthalene) are given in Figure 3.40.

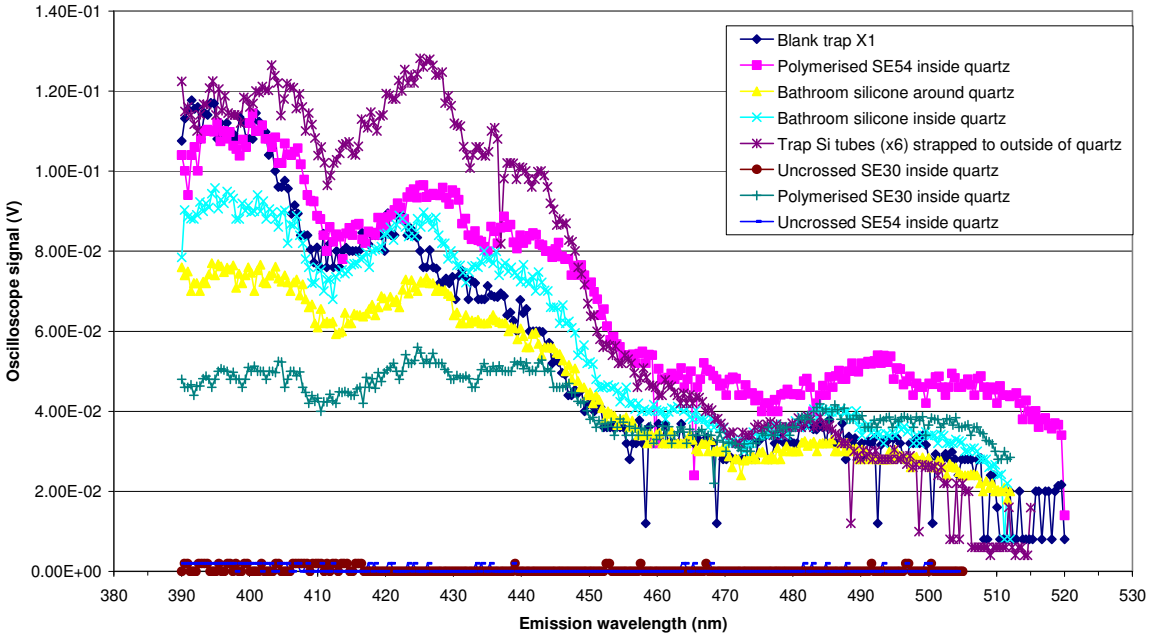

Figure 3.39: Fluorescence spectra of various blank quartz traps, with 302 nm excitation provided by the dye laser system. Blank trap X1 refers to the standard quartz multi-channel silicone rubber traps used in the other experiments.

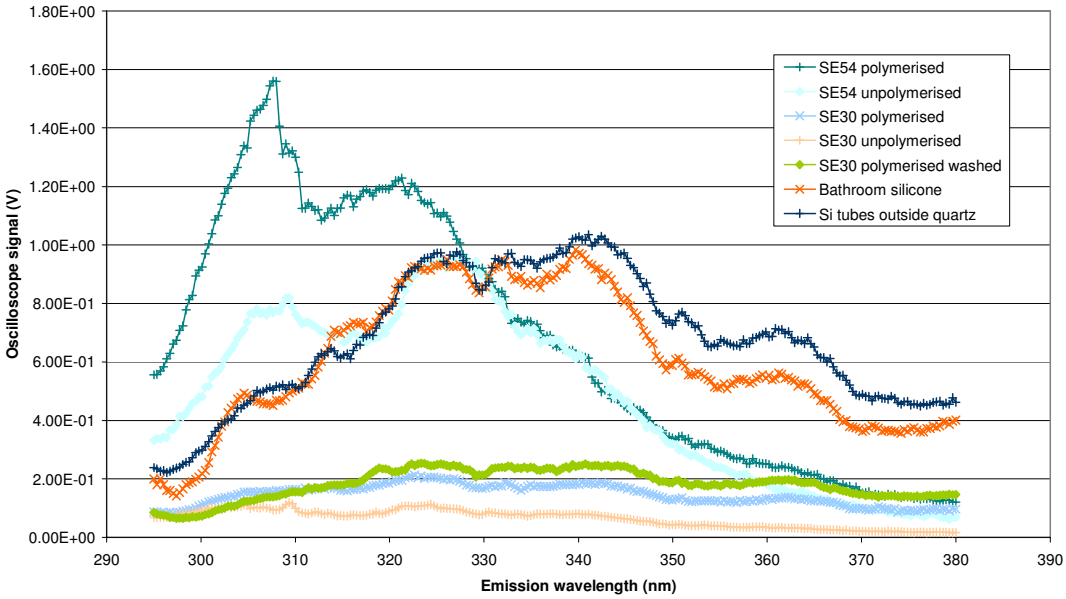

Figure 3.40: Fluorescence spectra of various blank quartz traps, with 292 nm excitation provided by the dye laser system.

3.2.6.3 Discussion and conclusion

In terms of the production of silicone rubber sheets, the results of the various preparation experiments conducted showed that silicone SE-52 (95 % methyl, 5 % phenyl) with (~ 25 % mass/mass) bis(α,α-dimethylbenzylperoxide) yielded a less sticky, more elastic product, which was clear, thus experiment 12 in Table 3.20 yielded the most promising results. The Teflon plate was the most suitable curing surface, as it facilitated the removal of the product.

With respect to solvent rinsing, hexane : DCM :: 1 : 2 yielded the best results (experiment no. 7 in Table 3.21), as this mixture maintained the structure of the silicone rubber product and its clear, translucent property.

The results of the LIF tests are qualitative, as the mass of silicone used in each experiment was not the same. The experiments did, however, successfully show that the lowest background fluorescence signal was obtained for the silicone which had the least aromatic moieties in the final product, as would be expected due to their chromophoric properties.

Similar trends in the background fluorescence signals were found at both excitation wavelengths. A high signal was obtained for the silicone tubes (used to prepare the standard multi-channel silicone rubber traps) strapped to the outside of a quartz tube. This experiment was performed to determine the background signal of the silicone tubes alone, without the influence of the quartz. Presumably more incident light reached the silicone tubes in this case, as compared to when they are housed in quartz, which therefore produced a higher background fluorescence signal. This trend was reversed for the commercial bathroom silicone, however, where it appears that the quartz tube assisted with focusing the incident beam onto the silicone (the 292 nm bathroom silicone measurement also refers to this silicone inside a quartz tube), resulting in a higher fluorescence signal, although this effect was less than that of the silicone tubes, where the difference between oscilloscope signals was larger.

The uncross-linked monomer had a lower background signal, which is most likely due to the lack of influence of the aromatic moieties of the cross-linking agent (peroxide). Although washing of polymerized product would remove remaining excess reagents, the

washing of polymerized SE-30, in the case of 292 nm excitation, increased the fluorescence signal slightly, possibly due to the presence of impurities in the solvents used. The cross-linked SE-54 (methyl silicone, 5 % phenyl, 1 % vinyl silicone) resulted in a higher background signal as compared to SE-30 (methyl silicone), which gave the lowest background fluorescence of all the cross-linked products tested, as would be expected due to the lower aromatic moieties present in this product.

The SE-30 based silicone is therefore a potential alternative to the commercial silicone tubes, although the production methodology requires further development, in order to produce a silicone sheet of reproducible thickness and consistency, which can be rolled up and inserted into a quartz tube in a manner which allows for reproducible sampling flow rates and minimal pressure drop across the trap.

3.3 OVERALL CONCLUSION

The method described has the potential to serve as a screening tool to avoid the comprehensive analysis of samples which do not contain appreciable levels of PAHs. The LIF experimental procedure is simple and rapid, with acceptably low limits of detection, even with the initial, unoptimized optical arrangement and without extensive time-averaging. LIF also provides selectivity without the need for sample clean-up and separation processes, which may entail the use of organic solvents and cryogenic equipment.

The method is basically non-destructive and the sample traps may be subsequently analysed directly by TD-GC-MS. The method developed here may therefore find application in the analysis of combustion products arising from processes of relevance to developing countries including incineration; veld fires; sugar cane burning; and diesel fuel combustion, as described in Chapter 5.

The multi-channel silicone rubber traps allow for the pre-concentration of analytes and in addition they may provide a useful means of simultaneously physically separating mixtures of analytes in air samples in the trap, as a consequence of chromatographic frontal separation processes occurring through the trap during sampling. The first part of the trap may therefore

remove the less volatile PAHs from naphthalene, for example, which will move further down the trap. This physical resolution can then be utilized by focusing the laser on a spot lower down the trap to detect naphthalene, and may also allow for the deconvolution of more complex fluorescence spectra. Such a profiling example was evident in the LIF analysis of traps which had been used to sample emissions from a sugar cane burn, as discussed in Chapter 5.

Further development and optimization of the method is needed in order to ensure its robustness and to provide sufficiently accurate and reproducible results. Specifically the variation in incident energy provided by the laser system should be minimized, which was a challenge in this study due to the age of the laser system employed. In addition, signal averaging and the collection and detection of the fluorescence emission should be optimized, and the capability of the system to resolve the PAH emission spectra in mixtures should be further investigated. The use of time-gated fluorescence spectroscopy may also reduce background effects arising from fluorescence of the PDMS, which would reduce method detection limits. Such an approach has been demonstrated in aqueous systems, where pyrene was detected by LIF (Kuo et al., 2007), for example.

3.4 REFERENCES

Allain, L.R., Stratis, D.N., Cullum, B.M., Mobley, J., Hajaligol, M.R. and Vo-Dinh, T., *Journal of Analytical Applied Pyrolysis,* **2003**, *66*, 145-154.

Agency for Toxic Substances and Disease Registry (ATSDR), USA Department of Health and Human Services, August **1995**, Agency for Toxic Substances and Disease Registry, Public Health Statement: Naphthalene, 1-methylnaphthalene, and 2-methylnaphthalene, accessed on 14 September 2007 at http://www.atsdr.cdc.gov/toxpro2

Agency for Toxic Substances and Disease Registry (ATSDR), USA Department of Health and Human Services, August **2005**, Agency for Toxic Substances and Disease Registry, Public Health Statement: Polycyclic Aromatic Hydrocarbons, accessed on 14 September 2007 at http://www.atsdr.cdc.gov/toxpro2

Balthussen, E., David, F., Sandra, P., Janssen, H.-G. and Cramers, C.A., *Journal of High Resolution Chromatography*, **1998**, *21*, 332-340.

Baltussen, E., Janssen, H.-G., Sandra, P. and Cramers, C.A., *Journal of High Resolution Chromatography*, **1997**, *20*, 385-393.

Behymer, T.D. and Hites, R.A., *Environmental Science and Technology,* **1985**, *19*, 1004-1006.

Boström, C.-E., Gerde, P., Hanberg, A., Jernström, B., Johansson, C., Kyrklund, T., Rannug, A., Törnqvist, M., Victorin, K. and Westerholm, R., *Environmental Health Perspectives*, **2002**, *110* (Suppl. 3), 451-488.

Brackmann, U., **1986**, Lambdachrome Laser Dyes, Lambda Physik.

Chang, K.-F., Fang, G.-C., Chen, J.-C. and Wu, Y.-S., *Environmental Pollution*, **2006**, *142*, 388-396.

Chi, Z., Cullum, B.M., Stokes, D.L., Mobley, J., Miller, G.H., Hajaligol, M.R. and Vo-Dinh, T., *Spectrochimica Acta Part A*, **2001**, *57*, 1377-1384.

Chiang, P.-C., You, J.-H., Chang, S.-C. and Wei, Y.-H., *Journal of Hazardous Materials*, **1992**, *31*, 29-37.

De Coensel, N., Desmet, K., Sandra, P. and Górecki, T., *Chemosphere*, **2008**, *71*, 711-716.

Dos Santos, C.Y.M., de Almeida Azevedo, D. and de Aquino Neto, F. R., *Atmospheric Environment*, **2002**, *36*, 3009-3019.

Fang, M., Zheng, M., Wang, F., To, K.L., Jaafar, A.B. and Tong, S.L., *Atmospheric Environment*, **1999**, *33*, 783-795.

Gevao, B., Al-Omair, A., Sweetman, A., Al-Ali, L., Al-Bahloul, M., Helaleh, M. and Zafar, J., *Environmental Toxicology and Chemistry*, **2006**, *25* (6), 1496-1502.

Gridin, V.V., Inoue, T., Ogawa, T. and Schechter, I., *Instrumentation Science and Technology*, **2000**, *28* (2), 131-141.

Grundl, T.J., Aldstadt, J.H., Harb, J.G., St Germain, R.W. and Schweitzer, R.C., *Environmental Science and Technology*, **2003**, *37* (6), 1189-1197.

Guillard, C., Delprat, H., Hoang-Van, C. and Pichat, P., *Journal of Atmospheric Chemistry*, **1993**, *16*, 47-59.

Gundel, L.A., Lee, V.C., Mahanama, K.R.R., Stevens, R.K. and Daisey, J.M., *Atmospheric Environment*, **1995**, *29* (14), 1719-1733.

Handa, T., Kato, Y., Yamamura, T., Tshii, T. and Matsushita, H., *Journal of Environmental Science and Health*, **1980**, *A15* (6), 573-599.

Harrison, R.M., Smith, D.J.T. and Luhana, L., *Environmental Science and Technology*, **1996**, *30*, 825-832.

Hart, K.M., McDow, S.R., Giger, W., Steiner, D. and Burtscher, H., *Water, Air, and Soil Pollution*, **1993**, *68*, 75-90.

Hawthorne, S.B., St. Germain, R.W. and Azzolina, N.A., *Environmental Science and Technology*, **2008**, *42* (21), 8021-8026.

Hays, M.D., Smith, N.D., Kinsey, J., Dong, Y. and Kariher, P. *Aerosol Science*, **2003**, *34*, 1061-1084.

Jang, M. and McDow, S.R., *Environmental Science and Technology,* **1997**, *31*, 1046-1053.

Jaward, F.M., Farrar, N.J., Harner, T., Sweetman, A.J. and Jones, K.C. *Environmental Toxicology and Chemistry,* **2004**, *23* (6), 1355-1364.

Johnsen, A.R., Wick, L.Y. and Harms, H., *Environmental Pollution*, **2005**, *133*, 71-84.

Kamens, R.M., Guo, J., Guo, Z. and McDow, S.R., *Atmospheric Environment*, **1990**, *24(A)* (5), 1161-1173.

Kamens, R.M., Zhishi, G., Fulcher, J.N. and Bell, D.A., *Environmental Science and Technology*, **1988**, *22*, 103-108.

Kamens, R.M.., Fulcher, J.N. and Zhishi, G., *Atmospheric Environment*, **1986**, *20* (8), 1579-1587.

Kirsh, B.A. and Winefordner, J.D., *Analytical Chemistry*, **1987**, *59* (14), 1874-1879.

Knorr, F.J. and Harris, J.M., *Analytical Chemistry*, **1981**, *53*, 272-276.

Korfmacher, W.A., Natusch, D.F.S., Taylor, D.R., Mamantov, G. and Wehry, E.L., *Science*, **1980a**, *207*, 763-765.

Korfmacher, W.A., Wehry, E.L., Mamantov, G. and Natusch, D.F.S., *Environmental Science and Technology*, **1980b**, *14* (9), 1094-1099.

Kotzick, R. and Niessner, R., *Fresenius Journal of Analytical Chemistry*, **1996**, *354*, 72-76.

Koziel, J.A., Odziemkowski, M. and Pawliszyn, J., *Analytical Chemistry,* **2001**, *73*, 47-54.

Kumke, M.U., Löhmannsröben, H.-G. and Roch, Th., *Journal of Fluorescence*, **1995**, *5* (2), 139-153.

Kuo, D.T.F., Adams, R.G., Rudnick, S.M., Chen, R.F. and Gschwend, P.M., *Environmental Science and Technology*, **2007**, *41* (22), 7752-7758.

Lehto, K.-M., Vuorimaa, E. and Lemmetyinen, H., *Journal of Photochemistry and Photobiology A: Chemistry*, **2000**, *136*, 53-60.

Liu, L.-B., Liu, Y., Lin, J.-M., Ning, T., Hayakawa K. and Maeda, T., *Journal of Environmental Sciences.* **2007**, *19*, 1-11.

Lohmann, R., Northcott, G.L. and Jones, K.C., *Environmental Science and Technology,* **2000**, *34*, 2892-2899.

Low, G., Batley, G. and Brockbank, C.I., *Journal of Chromatography*, **1987**, *392*, 199-210.

Lu, R., Wu, J., Turco, R.P., Winer, A.M., Atkinson, R., Arey, J., Paulson, S.E., Lurmann, F.W., Miguel, A.H. and Eiguren-Fernandez, A., *Atmospheric Environment*, **2005**, *39*, 489-507.

Manahan, S.E., **2000**, Environmental Chemistry, 7th edition, Lewis Publishers, USA, 313.

Marr, L.C., Grogan, L.A., Wöhrnschimmel, H., Molina, L., Molina, M.J., Smith, T.J. and Garshick, E., *Environmental Science and Technology,* **2004**, *38* (9), 2584-2592.

Marr, L.C., Kirchstetter, T.W., Harley, R.A., Miguel, A.H., Hering, S.V. and Hammond, S.K., *Environmental Science and Technology,* **1999**, *33*, 3091-3099.

Martinez, M., Harder, H., Ren, X., Lesher, R.L. and Brune, W.H., *Atmospheric Chemistry and Physics*, **2004**, *4*, 563-569.

Matsuzawa, S., Nasser-Ali, L. and Garrigues, P., *Environmental Science and Technology,* **2001**, *35*, 3139-3143.

Mayer, P., Vaes, W. H. J. and Hermens, J.L.M., *Analytical Chemistry,* **2000**, *72*, 459-464.

Menichini, E., Monfredini, F. and Merli, F., *Atmospheric Environment,* **1999**, *33*, 3739-3750.

Nadal, M., Wargent, J.J., Jones, K.C., Paul, N.D., Schuhmacher, M. and Domingo, J.L., *Journal of Atmospheric Chemistry*. **2006**, *55*, 241-252.

Niessner, R., Robers, W. and Krupp, A., *Fresenius Journal of Analytical Chemistry*, **1991**, *341*, 207-213.

Nikolaou, K., Masclet, P. and Mouvier, G., *Science of the Total Environment*, **1984**, *32*, 103-132.

NIOSH Manual of Analytical Methods, 15 January **1998**, 4th edition, Method 5800: Polycyclic aromatic hydrocarbons (total), Issue 1.

NIOSH Manual of Analytical Methods, 15 January **1998**, 4th edition, Method 5506: Polynuclear aromatic hydrocarbons by HPLC, Issue 3.

Nisbet, I.C.T. and LaGoy, P.K., *Regulatory Toxicology and Pharmacology,* **1992**, *16*, 290-300.

Niu, J., Chen, J., Martens, D., Henkelmann, B., Quan, X., Yang, F., Seidlitz, H.K. and Schramm, K.-W., *Science of the Total Environment*, **2004**, *322*, 231-241.

Niu, J., Chen, J., Martens, D., Quan, X., Yang, F., Kettrup, A. and Schramm, K.-W., *Environmental Pollution*, **2003**, *123*, 39-45.

Odabasi, M., Vadar, N., Sofuoglu, A., Tasdemir, Y. and Holsen, T.M., *The Science of the Total Environment*, **1999**, *227*, 57-67.

Odziemkowski, M., Koziel, J.A., Irish, D.E. and Pawliszyn, J., *Analytical Chemistry,* **2001**, *73*, 3131-3139.

Ohura, T., Amagai, T., Sugiyama, T., Fusaya, M. and Matsushita, H., *Environmental Science and Technology,* **2004a**, *38*, 2045-2054.

Ohura, T., Amagai, T., Sugiyama, T., Fusaya, M. and Matsushita, H., *Atmospheric Environment*, **2004b**, *38*, 2045-2054.

Ono-Ogasawara, M. and Smith, T.J., *Industrial Health*, **2004**, *42*, 389-399.

Ortner, E.K. and Rohwer, E.R., *Journal of High Resolution Chromatography,* **1996**, *19*, 339-344.

Ortner, E.K., August, **1994**, Alternative concentration techniques for the trace analysis of semi-volatile organic air pollutants by capillary gas chromatography, MSc Thesis, University of Pretoria.

Panne, U., Knöller, A., Kotzick, R. and Niessner, R., *Fresenius Journal of Analytical Chemistry*, **2000**, *366*, 408-414.

Park, S.S., Kim, Y.J. and Kang, C.H., *Atmospheric Environment*, **2002**, *36*, 2917-2924.

Prevedouros, K., Brorström-Lundén, E., Halsall, C.J., Jones, K.C., Lee, R.G.M. and Sweetman, A.J., *Environmental Pollution*, **2004**, *128*, 17-27.

Primbs, T., Piekarz, A., Wilson, G., Schmedding, D., Higginbotham, C., Field, J. and Simonich, S.M., *Environmental Science and Technology*, **2008**, *42*, 6385-6391.

Ravindra, K., Wauters, E. and Van Grieken, R., *Science of the Total Environment*, **2008**, *396*, 100-110.

Roper, J.C., Brown, D.M., Sullivan, M.A., Schoonhoven, R., Swenberg, J.A. and Pfaender, F.K., *Environmental Toxicology and Chemistry*, **2006**, *25* (12), 3093-3100.

Rosenberg, C., Winiwarter, W., Gregori, M., Pech, G., Casensky, V. and Puxbaum, H., *Fresenius Journal of Analytical Chemistry*, **1988**, *331*, 1-7.

Rusina, T.P., Smedes, F., Klanova, J., Booij, K. and Holoubek, I., *Chemosphere*, **2007**, *68*, 1344-1351.

Sawicki, E., Elbert, W., Stanley, T.W., Hauser, T.R. and Fox, F.T., *Analytical Chemistry*, **1960**, *32* (7), 811-815.

Schwarzenbach, R.P., Gschwend, P.M. and Imboden, D.M., **2003**, Environmental Organic Chemistry, 2nd edition, Wiley Interscience, USA.

Shekiro, J.M., Skogerboe, R.K. and Taylor, H.E. *Environmental Science and Technology*, **1988**, *22,* 338-344.

Šišović, A., Bešlić, I., Šega, K. and Vadjić, V., *Environment International*, **2008**, *34* (5), 580-584.

Song, J.M., Jagannathan, R., Stokes, D.L., Vo-Dinh, T. and Hajaligol, M.R., *Polycyclic Aromatic Compounds*, **2003**, *23*, 429-439.

Subramanyam, V., Valsaraj, K.T., Thibodeaux, L.J. and Reible, D.D., *Atmospheric Environment*, **1994**, *28* (19), 3083-3091.

Tang, S., Johnson, R., Lanni, T., Webster, W., Tagliaferro, T., Munn, J., Barnes, C., Barnes, D., Newkirk, K., Rivenburgh, D. and Guerrieri, D., **2001**, Monitoring of PM-bound polycyclic aromatic hydrocarbons from diesel vehicles by photoelectric aerosol sensor (PAS); Automotive Emissions Laboratory: New York, accessed at www.ecochem.biz/library/nydec.pdf

Temime-Roussel, B., Monod, A., Massiani, C. and Wortham, H., *Atmospheric Environment*, **2004**, *38*, 1913-1924.

Tsapakis, M. and Stephanou, E.G., *Environmental Pollution*, **2005**, *133*, 147-156.

USA EPA, **2002**, Health Assessment Document for Diesel Engine Exhaust. U.S. Environmental Protection Agency, Office of Research and Development, National Center for Environmental Assessment, Washington Office, Washington, DC, EPA/600/8-90/057F.

Vander Wal, R.L., Jensen, K.A. and Choi, M.Y., *Combustion and Flame*, **1997**, *109*, 399-414.

Wang, D., Chen, J., Xu, Z., Qiao, X. and Huang, L., *Atmospheric Environment*, **2005**, *39*, 4583-4591.

Wauters, E., Van Caeter, P., Desmet, G., David, F., Devos, C. and Sandra, P., *Journal of Chromatography A*, **2008**, *1190*, 286-293.

Westerholm, R.N., Almén, J., Li, H., Rannug, J.U., Egebäck, K.-E. and Grägg, K., *Environmental Science and Technology,* **1991**, *25*, 332-338.

Whitcomb, J.L., Bystol, A. J. and Campiglia, A.D., *Analytica Chimica Acta,* **2002**, *464*, 261-272.

Wild, E., Dent, J., Thomas, G.O. and Jones, K.C., *Environmental Toxicology and Chemistry,* **2007**, *26* (12), 2486-2493.

Wild, E., Dent, J., Thomas, G.O. and Jones, K.C., *Environmental Science and Technology,* **2005**, *39*, 268-273.

Wild, S.R. and Jones, K.C., *Environmental Pollution,* **1995**, *88*, 91-108.

Yang, H.-H., Tsai, C.-H., Chao, M.-R., Su, Y.-L. and Chien, S.-M., *Atmospheric Environment*, **2006**, *40*, 1266-1274.

Yokley, R.A., Garrison, A.A., Wehry, E.L. and Mamantov, G., *Environmental Science and Technology*, **1986**, *20*, 86-90.

Zhang, X., Cheng, S., Zhu, C. and Sun, S., *Pedosphere*, **2006**, *16* (5), 555-565.